Physics Reports 503 (2011) 1–75

Contents lists available at ScienceDirect

Physics Reports

journal homepage: www.elsevier.com/locate/physrep

Chiral effective field theory and nuclear forces

R. Machleidt [a,*], D.R. Entem [b]

[a] Department of Physics, University of Idaho, Moscow, ID 83844, USA

[b] Grupo de Fisica Nuclear and IUFFyM, University of Salamanca, E-37008 Salamanca, Spain

ARTICLE INFO

Article history:
Accepted 14 February 2011
Available online 19 February 2011
editor: W. Weise

Keywords:
Low-energy QCD
Effective field theory
Chiral perturbation theory
Nuclear forces
Nucleon–nucleon scattering

ABSTRACT

We review how nuclear forces emerge from low-energy QCD via chiral effective field theory. The presentation is accessible to the non-specialist. At the same time, we also provide considerable detailed information (mostly in appendices) for the benefit of researchers who wish to start working in this field.

Contents

* Corresponding author.
E-mail addresses: machleid@uidaho.edu (R. Machleidt), entem@usal.es (D.R. Entem).

0370-1573/$ – see front matter © 2011 Elsevier B.V. All rights reserved.
doi:10.1016/j.physrep.2011.02.001

1. Introduction and historical perspective

The theory of nuclear forces has a long history (cf. Table 1). Based upon the seminal idea by Yukawa [1], first field-theoretic attempts to derive the nucleon–nucleon (*NN*) interaction focused on pion exchange. While the one-pion exchange turned out to be very useful in explaining *NN* scattering data and, in particular, the properties of the deuteron [2], multi-pion exchange was beset with serious ambiguities [3,4] that could not be resolved in a satisfactory way. Thus, the "pion theories" of the 1950s are generally judged as failures—for reasons we understand today: pion dynamics is constrained by chiral symmetry, a crucial point that was unknown in the 1950s.

Historically, the experimental discovery of heavy mesons [5] in the early 1960s saved the situation. The one-boson-exchange (OBE) model [6–11] emerged, which still today is the most economical and quantitative phenomenology for describing the *NN* interaction [12–14]. The weak point of this model, however, is the scalar–isoscalar "sigma" or "epsilon" boson, for which empirical evidence remains controversial. Since this boson is associated with the correlated (or resonant) exchange of two pions, a vast theoretical effort was launched to derive the 2π-exchange contribution of the nuclear force, which creates the intermediate-range attraction. During this effort, which occupied more than a decade, dispersion theory (Stony Brook [15,16] and Paris [17,18] potentials) as well as field theory (Partovi–Lomon model [19], Bonn potential [11,20]) were invoked.

Table 1
The theory of nuclear forces: seven decades of struggle.

1935	**Yukawa: Meson theory**
1950's	*The "Pion Theories"*. One-pion exchange: good; multi-pion exchange: disaster.
1960's	Many pions ≡ multi-pion resonances: σ, ρ, ω,.... The One-Boson-Exchange Model: success.
1970's	Diverse two-pion-exchange models: Partovi–Lomon, Stony Brook, Paris, Bonn.
1980's	Nuclear physicists discover **QCD**: Quark Models.
1990's and beyond	Nuclear physicists discover **EFT**; Weinberg, van Kolck, ..., **Back to Meson (Pion) Theory!** *But, constrained by Chiral Symmetry.*

The nuclear force problem appeared to be solved; however, with the discovery of quantum chromodynamics (QCD), all "meson theories" were relegated to the status of models and the attempts to derive the nuclear force had to start all over again.

The problem with a derivation of nuclear forces from QCD is that this theory is nonperturbative in the low-energy regime characteristic of nuclear physics, which makes direct solutions very difficult. Therefore, during the first round of new attempts, QCD-inspired quark models [21–31] became popular. The positive aspect of these models is that they try to explain hadron structure and hadron–hadron interactions on an equal footing and, indeed, some of the gross features of the *NN* interaction are explained successfully. However, on a critical note, it must be pointed out that these quark-based approaches are nothing but another set of models and, thus, do not represent fundamental progress. For the purpose of describing hadron–hadron interactions, one may equally well stay with the simpler and much more quantitative meson models.

A major breakthrough occurred when the concept of an effective field theory (EFT) was introduced and applied to low-energy QCD. As outlined by Weinberg in a seminal paper [32], one has to write down the most general Lagrangian consistent with the assumed symmetry principles, particularly the (broken) chiral symmetry of QCD. At low energy, the effective degrees of freedom are pions (the Goldstone bosons of the broken symmetry) and nucleons rather than quarks and gluons; heavy mesons and nucleon resonances are "integrated out". So, the circle of history is closing and we are *back to Yukawa's meson (pion) theory*, except that we have finally learned how to deal with it: broken chiral symmetry is a crucial constraint that generates and controls the dynamics and establishes a clear connection with the underlying theory, QCD.

The idea of chiral symmetry has an interesting history of its own. The modern understanding is that this symmetry arises because the up and down quarks happen to have relatively small masses. However, chiral symmetry and its significance for low-energy hadron (pion) physics was discovered long before QCD. In 1960, based upon concepts proposed by Schwinger [33], Gell-Mann and Levy [34] developed the sigma model, which is a linear realization of chiral symmetry.[1] One major problem researchers had been struggling with in the 1950's was that the pion–nucleon scattering length came out two orders of magnitude too large when the (renormalizable) pseudoscalar (γ_5) πN interaction was used. This unrealistic prediction was due to very large contributions from virtual anti-nucleon states (the so-called "pair terms" or "Z-graphs"). Similar problems occurred in the 2π-exchange contribution to the *NN* interaction. In the sigma model, the large pair terms are canceled by processes involving the (fictitious) σ boson. In this way, the linear sigma model demonstrates how imposing chiral invariance fixes the problem with low-energy π–N scattering. However, the fictitious character of the σ particle as well as the reliance on the perfect cancelation of huge terms are uncomfortable features. In 1967, motivated by the current algebra approach to soft pion physics, Weinberg [36] worked out what has become known as the non-linear sigma model, which does not include a σ anymore and has pions and nucleons interact via pseudo-vector (derivative, $\gamma_5\gamma^\mu\partial_\mu$) coupling besides a new (non-linear) $\pi\pi NN$ term also involving a derivative ("Weinberg–Tomozawa term" [37,38]). The derivative (equivalent to momentum) guarantees that the interaction vanishes when the momentum goes to zero providing a natural explanation for the weakness of the interaction by soft pions which does not rely on the cancelation of large terms. Following suggestions by Schwinger, Weinberg [39] developed, soon after, a general theory of non-linear realizations of chiral symmetry, which was further generalized in an elegant way by Callan et al. [40].

Even though the original work on chiral symmetry was obviously all performed by particle physicists, it must be stated – to the honor of nuclear physics – that there have been some far-sighted nuclear physicists who early on understood and appreciated the significance of chiral symmetry for low-energy hadron interactions. One of them was Gerry Brown, who as early as 1968 published with two co-workers a paper [41] on three-nucleon forces, where the consequences of chiral symmetry are fully exploited. In 1970, Brown wrote a remarkable Comment [42] and, in 1979, he published a book chapter entitled "Chiral symmetry and the nucleon–nucleon interaction"[43]. Moreover, in the more sophisticated relativistic meson models of the past [20,44–46] the pseudo-vector coupling was applied in πNN vertices (instead of the simpler pseudoscalar one that was commonly in use) in recognition of chiral symmetry. However, this chiral patch work, even though it points into the right direction, cannot be perceived as a serious chirally invariant theory. Moreover, one has to face the problem that the derivative coupling is not renormalizable in the conventional sense.

Therefore, ideas were still needed for how to implement chiral symmetry consistently in the theory of pionic and nuclear interactions and how to deal with the renormalization issue. In his contribution to the 'Festschrift' in honor of Schwinger of 1979 [32,47], Weinberg proposed to consider the most general possible Lagrangian including all higher-derivative terms

[1] For a pedagogical introduction into chiral symmetry and the sigma model, see [35].

that are consistent with chiral symmetry (besides the other commonly accepted symmetry principles). For this theory to be manageable, one needs to assume some sort of perturbative expansion such that only a finite number of terms contribute at a given order. This expansion is provided by powers of small external momenta over the chiral symmetry breaking scale, $\Lambda_\chi \sim 1$ GeV. The higher-derivative terms supply the counterterms that make possible an order-by-order renormalization, which is the appropriate renormalization procedure for an effective field theory. Weinberg's suggestions were soon picked up by Gasser, Leutwyler, and associates who worked out, to one loop, the cases of $\pi\pi$ [48] and πN scattering [49] with great success.

But there was still the problem of the nuclear force which is more difficult, since nuclear interactions do not vanish in the chiral limit ($q \to 0$; $m_{u/d}$, $m_\pi \to 0$) and require a nonperturbative treatment because of the existence of nuclear bound states. In a series of papers published around 1990 [50–52], Weinberg picked up the nuclear force issue and suggested to calculate the *NN* potential perturbatively in the chiral expansion and then iterate it to all orders in a Schroedinger or Lippmann–Schwinger equation to obtain the nuclear amplitude. Here, the introduction of four-nucleon contact terms is crucial for renormalization.

Following the Weinberg proposal, pioneering work was performed by Ordóñez et al. [53,54] who applied time-ordered perturbation theory to construct a *NN* potential up to next-to-next-to-leading order (NNLO). The results were encouraging and nuclear EFT quickly developed into one of the most popular branches of modern nuclear physics. The Munich group used covariant perturbation theory and dimensional regularization to calculate the perturbative *NN* amplitude without [55] and with $\Delta(1232)$-isobar degrees of freedom [56] at NNLO. Besides this, the Munich group worked out important loop contributions of higher order [57–61]. A relativistic approach was also taken by the Brazil group [62,63]. The Bochum–Jülich group devised a method of unitarity transformations to eliminate the energy dependence of time-ordered perturbation theory amplitudes and calculated the *NN* potentials up to NNLO [64,65]. The Idaho group managed to construct a chiral *NN* potential at next-to-next-to-next-to-leading order (N^3LO) and showed that only at this order can one achieve the precision necessary for reliable few-nucleon and nuclear structure calculations [66–69]. Progress extended beyond the *NN* interaction, as nuclear many-body forces based upon chiral perturbation theory were also developed [52,70–73].

During the past decade or so, chiral two-nucleon forces have been used in many microscopic calculations of nuclear reactions and structure [74–88] and the combination of chiral two- and three-nucleon forces has been applied in few-nucleon reactions [71,89–97], structure of light- and medium-mass nuclei [98–101], and nuclear and neutron matter [102,103]—with a great deal of success. The majority of nuclear structure calculations is nowadays based upon chiral forces.

Consequently, it may be of interest to the community to have a good understanding of these forces and their background. It is therefore the purpose of this report to provide an accessible review on how nuclear forces emerge from low-energy QCD via chiral effective field theory. A pedagogical introduction into the phenomenology and the traditional view of nuclear forces can be found in Refs. [11,104]. Alternative reviews on various aspects of the modern perspective are published in Refs. [105–108].

This article is organized as follows. In Section 2, we sketch the foundations of an EFT for low-energy QCD including the effective Lagrangians. Section 3 provides an overview on nuclear forces derived from chiral EFT. The two-nucleon force is then discussed in detail in Section 4 and many-body forces in Section 5. The extension of the theory through the introduction of $\Delta(1232)$-isobar degrees of freedom and higher order contributions to nuclear forces are considered in Section 6. Finally, Section 7 contains our conclusions. The appendices provide many mathematical details which may be useful to researchers who wish to start working in the field.

2. Effective field theory for low-energy QCD

Quantum chromodynamics (QCD) is the theory of strong interactions. It deals with quarks, gluons and their interactions and is part of the Standard Model of Particle Physics. QCD is a non-Abelian gauge field theory with color $SU(3)$ the underlying gauge group. The non-Abelian nature of the theory has dramatic consequences. While the interaction between colored objects is weak at short distances or high-momentum transfer ("asymptotic freedom"); it is strong at long distances ($\gtrsim$1 fm) or low energies, leading to the confinement of quarks into colorless objects, the hadrons. Consequently, QCD allows for a perturbative analysis at large energies, whereas it is highly nonperturbative in the low-energy regime. Nuclear physics resides at low energies and the force between nucleons is a residual color interaction similar to the van der Waals force between neutral molecules. Therefore, in terms of quarks and gluons, the nuclear force is a very complicated problem that, nevertheless, can be attacked with brute computing power on a discretized, Euclidean space-time lattice (known as lattice QCD). In a recent study [109], the neutron–proton scattering lengths in the singlet and triplet S waves have been determined in fully dynamical lattice QCD, with a smallest pion mass of 354 MeV. This result is then extrapolated to the physical pion mass with the help of chiral perturbation theory. The pion mass of 354 MeV is still too large to allow for reliable extrapolations, but the feasibility has been demonstrated and more progress can be expected for the near future. In a lattice calculation of a very different kind, the nucleon–nucleon (NN) potential was studied [110,111]. The *NN* potential is extracted from the equal-time Bethe–Salpeter amplitude with local interpolating operators for the nucleons. The central part of the potential shows a repulsive core plus attraction of intermediate range. This is a very promising result, but it must be noted that also in this investigation still rather large pion masses are being used. In any case, advanced lattice QCD calculations are under way and continuously improved. However, since these calculations are very time-consuming and

expensive, they can only be used to check a few representative key issues. For everyday nuclear structure physics, a more efficient approach is needed.

The efficient approach is an effective field theory. For the development of an EFT, it is crucial to identify a separation of scales. In the hadron spectrum, a large gap between the masses of the pions and the masses of the vector mesons, like $\rho(770)$ and $\omega(782)$, can clearly be identified. Thus, it is natural to assume that the pion mass sets the soft scale, $Q \sim m_\pi$, and the rho mass the hard scale, $\Lambda_\chi \sim m_\rho$, also known as the chiral symmetry breaking scale. This is suggestive of considering an expansion in terms of the soft scale over the hard scale, Q/Λ_χ. Concerning the relevant degrees of freedom, we noticed already that, for the ground state and the low-energy excitation spectrum of an atomic nucleus as well as for conventional nuclear reactions, quarks and gluons are ineffective degrees of freedom, while nucleons and pions are the appropriate ones. To make sure that this EFT is not just another phenomenology, it must have a firm link with QCD. The link is established by having the EFT observe all relevant symmetries of the underlying theory. This requirement is based upon a 'folk theorem' by Weinberg [32]:

> If one writes down the most general possible Lagrangian, including *all* terms consistent with assumed symmetry principles, and then calculates matrix elements with this Lagrangian to any given order of perturbation theory, the result will simply be the most general possible S-matrix consistent with analyticity, perturbative unitarity, cluster decomposition, and the assumed symmetry principles.

In summary, the EFT program consists of the following steps:

1. Identify the soft and hard scales, and the degrees of freedom appropriate for (low-energy) nuclear physics.
2. Identify the relevant symmetries of low-energy QCD and investigate if and how they are broken.
3. Construct the most general Lagrangian consistent with those symmetries and symmetry breakings.
4. Design an organizational scheme that can distinguish between more and less important contributions: a low-momentum expansion.
5. Guided by the expansion, calculate Feynman diagrams for the problem under consideration to the desired accuracy.

In the following (sub)sections, we will elaborate on these steps, one by one. Since we discussed the first step already, we will address now step two.

2.1. Symmetries of low-energy QCD

In this section, we will give a brief introduction into (low-energy) QCD, its symmetries and symmetry breakings. More detailed presentations of this topic are provided in Refs. [112–114].

2.1.1. Chiral symmetry

The QCD Lagrangian reads

$$\mathcal{L}_{\rm QCD} = \bar{q}(i\gamma^\mu \mathcal{D}_\mu - \mathcal{M})q - \frac{1}{4}\mathcal{G}_{\mu\nu,a}\mathcal{G}_a^{\mu\nu} \tag{2.1}$$

with the gauge-covariant derivative

$$\mathcal{D}_\mu = \partial_\mu - ig\frac{\lambda_a}{2}\mathcal{A}_{\mu,a} \tag{2.2}$$

and the gluon field strength tensor[2]

$$\mathcal{G}_{\mu\nu,a} = \partial_\mu \mathcal{A}_{\nu,a} - \partial_\nu \mathcal{A}_{\mu,a} + g f_{abc}\mathcal{A}_{\mu,b}\mathcal{A}_{\nu,c}. \tag{2.3}$$

In the above, q denotes the quark fields and $\mathcal{M}$ the quark mass matrix. Further, g is the strong coupling constant and $\mathcal{A}_{\mu,a}$ are the gluon fields. The λ_a are the Gell-Mann matrices and the f_{abc} the structure constants of the $SU(3)_{\rm color}$ Lie algebra ($a, b, c = 1, \ldots, 8$); summation over repeated indices is always implied. The gluon–gluon term in the last equation arises from the non-Abelian nature of the gauge theory and is the reason for the peculiar features of the color force.

The masses of the up (u), down (d), and strange (s) quarks are [115]:

$$m_u = 2.5 \pm 0.8 \text{ MeV}, \tag{2.4}$$

$$m_d = 5 \pm 0.9 \text{ MeV}, \tag{2.5}$$

$$m_s = 101 \pm 25 \text{ MeV}. \tag{2.6}$$

These masses are small as compared to a typical hadronic scale, i.e., a scale of low-mass hadrons which are not Goldstone bosons, e.g., $m_\rho = 0.78$ GeV ≈ 1 GeV.

[2] For $SU(N)$ group indices, we use Latin letters, $\ldots, a, b, c, \ldots, i, j, k, \ldots$, and, in general, do not distinguish between subscripts and superscripts.

It is therefore of interest to discuss the QCD Lagrangian in the limit of vanishing quark masses:

$$\mathcal{L}^0_{\rm QCD} = \bar{q} i\gamma^\mu \mathcal{D}_\mu q - \frac{1}{4}\mathcal{G}_{\mu\nu,a}\mathcal{G}^{\mu\nu}_a. \tag{2.7}$$

Defining right- and left-handed quark fields,

$$q_R = P_R q, \qquad q_L = P_L q, \tag{2.8}$$

with

$$P_R = \frac{1}{2}(1+\gamma_5), \qquad P_L = \frac{1}{2}(1-\gamma_5), \tag{2.9}$$

we can rewrite the Lagrangian as follows:

$$\mathcal{L}^0_{\rm QCD} = \bar{q}_R i\gamma^\mu \mathcal{D}_\mu q_R + \bar{q}_L i\gamma^\mu \mathcal{D}_\mu q_L - \frac{1}{4}\mathcal{G}_{\mu\nu,a}\mathcal{G}^{\mu\nu}_a. \tag{2.10}$$

Restricting ourselves now to up and down quarks, we see that $\mathcal{L}^0_{\rm QCD}$ is invariant under the global unitary transformations

$$q_R = \begin{pmatrix} u_R \\ d_R \end{pmatrix} \longmapsto g_R\, q_R = \exp\left(-i\Theta^R_i \frac{\tau_i}{2}\right)\begin{pmatrix} u_R \\ d_R \end{pmatrix} \tag{2.11}$$

and

$$q_L = \begin{pmatrix} u_L \\ d_L \end{pmatrix} \longmapsto g_L\, q_L = \exp\left(-i\Theta^L_i \frac{\tau_i}{2}\right)\begin{pmatrix} u_L \\ d_L \end{pmatrix}, \tag{2.12}$$

where τ_i ($i = 1, 2, 3$) are the generators of $SU(2)_{\rm flavor}$, the usual Pauli spin matrices with commutation relations

$$\left[\frac{\tau_i}{2}, \frac{\tau_j}{2}\right] = i\epsilon^{ijk}\frac{\tau_k}{2}, \tag{2.13}$$

and g_R and g_L are elements of $SU(2)_R$ and $SU(2)_L$, respectively. In conclusion: *The right- and left-handed components of massless quarks do not mix.* This is $SU(2)_R \times SU(2)_L$ symmetry, also known as *chiral symmetry*. Noether's Theorem implies the existence of six conserved currents; three right-handed currents

$$R^\mu_i = \bar{q}_R \gamma^\mu \frac{\tau_i}{2} q_R \quad \text{with } \partial_\mu R^\mu_i = 0 \tag{2.14}$$

and three left-handed currents

$$L^\mu_i = \bar{q}_L \gamma^\mu \frac{\tau_i}{2} q_L \quad \text{with } \partial_\mu L^\mu_i = 0. \tag{2.15}$$

It is useful to consider the following linear combinations; namely, three vector-currents

$$V^\mu_i = R^\mu_i + L^\mu_i = \bar{q}\gamma^\mu \frac{\tau_i}{2} q \quad \text{with } \partial_\mu V^\mu_i = 0 \tag{2.16}$$

and three axial-vector currents

$$A^\mu_i = R^\mu_i - L^\mu_i = \bar{q}\gamma^\mu\gamma_5 \frac{\tau_i}{2} q \quad \text{with } \partial_\mu A^\mu_i = 0, \tag{2.17}$$

which got their names from the fact that they transform under parity as vector and axial-vector current densities, respectively. The vector transformations are given by

$$q = \begin{pmatrix} u \\ d \end{pmatrix} \longmapsto \exp\left(-i\Theta^V_i \frac{\tau_i}{2}\right)\begin{pmatrix} u \\ d \end{pmatrix}, \tag{2.18}$$

which are isospin rotations and, therefore, invariance under vector transformations can be identified with isospin symmetry.

There are six conserved charges,

$$Q^R_i = \int d^3x\, R^0_i = \int d^3x\, q^\dagger_R(t,\vec{x})\frac{\tau_i}{2} q_R(t,\vec{x}) \quad \text{with } \frac{dQ^R_i}{dt} = 0 \tag{2.19}$$

and

$$Q^L_i = \int d^3x\, L^0_i = \int d^3x\, q^\dagger_L(t,\vec{x})\frac{\tau_i}{2} q_L(t,\vec{x}) \quad \text{with } \frac{dQ^L_i}{dt} = 0, \tag{2.20}$$

or, alternatively,

$$Q_i^V = \int d^3x\, V_i^0 = \int d^3x\, q^\dagger(t,\vec{x})\frac{\tau_i}{2}q(t,\vec{x}) \quad \text{with } \frac{dQ_i^V}{dt} = 0 \tag{2.21}$$

and

$$Q_i^A = \int d^3x\, A_i^0 = \int d^3x\, q^\dagger(t,\vec{x})\gamma_5\frac{\tau_i}{2}q(t,\vec{x}) \quad \text{with } \frac{dQ_i^A}{dt} = 0. \tag{2.22}$$

The Q_i^L and Q_i^R satisfy the commutation relations of the Lie algebra of $SU(2)_R \times SU(2)_L$ (chiral algebra),

$$\left[Q_i^R, Q_j^R\right] = i\epsilon^{ijk}Q_k^R, \qquad \left[Q_i^L, Q_j^L\right] = i\epsilon^{ijk}Q_k^L, \qquad \left[Q_i^R, Q_j^L\right] = 0. \tag{2.23}$$

For Q_i^V and Q_i^A, the commutation relations read,

$$\left[Q_i^V, Q_j^V\right] = i\epsilon^{ijk}Q_k^V, \qquad \left[Q_i^A, Q_j^A\right] = i\epsilon^{ijk}Q_k^V, \qquad \left[Q_i^V, Q_j^A\right] = i\epsilon^{ijk}Q_k^A. \tag{2.24}$$

For reasons of completeness, we mention that massless u and d quarks satisfy an even larger symmetry group, namely, $SU(2)_R \times SU(2)_L \times U(1)_V \times U(1)_A$. While the $U(1)_V$ symmetry corresponds to quark number conservation, the $U(1)_A$ is broken on the quantum level ("$U(1)_A$ anomaly") and is not a symmetry of the system.

2.1.2. Explicit symmetry breaking

The mass term $-\bar{q}\mathcal{M}q$ in the QCD Lagrangian Eq. (2.1) breaks chiral symmetry explicitly. To better see this, let us rewrite $\mathcal{M}$ for the two-flavor case,

$$\begin{aligned}\mathcal{M} &= \begin{pmatrix} m_u & 0 \\ 0 & m_d \end{pmatrix} \\ &= \frac{1}{2}(m_u + m_d)\begin{pmatrix} 1 & 0 \\ 0 & 1 \end{pmatrix} + \frac{1}{2}(m_u - m_d)\begin{pmatrix} 1 & 0 \\ 0 & -1 \end{pmatrix} \\ &= \frac{1}{2}(m_u + m_d)\, I + \frac{1}{2}(m_u - m_d)\, \tau_3. \end{aligned} \tag{2.25}$$

The first term in the last equation in invariant under $SU(2)_V$ (isospin symmetry) and the second term vanishes for $m_u = m_d$. Thus, isospin is an exact symmetry if $m_u = m_d$. However, both terms in Eq. (2.25) break chiral symmetry. Since the up and down quark masses [Eqs. (2.4) and (2.5)] are small as compared to the typical hadronic mass scale of $\sim$1 GeV, the explicit chiral symmetry breaking due to non-vanishing quark masses is very small. Note also that, as a consequence of the non-vanishing quark masses, the axial-vector current, Eq. (2.17), is not conserved anymore.

2.1.3. Spontaneous symmetry breaking

A (continuous) symmetry is said to be *spontaneously broken* if a symmetry of the Lagrangian is not realized in the ground state of the system. There is evidence that the (approximate) chiral symmetry of the QCD Lagrangian is spontaneously broken—for dynamical reasons of nonperturbative origin which are not fully understood at this time. The most plausible evidence comes from the hadron spectrum.

Since the conserved quantity Q_i^A, Eq. (2.22), commutes with the Hamiltonian and has negative parity, one naively expects the existence of degenerate hadron multiplets of opposite parity, i.e., for any hadron of positive parity one would expect a degenerate hadron state of negative parity and vice versa. However, these "parity doublets" are not observed in nature. For example, take the ρ meson which is a vector meson of negative parity ($J^P = 1^-$) and mass 776 MeV. There does exist a 1^+ meson, the a_1, but it has a mass of 1230 MeV and, therefore, cannot be perceived as degenerate with the ρ. On the other hand, the ρ meson comes in three charge states (equivalent to three isospin states), the $\rho^\pm$ and the ρ^0, with masses that differ by at most a few MeV. Thus, in the hadron spectrum, $SU(2)_V$ (isospin) symmetry is well observed, while axial symmetry is broken: $SU(2)_R \times SU(2)_L$ is broken down to $SU(2)_V$. As a consequence of this, the vacuum (QCD ground state) is invariant under vector transformations, i. e., $Q_i^V|0\rangle = 0$, while this is not the case for axial transformations, $Q_i^A|0\rangle \neq 0$, where $|0\rangle$ denotes the vacuum.

A spontaneously broken global symmetry implies the existence of (massless) Goldstone bosons with the quantum numbers of the broken generators [116,117]. The broken generators are the Q_i^A of Eq. (2.22) which are pseudoscalar. The Goldstone bosons are identified with the isospin triplet of the (pseudoscalar) pions, which explains why pions are so light. The pion masses are not exactly zero because the up and down quark masses are not exactly zero either (explicit symmetry breaking). Thus, pions are a truly remarkable species: they reflect spontaneous as well as explicit symmetry breaking. Goldstone bosons interact weakly at low energy. They are degenerate with the vacuum and, therefore, interactions between them must vanish at zero momentum and in the chiral limit ($m_\pi \to 0$).

2.2. Chiral effective Lagrangians

2.2.1. Relativistic formulation

The next step in our EFT program is to build the most general Lagrangian consistent with the (broken) symmetries discussed above. An elegant formalism for the construction of such Lagrangians was developed by Callan et al. (CCWZ) [40] who worked out the group-theoretical foundations of non-linear realizations of chiral symmetry.[3] It is characteristic for these non-linear realizations that, whenever functions of the Goldstone bosons appear in the Lagrangian, they are always accompanied with at least one space-time derivative. The Lagrangians given below are built upon the CCWZ formalism.

As discussed, the relevant degrees of freedom are pions (Goldstone bosons) and nucleons. Since the interactions of Goldstone bosons must vanish at zero momentum transfer and in the chiral limit ($m_\pi \to 0$), the low-energy expansion of the Lagrangian is arranged in powers of derivatives and pion masses. The hard scale is the chiral symmetry breaking scale, $\Lambda_\chi \approx 1$ GeV. Thus, the expansion is in terms of powers of Q/Λ_χ where Q is a (small) momentum or pion mass. This is chiral perturbation theory (ChPT).

The effective Lagrangian can formally be written as,

$$\mathcal{L}_{\rm eff} = \mathcal{L}_{\pi\pi} + \mathcal{L}_{\pi N} + \cdots, \tag{2.26}$$

where $\mathcal{L}_{\pi\pi}$ deals with the dynamics among pions, $\mathcal{L}_{\pi N}$ describes the interaction between pions and a nucleon, and the ellipsis stands for terms that involve pions and two or more nucleons. The individual Lagrangians are organized as follows:

$$\mathcal{L}_{\pi\pi} = \mathcal{L}^{(2)}_{\pi\pi} + \mathcal{L}^{(4)}_{\pi\pi} + \cdots \tag{2.27}$$

and

$$\mathcal{L}_{\pi N} = \mathcal{L}^{(1)}_{\pi N} + \mathcal{L}^{(2)}_{\pi N} + \mathcal{L}^{(3)}_{\pi N} + \cdots, \tag{2.28}$$

where the superscript refers to the number of derivatives or pion-mass insertions (chiral dimension) and the ellipsis stands for terms of higher dimensions.

To construct chiral Lagrangians, we introduce the following $SU(2)$ matrix U in flavor space which collects the Goldstone pion fields, $\boldsymbol{\pi}$:

$$U = 1 + \frac{i}{f_\pi}\boldsymbol{\tau}\cdot\boldsymbol{\pi} - \frac{1}{2f_\pi^2}\boldsymbol{\pi}^2 - \frac{i\alpha}{f_\pi^3}(\boldsymbol{\tau}\cdot\boldsymbol{\pi})^3 + \frac{8\alpha-1}{8f_\pi^4}\boldsymbol{\pi}^4 + \cdots, \tag{2.29}$$

where f_π denotes the pion decay constant. In this expansion, the coefficient of the term linear in the pion field $\boldsymbol{\pi}$ is fixed such as to produce the correct kinetic term in the $\pi\pi$ Lagrangian, below, and the coefficient of the quadratic term is chosen to satisfy the unitary condition $U^\dagger U = 1$, at second order in the pion field. However, the coefficient α of the third order is arbitrary because of our freedom of choice for the interpolating pion fields (constrained only by U unitary and $\det U = 1$). The coefficient of the fourth order is then dictated by the unitarity condition, $U^\dagger U = 1$, at fourth order. Note that (on-shell) observables must not depend on the choice for the pion fields or, in other words, they must not depend on the (unphysical) parameter α (and there are more such parameters as you continue to higher orders in the above expansion of U). Therefore, diagrams with vertices that involve three or four pions must always be grouped together such that the α dependence drops out. For more on this issue, see the calculation of the two-loop 2π and 3π contributions, below, where those vertices enter. Popular choices for the pion fields are the exponential parametrization $U = \exp(i\boldsymbol{\tau}\cdot\boldsymbol{\pi}/f_\pi)$ which corresponds to $\alpha = 1/6$ and the so-called sigma representation $U = (\sigma + i\boldsymbol{\tau}\cdot\boldsymbol{\pi})/f_\pi$ with $\sigma = \sqrt{f_\pi^2 - \boldsymbol{\pi}^2}$ which is equivalent to $\alpha = 0$.

The leading order (LO) $\pi\pi$ Lagrangian is now given by [48]

$$\mathcal{L}^{(2)}_{\pi\pi} = \frac{f_\pi^2}{4}\,{\rm tr}\left[\partial_\mu U \partial^\mu U^\dagger + m_\pi^2 (U + U^\dagger)\right], \tag{2.30}$$

where tr denotes the trace in flavor space and m_π is the pion mass. Since Goldstone bosons can interact only when they carry momentum, the interaction between pions comes in powers of $\partial_\mu U$. Only even powers are allowed because of Lorentz invariance. Note that the U field transforms under global chiral rotations via

$$U \longmapsto g_L\, U\, g_R^\dagger \tag{2.31}$$

with g_R and g_L elements of $SU(2)_R$ and $SU(2)_L$, respectively, cf. Eqs. (2.11) and (2.12). Since we consider global chiral rotations, g_R and g_L do not depend on space-time and, therefore, $\partial_\mu U$ transforms in the same way as U. Thus, the first term in Eq. (2.30) is clearly chiral invariant. The second term breaks chiral symmetry explicitly with the coefficient chosen such as to reproduce the correct mass term, which can be seen by inserting U and expanding in numbers of pion fields:

$$\mathcal{L}^{(2)}_{\pi\pi} = \frac{1}{2}\partial_\mu\boldsymbol{\pi}\cdot\partial^\mu\boldsymbol{\pi} - \frac{1}{2}m_\pi^2\boldsymbol{\pi}^2 \tag{2.32}$$

$$+ \frac{1-4\alpha}{2f_\pi^2}(\boldsymbol{\pi}\cdot\partial_\mu\boldsymbol{\pi})(\boldsymbol{\pi}\cdot\partial^\mu\boldsymbol{\pi}) - \frac{\alpha}{f_\pi^2}\boldsymbol{\pi}^2\partial_\mu\boldsymbol{\pi}\cdot\partial^\mu\boldsymbol{\pi} + \frac{8\alpha-1}{8f_\pi^2}m_\pi^2\boldsymbol{\pi}^4 + \mathcal{O}(\boldsymbol{\pi}^6), \tag{2.33}$$

where we dropped the constant term $f_\pi^2 m_\pi^2$, since it does not contribute to the dynamics.

[3] An accessible introduction into the rather involved CCWZ formalism can be found in Ref. [113].

Baryon fields can also be incorporated into the effective field theory in a chirally consistent manner. Gasser et al. [49] have derived the LO relativistic πN Lagrangian to be

$$\mathcal{L}^{(1)}_{\pi N} = \bar{\Psi}\left(i\gamma^\mu D_\mu - M_N + \frac{g_A}{2}\gamma^\mu\gamma_5 u_\mu\right)\Psi \tag{2.34}$$

with

$$D_\mu = \partial_\mu + \Gamma_\mu \tag{2.35}$$

the chirally covariant derivative which introduces the so-called chiral connection (an analogy to a gauge term)

$$\Gamma_\mu = \frac{1}{2}\left[\xi^\dagger, \partial_\mu\xi\right] = \frac{1}{2}\left(\xi^\dagger\partial_\mu\xi + \xi\partial_\mu\xi^\dagger\right) \tag{2.36}$$

$$= \frac{i}{4f_\pi^2}\boldsymbol{\tau}\cdot(\boldsymbol{\pi}\times\partial_\mu\boldsymbol{\pi}) + \mathcal{O}(\boldsymbol{\pi}^4), \tag{2.37}$$

representing a vector current that leads to a coupling of even numbers of pions with the nucleon. Besides this, the Lagrangian includes a coupling term which involves the axial-vector

$$u_\mu = i\left\{\xi^\dagger, \partial_\mu\xi\right\} = i\left(\xi^\dagger\partial_\mu\xi - \xi\partial_\mu\xi^\dagger\right) \tag{2.38}$$

$$= -\frac{1}{f_\pi}\boldsymbol{\tau}\cdot\partial_\mu\boldsymbol{\pi} + \frac{4\alpha-1}{2f_\pi^3}(\boldsymbol{\tau}\cdot\boldsymbol{\pi})(\boldsymbol{\pi}\cdot\partial_\mu\boldsymbol{\pi}) + \frac{\alpha}{f_\pi^3}\boldsymbol{\pi}^2(\boldsymbol{\tau}\cdot\partial_\mu\boldsymbol{\pi}) + \mathcal{O}(\boldsymbol{\pi}^5), \tag{2.39}$$

which couples an odd number of pions to the nucleon. The definition of ξ used in the above is

$$\xi = \sqrt{U} = 1 + \frac{i}{2f_\pi}\boldsymbol{\tau}\cdot\boldsymbol{\pi} - \frac{1}{8f_\pi^2}\boldsymbol{\pi}^2 - \frac{i(8\alpha-1)}{16f_\pi^3}(\boldsymbol{\tau}\cdot\boldsymbol{\pi})^3 + \cdots. \tag{2.40}$$

Note that $\xi\xi^\dagger = 1$; therefore, $\partial_\mu(\xi\xi^\dagger) = (\partial_\mu\xi)\xi^\dagger + \xi\partial_\mu\xi^\dagger = 0$, which is applied in Eqs. (2.36) and (2.38).

Thus, more explicitly, the LO relativistic πN Lagrangian, Eq. (2.34), reads

$$\mathcal{L}^{(1)}_{\pi N} = \bar{\Psi}\left(i\gamma^\mu\partial_\mu - M_N - \frac{1}{4f_\pi^2}\gamma^\mu\boldsymbol{\tau}\cdot(\boldsymbol{\pi}\times\partial_\mu\boldsymbol{\pi}) - \frac{g_A}{2f_\pi}\gamma^\mu\gamma_5\boldsymbol{\tau}\cdot\partial_\mu\boldsymbol{\pi} + \cdots\right)\Psi. \tag{2.41}$$

In this equation, Ψ is the relativistic four-component Dirac spinor field representing the nucleon, M_N denotes the nucleon mass and g_A the axial-vector coupling constant. Numerical values will be given later. The term proportional to $g_A/2f_\pi$ is the familiar axial-vector coupling of one pion to the nucleon, while the non-linear term proportional to $1/4f_\pi^2$ is known as the Weinberg–Tomozawa coupling (a 2π contact term) [37,38], which is crucial for π–N s-wave scattering at threshold.

2.2.2. Heavy baryon formalism

The relativistic treatment of baryons in chiral perturbation theory leads to problems. The reason for the problems is the fact that the time-derivative of a relativistic baryon field generates a factor $E \approx M$ (where M denotes the baryon mass) which is not small as compared to the chiral symmetry breaking scale $\Lambda_\chi \approx 1$ GeV; in fact, $M_N/\Lambda_\chi \approx 1$. Note also that the nucleon mass does not vanish in the chiral limit. The consequence of all this is that the one-to-one correspondence between the expansion in pion loops, on the one hand, and the expansion in terms of small external momenta and pion masses, on the other side, is destroyed [49,118,119].

A solution to these problems has been proposed by Jenkins and Manohar [120] using effective field theory techniques originally developed by Georgi [121] for the study of heavy quark systems. The basic idea is to treat the baryons as heavy static sources ("extreme nonrelativistic limit") such that the momentum transfer between baryons by pion exchange is small as compared to the baryon mass. The expansion is performed in terms of these small momenta over the baryon mass and has become known as heavy baryon (HB) chiral perturbation theory (HBChPT). We will now briefly sketch this approach.

The four-momentum of the heavy baryon is parametrized as

$$p^\mu = Mv^\mu + l^\mu \tag{2.42}$$

where v^μ is the four-velocity satisfying $v^2 = 1$ and l^μ is a small residual momentum, $v\cdot l \ll M$. Defining projection operators

$$P_v^\pm = \frac{1 \pm \gamma_\mu v^\mu}{2}, \qquad P_v^+ + P_v^- = 1, \tag{2.43}$$

we introduce the so-called velocity-dependent fields

$$N = e^{iMv\cdot x}P_v^+\Psi, \qquad h = e^{iMv\cdot x}P_v^-\Psi, \tag{2.44}$$

such that the relativistic four-component Dirac spinor field representing the baryon can be written as

$$\Psi = e^{-iMv\cdot x}(N + h). \tag{2.45}$$

The exponential factor in Eq. (2.44) eliminates the kinematical dependence on the baryon mass. To make the meaning of the fields N and h more transparent, consider a positive-energy plane wave solution of the Dirac equation

$$\psi_p(x) = u(\vec{p}, s)e^{-ip\cdot x}, \qquad u(\vec{p}, s) = \sqrt{\frac{E+M}{2M}}\begin{pmatrix} I \\ \dfrac{\vec{\sigma}\cdot\vec{p}}{E+M}\end{pmatrix}\chi_s, \tag{2.46}$$

where I is the two-dimensional identity matrix, $p^0 = E = \sqrt{\vec{p}^{\,2} + M^2}$, and χ_s a Pauli spinor describing the spin state of the baryon. Assuming for the four-velocity $v^\mu = (1, 0, 0, 0)$, which is what we have in the rest frame of the baryon, the explicit expressions for the wave function components N_p and h_p are

$$N_p = \sqrt{\frac{E+M}{2M}}\begin{pmatrix}\chi_s \\ 0\end{pmatrix}e^{-i(E-M)t+i\vec{p}\cdot\vec{x}} \longmapsto \begin{pmatrix}\chi_s \\ 0\end{pmatrix}e^{-i(E-M)t+i\vec{p}\cdot\vec{x}}, \tag{2.47}$$

$$h_p = \sqrt{\frac{E+M}{2M}}\begin{pmatrix} 0 \\ \dfrac{\vec{\sigma}\cdot\vec{p}}{E+M}\chi_s\end{pmatrix}e^{-i(E-M)t+i\vec{p}\cdot\vec{x}}, \tag{2.48}$$

where the 0 represents a column vector that consists of two zeros. The arrow indicates the properly normalized spinor at leading order. So, for $v^\mu = (1, 0, 0, 0)$, N_p represents the large/upper component and h_p the small/lower component of the Dirac wave function ψ_p. Note also that the energy of N_p and h_p is different from ψ_p; namely, they carry the small residual energy [cf. Eq. (2.42)]

$$l_0 = E - M \approx 0 + \frac{\vec{p}^{\,2}}{2M} + \cdots. \tag{2.49}$$

Thus, l_0 is zero in leading order and $\vec{p}^{\,2}/2M$ at next-to-leading order (NLO).

To derive the leading order heavy baryon Lagrangian, we start from the leading order relativistic one,

$$\mathcal{L}^{(1)}_{\pi N} = \bar{\Psi}\left(i\gamma^\mu D_\mu - M + \frac{g_A}{2}\gamma^\mu\gamma_5 u_\mu\right)\Psi, \tag{2.50}$$

and insert Eq. (2.45), assuming $v^\mu = (1, 0, 0, 0)$ for simplicity.[4] One immediate result is that the e^{-iMt} factor of Eq. (2.45) generates a term $\gamma_0 M$ which kills the troublesome baryon mass term $(-M)$ in the upper-component projection yielding

$$\mathcal{L}^{(1)}_{\pi N} = \bar{N}\left(i\gamma^\mu D_\mu + \frac{g_A}{2}\gamma^\mu\gamma_5 u_\mu\right)N + \cdots \tag{2.51}$$

where the ellipsis stands for additional expressions involving the lower-component field h. Since N contains only upper components, Eq. (2.51) collapses to

$$\widehat{\mathcal{L}}^{(1)}_{\pi N} = \bar{N}\left(iD_0 - \frac{g_A}{2}\,\vec{\sigma}\cdot\vec{u}\right)N \tag{2.52}$$

plus $1/M$ corrections which are generated by expressing h in terms of N via the equations of motion for N and h. The first such $1/M$ corrections are shown in Eq. (2.56), below.

Eq. (2.52) is the leading order πN Lagrangian in the HB formalism (as indicated by the hat). Expanding in numbers of pion fields, this Lagrangian reads

$$\begin{aligned}\widehat{\mathcal{L}}^{(1)}_{\pi N} = \bar{N}\Big\{ & i\partial_0 - \frac{1}{4f_\pi^2}\,\boldsymbol{\tau}\cdot(\boldsymbol{\pi}\times\partial_0\boldsymbol{\pi}) - \frac{g_A}{2f_\pi}\,\boldsymbol{\tau}\cdot(\vec{\sigma}\cdot\vec{\nabla})\boldsymbol{\pi} \\ & + \frac{g_A(4\alpha-1)}{4f_\pi^3}\,(\boldsymbol{\tau}\cdot\boldsymbol{\pi})\Big[\boldsymbol{\pi}\cdot(\vec{\sigma}\cdot\vec{\nabla})\boldsymbol{\pi}\Big] + \frac{g_A\alpha}{2f_\pi^3}\,\boldsymbol{\pi}^2\Big[\boldsymbol{\tau}\cdot(\vec{\sigma}\cdot\vec{\nabla})\boldsymbol{\pi}\Big]\Big\}N + \cdots\end{aligned} \tag{2.53}$$

where the ellipsis stands for terms involving four or more pions.

At dimension two, the relativistic πN Lagrangian reads

$$\mathcal{L}^{(2)}_{\pi N} = \sum_{i=1}^{4} c_i \bar{\Psi} O_i^{(2)} \Psi. \tag{2.54}$$

The various operators $O_i^{(2)}$ are given in Ref. [122]. The fundamental rule by which this Lagrangian – as well as all the other ones – are assembled is that they must contain *all* terms consistent with chiral symmetry and Lorentz invariance (apart from other trivial symmetries) at a given chiral dimension (here: order two). The parameters c_i are known as low-energy constants (LECs) and are determined empirically from fits to πN data.

[4] For a full-fledged derivation, see Ref. [113].

The HB projected πN Lagrangian at order two is most conveniently broken up into two pieces,

$$\widehat{\mathcal{L}}^{(2)}_{\pi N} = \widehat{\mathcal{L}}^{(2)}_{\pi N,\,\mathrm{fixed}} + \widehat{\mathcal{L}}^{(2)}_{\pi N,\,\mathrm{ct}}, \tag{2.55}$$

with

$$\begin{aligned}\widehat{\mathcal{L}}^{(2)}_{\pi N,\,\mathrm{fixed}} &= \bar N\left[\frac{1}{2M_N}\vec D\cdot\vec D + i\,\frac{g_A}{4M_N}\{\vec\sigma\cdot\vec D, u_0\}\right]N \\ &= \bar N\Big\{\frac{\vec\nabla^2}{2M_N} - \frac{ig_A}{4M_N f_\pi}\boldsymbol{\tau}\cdot\Big[\vec\sigma\cdot\Big(\overleftarrow{\nabla}\,\partial_0\boldsymbol{\pi} - \partial_0\boldsymbol{\pi}\,\overrightarrow{\nabla}\Big)\Big] \\ &\quad - \frac{i}{8M_N f_\pi^2}\boldsymbol{\tau}\cdot\Big[\overleftarrow{\nabla}\cdot(\boldsymbol{\pi}\times\vec\nabla\boldsymbol{\pi}) - (\boldsymbol{\pi}\times\vec\nabla\boldsymbol{\pi})\cdot\overrightarrow{\nabla}\Big]\Big\}N + \cdots\end{aligned} \tag{2.56}$$

and

$$\begin{aligned}\widehat{\mathcal{L}}^{(2)}_{\pi N,\,\mathrm{ct}} &= \bar N\left[2\,c_1\,m_\pi^2\,(U+U^\dagger) + \left(c_2 - \frac{g_A^2}{8M_N}\right)u_0^2 + c_3\,u_\mu u^\mu + \frac{i}{2}\left(c_4 + \frac{1}{4M_N}\right)\vec\sigma\cdot(\vec u\times\vec u)\right]N \\ &= \bar N\left[4c_1 m_\pi^2 - \frac{2c_1}{f_\pi^2}\,m_\pi^2\,\boldsymbol{\pi}^2 + \left(c_2 - \frac{g_A^2}{8M_N}\right)\frac{1}{f_\pi^2}(\partial_0\boldsymbol{\pi}\cdot\partial_0\boldsymbol{\pi}) + \frac{c_3}{f_\pi^2}\,(\partial_\mu\boldsymbol{\pi}\cdot\partial^\mu\boldsymbol{\pi})\right. \\ &\quad \left. - \left(c_4 + \frac{1}{4M_N}\right)\frac{1}{2f_\pi^2}\epsilon^{ijk}\epsilon^{abc}\sigma^i\tau^a(\partial^j\pi^b)(\partial^k\pi^c)\right]N + \ldots,\end{aligned} \tag{2.57}$$

where we neglected the isospin breaking c_5-term proportional to $(m_u - m_d)$; the ellipsis represents terms involving more pions.

Note that $\widehat{\mathcal{L}}^{(2)}_{\pi N,\,\mathrm{fixed}}$ is created entirely from the HB expansion of the relativistic $\mathcal{L}^{(1)}_{\pi N}$ and thus has no free parameters ("fixed"), while $\widehat{\mathcal{L}}^{(2)}_{\pi N,\,\mathrm{ct}}$ is made up by the new πN contact terms proportional to the c_i parameters (plus those $1/M_N$ corrections which happen to have the same mathematical structure as c_i terms).

At dimension three, the relativistic πN Lagrangian can be formally written as

$$\mathcal{L}^{(3)}_{\pi N} = \sum_{i=1}^{31} d_i\bar\Psi O_i^{(3)}\Psi, \tag{2.58}$$

with the operators, $O_i^{(3)}$, listed in Refs. [122,123]; not all 31 terms will be of interest here. The new LECs that occur at this order are the d_i. Similar to the order two case, the HB projected Lagrangian at order three can be broken into two pieces,

$$\widehat{\mathcal{L}}^{(3)}_{\pi N} = \widehat{\mathcal{L}}^{(3)}_{\pi N,\,\mathrm{fixed}} + \widehat{\mathcal{L}}^{(3)}_{\pi N,\,\mathrm{ct}}, \tag{2.59}$$

with $\widehat{\mathcal{L}}^{(3)}_{\pi N,\,\mathrm{fixed}}$ and $\widehat{\mathcal{L}}^{(3)}_{\pi N,\,\mathrm{ct}}$ given in Refs. [122,123].

2.3. Nucleon contact Lagrangians

Two-nucleon contact interactions consist of four-nucleon fields (four-nucleon legs) and no meson fields. Such terms are needed to renormalize loop integrals, to make results reasonably independent of regulators, and to parametrize the unresolved short-distance dynamics of the nuclear force. For more on the role of contact terms, see Section 4.3.

Because of parity, nucleon contact interactions come only in even powers of derivatives, thus,

$$\widehat{\mathcal{L}}_{NN} = \widehat{\mathcal{L}}^{(0)}_{NN} + \widehat{\mathcal{L}}^{(2)}_{NN} + \widehat{\mathcal{L}}^{(4)}_{NN} + \cdots. \tag{2.60}$$

The lowest order (or leading order) NN Lagrangian has no derivatives and reads [50,51]

$$\widehat{\mathcal{L}}^{(0)}_{NN} = -\frac{1}{2}C_S\bar N N\bar N N - \frac{1}{2}C_T(\bar N\vec\sigma N)\cdot(\bar N\vec\sigma N), \tag{2.61}$$

where N is the heavy baryon nucleon field ($\bar N = N^\dagger$). C_S and C_T are unknown constants which are determined by a fit to the NN data. The second order NN Lagrangian can be stated as follows [54]

$$\begin{aligned}\widehat{\mathcal{L}}^{(2)}_{NN} &= -C_1'\left[(\bar N\vec\nabla N)^2 + (\overline{\vec\nabla N}N)^2\right] - C_2'(\bar N\vec\nabla N)\cdot(\overline{\vec\nabla N}N) - C_3'\bar N N\left[\bar N\vec\nabla^2 N + \overline{\vec\nabla^2 N}N\right] \\ &\quad - iC_4'\left[\bar N\vec\nabla N\cdot(\overline{\vec\nabla N}\times\vec\sigma N) + \overline{(\vec\nabla N)}N\cdot(\bar N\vec\sigma\times\vec\nabla N)\right] \\ &\quad - iC_5'\bar N N(\overline{\vec\nabla N}\cdot\vec\sigma\times\vec\nabla N) - iC_6'(\bar N\vec\sigma N)\cdot(\overline{\vec\nabla N}\times\vec\nabla N)\end{aligned}$$

$$
\begin{aligned}
&- \left(C_7'\delta_{ik}\delta_{jl} + C_8'\delta_{il}\delta_{kj} + C_9'\delta_{ij}\delta_{kl}\right)\left[\bar{N}\sigma_k\partial_i N\bar{N}\sigma_l\partial_j N + \overline{\partial_i N}\sigma_k N\overline{\partial_j N}\sigma_l N\right] \\
&- \left(C_{10}'\delta_{ik}\delta_{jl} + C_{11}'\delta_{il}\delta_{kj} + C_{12}'\delta_{ij}\delta_{kl}\right)\bar{N}\sigma_k\partial_i N\overline{\partial_j N}\sigma_l N \\
&- \left(\frac{1}{2}C_{13}'(\delta_{ik}\delta_{jl} + \delta_{il}\delta_{kj}) + C_{14}'\delta_{ij}\delta_{kl}\right)\left[\overline{\partial_i N}\sigma_k\partial_j N + \overline{\partial_j N}\sigma_k\partial_i N\right]\bar{N}\sigma_l N. \qquad (2.62)
\end{aligned}
$$

For a thorough discussion of second order contact Lagrangians, see Refs. [124,125].

Similar to C_S and C_T of Eq. (2.61), the C_i' of Eq. (2.62) are unknown constants which are fixed in a fit to the *NN* data. Obviously, these contact Lagrangians blow up quite a bit with increasing order, which is why we do not give $\widehat{\mathcal{L}}_{NN}^{(4)}$ explicitly here. The *NN* contact potentials that emerge from these Lagrangians are given in Section 4.3.

Besides the above contact Lagrangians involving two nucleons, there exist contact interactions among three or more nucleons representing nuclear many-body forces (cf. last term of Eq. (2.66), below, and Section 5).

2.4. Summary: effective Lagrangians organized by interaction index Δ

To summarize, the effective Lagrangian needed to derive nuclear forces includes the following parts:

$$\mathcal{L}_{\rm eff} = \mathcal{L}_{\pi\pi} + \mathcal{L}_{\pi N} + \mathcal{L}_{NN} + \cdots, \qquad (2.63)$$

where the ellipsis stands for terms that involve two nucleons plus pions and three or more nucleons with or without pions, relevant for nuclear many-body forces (cf. last two terms of Eq. (2.66), below, and Section 5).

In previous sections, we organized the Lagrangians by the number of derivatives or pion-mass insertions. This is the standard way, appropriate particularly for considerations of π–π and π–N scattering. As it turns out (cf. Section 3.1), for interactions among nucleons, it is sometimes useful to also consider the so-called index of the interaction,

$$\Delta \equiv d + \frac{n}{2} - 2, \qquad (2.64)$$

where d is the number of derivatives or pion-mass insertions and n the number of nucleon field operators (nucleon legs). We will now rewrite the HB Lagrangian in terms of increasing values of the parameter Δ.

The leading order Lagrangian reads,

$$
\begin{aligned}
\widehat{\mathcal{L}}^{\Delta=0} &= \frac{1}{2}\partial_\mu\boldsymbol{\pi}\cdot\partial^\mu\boldsymbol{\pi} - \frac{1}{2}m_\pi^2\boldsymbol{\pi}^2 + \frac{1-4\alpha}{2f_\pi^2}(\boldsymbol{\pi}\cdot\partial_\mu\boldsymbol{\pi})(\boldsymbol{\pi}\cdot\partial^\mu\boldsymbol{\pi}) - \frac{\alpha}{f_\pi^2}\boldsymbol{\pi}^2\partial_\mu\boldsymbol{\pi}\cdot\partial^\mu\boldsymbol{\pi} + \frac{8\alpha-1}{8f_\pi^2}m_\pi^2\boldsymbol{\pi}^4 \\
&+ \bar{N}\left[i\partial_0 - \frac{g_A}{2f_\pi}\,\boldsymbol{\tau}\cdot(\vec{\sigma}\cdot\vec{\nabla})\boldsymbol{\pi} - \frac{1}{4f_\pi^2}\,\boldsymbol{\tau}\cdot(\boldsymbol{\pi}\times\partial_0\boldsymbol{\pi})\right]N \\
&+ \bar{N}\left\{\frac{g_A(4\alpha-1)}{4f_\pi^3}\,(\boldsymbol{\tau}\cdot\boldsymbol{\pi})\left[\boldsymbol{\pi}\cdot(\vec{\sigma}\cdot\vec{\nabla})\boldsymbol{\pi}\right] + \frac{g_A\alpha}{2f_\pi^3}\,\boldsymbol{\pi}^2\left[\boldsymbol{\tau}\cdot(\vec{\sigma}\cdot\vec{\nabla})\boldsymbol{\pi}\right]\right\}N \\
&- \frac{1}{2}C_S\bar{N}N\bar{N}N - \frac{1}{2}C_T(\bar{N}\vec{\sigma}N)\cdot(\bar{N}\vec{\sigma}N) + \cdots, \qquad (2.65)
\end{aligned}
$$

and subleading Lagrangians are,

$$
\begin{aligned}
\widehat{\mathcal{L}}^{\Delta=1} &= \bar{N}\left\{\frac{\vec{\nabla}^2}{2M_N} - \frac{ig_A}{4M_Nf_\pi}\boldsymbol{\tau}\cdot\left[\vec{\sigma}\cdot\left(\overleftarrow{\nabla}\,\partial_0\boldsymbol{\pi} - \partial_0\boldsymbol{\pi}\,\overrightarrow{\nabla}\right)\right] - \frac{i}{8M_Nf_\pi^2}\boldsymbol{\tau}\cdot\left[\overleftarrow{\nabla}\cdot(\boldsymbol{\pi}\times\vec{\nabla}\boldsymbol{\pi}) - (\boldsymbol{\pi}\times\overleftarrow{\nabla}\boldsymbol{\pi})\cdot\overrightarrow{\nabla}\right]\right\}N \\
&+ \bar{N}\left[4c_1m_\pi^2 - \frac{2c_1}{f_\pi^2}\,m_\pi^2\,\boldsymbol{\pi}^2 + \left(c_2 - \frac{g_A^2}{8M_N}\right)\frac{1}{f_\pi^2}(\partial_0\boldsymbol{\pi}\cdot\partial_0\boldsymbol{\pi})\right. \\
&\left. + \frac{c_3}{f_\pi^2}\,(\partial_\mu\boldsymbol{\pi}\cdot\partial^\mu\boldsymbol{\pi}) - \left(c_4 + \frac{1}{4M_N}\right)\frac{1}{2f_\pi^2}\epsilon^{ijk}\epsilon^{abc}\sigma^i\tau^a(\partial^j\pi^b)(\partial^k\pi^c)\right]N \\
&- \frac{D}{4f_\pi}(\bar{N}N)\bar{N}\left[\boldsymbol{\tau}\cdot(\vec{\sigma}\cdot\vec{\nabla})\boldsymbol{\pi}\right]N - \frac{1}{2}E(\bar{N}N)(\bar{N}\boldsymbol{\tau}N)\cdot(\bar{N}\boldsymbol{\tau}N) + \cdots, \qquad (2.66) \\
\widehat{\mathcal{L}}^{\Delta=2} &= \mathcal{L}_{\pi\pi}^{(4)} + \widehat{\mathcal{L}}_{\pi N}^{(3)} + \widehat{\mathcal{L}}_{NN}^{(2)} + \cdots, \qquad (2.67) \\
\widehat{\mathcal{L}}^{\Delta=4} &= \widehat{\mathcal{L}}_{NN}^{(4)} + \cdots, \qquad (2.68)
\end{aligned}
$$

where the ellipses represent terms that are irrelevant for the derivation of nuclear forces up to fourth order.

3. Nuclear forces from EFT: overview

In the beginning of Section 2, we listed the steps we have to take for carrying out the EFT program of a derivation of nuclear forces. So far, we discussed steps one to three. What is left are steps four (low-momentum expansion) and five (Feynman diagrams). In this section, we will say more about the expansion we are using and give an overview of the Feynman diagrams that arise order by order.

3.1. Chiral perturbation theory and power counting

Effective Lagrangians have infinitely many terms, and an unlimited number of Feynman graphs can be calculated from them. Therefore, we need a scheme that makes the theory manageable and calculable. This scheme which tells us how to distinguish between large (important) and small (unimportant) contributions is chiral perturbation theory (ChPT).

In ChPT, graphs are analyzed in terms of powers of small external momenta over the large scale: $(Q/\Lambda_\chi)^\nu$, where Q is generic for a momentum (nucleon three-momentum or pion four-momentum) or a pion mass and $\Lambda_\chi \sim 1$ GeV is the chiral symmetry breaking scale (hadronic scale, hard scale). Determining the power ν has become known as power counting.

For the moment, we will consider only so-called irreducible graphs; the problem of reducible or iterative diagrams and their relevance for the *NN* system will be discussed later (cf. Section 4.5). By definition, an irreducible graph is a diagram that cannot be separated into two by cutting only nucleon lines. Following the Feynman rules of covariant perturbation theory, a nucleon propagator is Q^{-1}, a pion propagator Q^{-2}, each derivative in any interaction is Q, and each four-momentum integration Q^4. This is also known as naive dimensional analysis. Applying then some topological identities, Weinberg obtained for the power of an irreducible diagram involving A nucleons [50–52]

$$\nu_W = 4 - A - 2C + 2L + \sum_i \Delta_i \tag{3.1}$$

with

$$\Delta_i \equiv d_i + \frac{n_i}{2} - 2, \tag{3.2}$$

where C denotes the number of separately connected pieces and L the number of loops in the diagram; d_i is the number of derivatives or pion-mass insertions and n_i the number of nucleon fields (nucleon legs) involved in vertex i; the sum runs over all vertices i contained in the diagram under consideration. Note that $\Delta_i \geq 0$ for all interactions allowed by chiral symmetry. Purely pionic interactions have at least two derivatives ($d_i \geq 2$, $n_i = 0$); interactions of pions with a nucleon have at least one derivative ($d_i \geq 1$, $n_i = 2$); and nucleon–nucleon contact terms ($n_i = 4$) have $d_i \geq 0$. This demonstrates how chiral symmetry guarantees a low-energy expansion.

The Weinberg formula, Eq. (3.1) works well for connected diagrams with $A \leq 2$ nucleons and any number of pions, but there are problems when applied in systems with $A \geq 3$.

To illustrate the problem, consider one-pion exchange ($L = 0$, $\Delta_i = 0$) between two nucleons in an $A = 2$ system ($C = 1$) which yields $\nu_W = 0$. Now, when the same interaction occurs in an $A = 3$ environment, then $C = 2$, since one nucleon is not interacting, and Eq. (3.1) produces $\nu_W = -3$. The reason for this result is that, by widespread convention [115], particle states are normalized to Dirac δ-functions,

$$\langle p'|p\rangle = \delta^3(\vec{p} - \vec{p}\,'), \tag{3.3}$$

which carry dimension Q^{-3}. A nucleon line passing through a diagram without interaction is represented by such a three-momentum-conserving δ-function.

The above-illustrated A dependence of the power ν_W is undesirable. As indicated, the reason for the problem is the dimension (-3) introduced for each nucleon through the normalization equation (3.3). Therefore, to fix the problem, we add $(+3A)$ to Eq. (3.1) and subtract 6 to have the $A = 2$ case unaltered. Thus, we introduce the new power $\nu = \nu_W + 3A - 6$, which reads explicitly,

$$\nu = -2 + 2A - 2C + 2L + \sum_i \Delta_i. \tag{3.4}$$

This definition of the power ν will be applied throughout this report. It is also what is used in other works [107]. Another way to get the formula, Eq. (3.4) is to define ν as the difference between ν_W and the smallest possible power, $\nu_{\min}$: $\nu = \nu_W - \nu_{\min}$. The minimal power $\nu_{\min}$ is obtained from Eq. (3.1) for the case of no loops ($L = 0$), $\Delta_i = 0$ for all vertices, and the maximal number of separately connected pieces, which is $C = A - 1$ if at least two nucleons interact; thus, $\nu_{\min} = 6 - 3A$.

Notice that, even though A still appears in Eq. (3.4), the formula is essentially A independent: when a non-interacting nucleon is added, A and C go up by one, which cancels. From the above derivation, it should also be clear that Eq. (3.4) is suitable only for systems with $A \geq 2$ nucleons while Eq. (3.1) may be used for connected graphs with $A \leq 2$.

An alternative method for developing a reasonable power formula has been presented by Friar [126], who considers the expectation value of an m-nucleon operator ($m \leq A$) in A-nucleon space. Working in configuration space generates

additional phase-space factors of power $3(A-1)$ to be added to Eq. (3.1). Thus, Friar's power is $\nu_F = \nu_W + 3A - 3 = \nu + 3$. The additional power of three by which Friar differs from Eq. (3.4) is due to an additional momentum-space integration that converts the units of a momentum-space potential into units of energy, which is reasonable. Finally, we note that normalizing the nucleon states in a box to a Kronecker-δ (instead of using the Dirac δ-function normalization of the continuum) should lead to Eq. (3.4) in a straightforward fashion.

In any case, the most important observation from power counting is that the powers are bounded from below and, specifically, $\nu \geq 0$. This fact is crucial for the convergence of the low-momentum expansion.

Moreover, the power formula, Eq. (3.4) allows to predict the leading orders of connected multi-nucleon forces. Consider a m-nucleon irreducibly connected diagram (m-nucleon force) in an A-nucleon system ($m \leq A$). The number of separately connected pieces is $C = A - m + 1$. Inserting this into Eq. (3.4) together with $L = 0$ and $\sum_i \Delta_i = 0$ yields $\nu = 2m - 4$. Thus, two-nucleon forces ($m = 2$) start at $\nu = 0$, three-nucleon forces ($m = 3$) at $\nu = 2$ (but they happen to cancel at that order), and four-nucleon forces at $\nu = 4$ (they do not cancel). More about this in the next subsection and Section 5.

For later purposes, we note that for an irreducible NN diagram ($A = 2$, $C = 1$), the power formula collapses to the very simple expression

$$\nu = 2L + \sum_i \Delta_i. \tag{3.5}$$

In summary, the chief point of the ChPT expansion is that, at a given order ν, there exists only a finite number of graphs. This is what makes the theory calculable. The expression $(Q/\Lambda_\chi)^{\nu+1}$ provides a rough estimate of the relative size of the contributions left out and, thus, of the accuracy at order ν. In this sense, the theory can be calculated to any desired accuracy and has predictive power.

3.2. The hierarchy of nuclear forces

Chiral perturbation theory and power counting imply that nuclear forces emerge as a hierarchy controlled by the power ν, Fig. 1.

In lowest order, better known as leading order (LO, $\nu = 0$), the NN amplitude is made up by two momentum-independent contact terms ($\sim Q^0$), represented by the four-nucleon-leg graph with a small-dot vertex shown in the first row of Fig. 1, and static one-pion exchange (1PE), second diagram in the first row of the figure. This is, of course, a rather crude approximation to the two-nucleon force (2NF), but accounts already for some important features. The 1PE provides the tensor force, necessary to describe the deuteron, and it explains NN scattering in peripheral partial waves of very high orbital angular momentum. At this order, the two contacts which contribute only in S waves provide the short- and intermediate-range interaction which is somewhat crude.

In the next order, $\nu = 1$, all contributions vanish due to parity and time-reversal invariance.

Therefore, the next-to-leading order (NLO) is $\nu = 2$. Two-pion exchange (2PE) occurs for the first time ("leading 2PE") and, thus, the creation of a more sophisticated description of the intermediate-range interaction is starting here. Since the loop involved in each pion diagram implies already $\nu = 2$ [cf. Eq. (3.5)], the vertices must have $\Delta_i = 0$. Therefore, at this order, only the lowest order πNN and $\pi\pi NN$ vertices are allowed which is why the leading 2PE is rather weak. Furthermore, there are seven contact terms of $\mathcal{O}(Q^2)$, shown by the four-nucleon-leg graph with a solid square, which contribute in S and P waves. The operator structure of these contacts include a spin–orbit term besides central, spin–spin, and tensor terms. Thus, essentially all spin–isospin structures necessary to describe the two-nucleon force phenomenologically have been generated at this order. The main deficiency at this stage of development is an insufficient intermediate-range attraction.

This problem is finally fixed at order three ($\nu = 3$), next-to-next-to-leading order (NNLO). The 2PE involves now the two derivative $\pi\pi NN$ seagull vertices (proportional to the c_i LECs) denoted by a large solid dot in Fig. 1. These vertices represent correlated 2PE as well as intermediate $\Delta(1232)$-isobar contributions. It is well known from the meson phenomenology of nuclear forces [18,20] that these two contributions are crucial for a realistic and quantitative 2PE model. Consequently, the 2PE now assumes a realistic size and describes the intermediate-range attraction of the nuclear force about right. Moreover, first relativistic corrections come into play at this order. There are no new contacts.

The reason why we talk of a hierarchy of nuclear forces is that two- and many-nucleon forces are created on an equal footing and emerge in increasing number as we go to higher and higher orders. At NNLO, the first set of non-vanishing three-nucleon forces (3NF) occur [70,71], cf. column '3N Force' of Fig. 1. In fact, at the previous order, NLO, irreducible 3N graphs appear already, however, it has been shown by Weinberg [52] and others [70,127,128] that these diagrams all cancel. Since non-vanishing 3NF contributions happen first at order $(Q/\Lambda_\chi)^3$, they are very weak as compared to 2NF which start at $(Q/\Lambda_\chi)^0$.

More 2PE is produced at $\nu = 4$, next-to-next-to-next-to-leading order (N^3LO), of which we show only a few symbolic diagrams in Fig. 1. Two-loop 2PE graphs show up for the first time and so does three-pion exchange (3PE) which necessarily involves two loops. 3PE was found to be negligible at this order [57,58]. Most importantly, 15 new contact terms $\sim Q^4$ arise and are represented by the four-nucleon-leg graph with a solid diamond. They include a quadratic spin–orbit term and contribute up to D waves. Mainly due to the increased number of contact terms, a quantitative description of the two-nucleon interaction up to about 300 MeV lab. energy is possible, at N^3LO (for details, see below). Besides further 3NF, four-nucleon

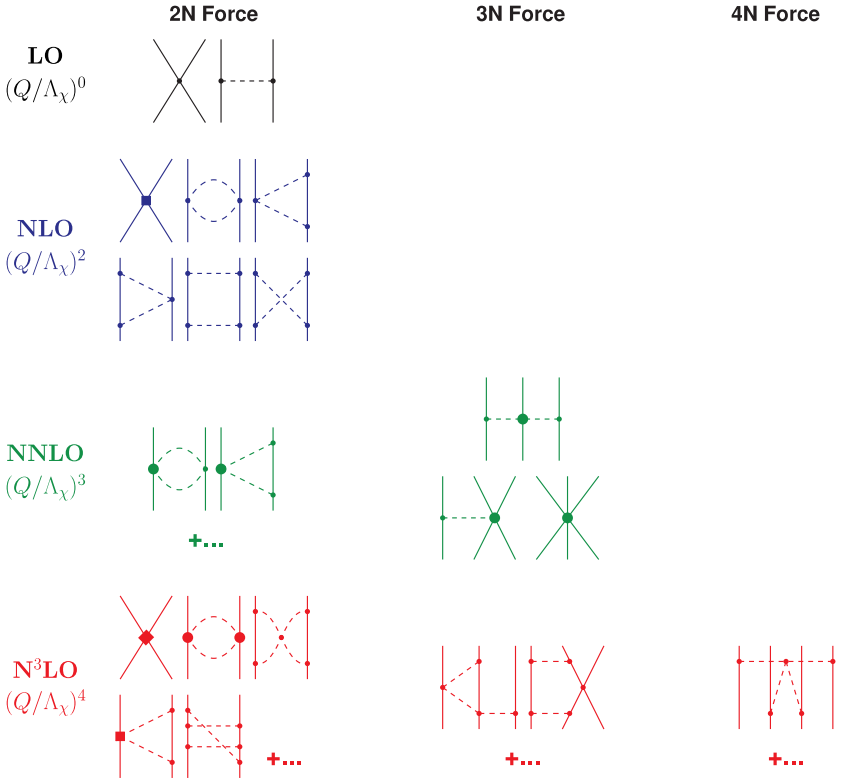

Fig. 1. Hierarchy of nuclear forces in ChPT. Solid lines represent nucleons and dashed lines pions. Small dots, large solid dots, solid squares, and solid diamonds denote vertices of index $\Delta = 0, 1, 2$, and 4, respectively. Further explanations are given in the text.

forces (4NF) start at this order. Since the leading 4NF come into existence one order higher than the leading 3NF, 4NF are weaker than 3NF. Thus, ChPT provides a straightforward explanation for the empirically known fact that 2NF $\gg$ 3NF $\gg$ 4NF ....

4. Two-nucleon interactions

The last section was just an overview. In this section, we will fill in all the details involved in the ChPT development of the *NN* interaction; and 3NF and 4NF will be discussed in Section 5. We start by talking about the various pion-exchange contributions.

4.1. Pion-exchange contributions in ChPT

Based upon the effective pion Lagrangians of Section 2.2, we will now derive the pion-exchange contributions to the *NN* interaction order by order.

As noted before, there are infinitely many pion-exchange contributions to the *NN* interaction and, thus, we need to get organized. First, we arrange the various pion-exchange contributions according to the number of pions being exchanged between the two nucleons:

$$V_\pi = V_{1\pi} + V_{2\pi} + V_{3\pi} + \cdots, \tag{4.1}$$

where the meaning of the subscripts is obvious and the ellipsis represents 4π and higher pion exchanges. Second, for each of the above terms, we assume a low-momentum expansion:

$$V_{1\pi} = V_{1\pi}^{(0)} + V_{1\pi}^{(2)} + V_{1\pi}^{(3)} + V_{1\pi}^{(4)} + \cdots \tag{4.2}$$

$$V_{2\pi} = V_{2\pi}^{(2)} + V_{2\pi}^{(3)} + V_{2\pi}^{(4)} + \cdots \tag{4.3}$$

$$V_{3\pi} = V_{3\pi}^{(4)} + \cdots, \tag{4.4}$$

where the superscript denotes the order ν and the ellipses stand for contributions of fifth and higher orders. Due to parity and time reversal, there are no first order contributions. Moreover, since n pions create $L = n - 1$ loops, the leading order for n-pion exchange occurs at $\nu = 2n - 2$ [cf. Eq. (3.5)].

In the following subsections, we will discuss $V_{1\pi}$, $V_{2\pi}$, and $V_{3\pi}$, one by one and order by order.

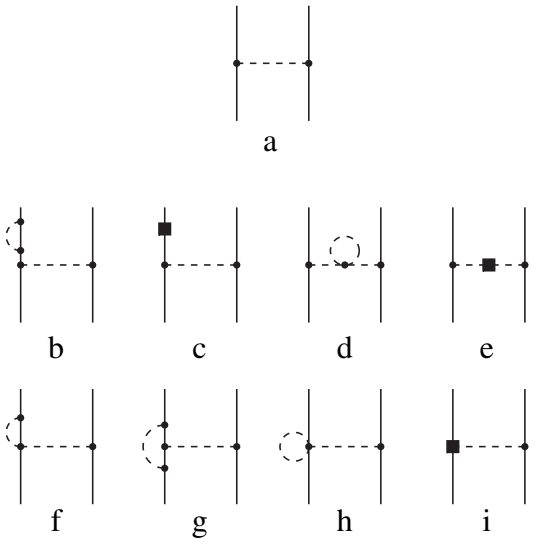

Fig. 2. One-pion-exchange contributions. Diagram (a) represents the leading order, while graphs (b)–(i) contribute to renormalization. Notation as in Fig. 1. Diagrams that result from interchange of nucleon lines and/or time reversal are not shown.

4.1.1. One-pion exchange

One-pion-exchange (1PE) diagrams are shown in Fig. 2. At leading order (LO, $\nu = 0$), we have the well-known static 1PE, diagram (a) of Fig. 2, which is given by [for notation, see Eq. (4.8) below]:

$$V_{1\pi}(\vec{p}\,', \vec{p}) = -\frac{g_A^2}{4f_\pi^2}\boldsymbol{\tau}_1 \cdot \boldsymbol{\tau}_2 \frac{\vec{\sigma}_1 \cdot \vec{q}\ \vec{\sigma}_2 \cdot \vec{q}}{q^2 + m_\pi^2}. \tag{4.5}$$

On-shell and in the center-of-mass system (CMS), there are no relativistic corrections at any order. Off-shell corrections come into play when the relativistic 1PE is iterated, i.e., in four-dimensional planar box diagrams. These corrections will be taken into account in the evaluation of those box diagrams up to the given order (see below).

At second order (NLO), the 1PE gets renormalized due to one-loop graphs and counterterm insertions, shown in the second and third row of Fig. 2. Graphs (b) and (c) renormalize the nucleon and graphs (d) and (e) the pion lines. Diagrams (f)–(i) renormalize the pion–nucleon coupling. In the one-loop graphs, all vertices are from the leading order Lagrangian $\widehat{\mathcal{L}}^{\Delta=0}$, Eq. (2.65), while counterterm insertions stem from $\widehat{\mathcal{L}}^{\Delta=2}$. Note that graph (f) vanishes because it involves an odd power of the loop momentum that is integrated over. In graph (i), the solid square includes the d_{18}-vertex from $\widehat{\mathcal{L}}^{(3)}_{\pi N}$ [which is part of $\widehat{\mathcal{L}}^{\Delta=2}$, Eq. (2.67)]. This correction, which is known as the Goldberger–Treiman discrepancy, can be taken care of by replacing

$$g_A \longrightarrow g_A - 2d_{18}m_\pi^2. \tag{4.6}$$

For more details on the NLO corrections to the 1PE see Ref. [129]. At NNLO, there are further one-loop corrections, but with one subleading vertex, which renormalize g_A.

Finally, at N^{3}LO, there are two-loop corrections with leading vertices only, as well as one-loop and tree diagrams including (sub-)subleading vertices. It has been shown [55,57] that these contributions renormalize various LECs and the pion mass m_π, but do not generate any πN form-factor-like functions. Furthermore, a correction to the Goldberger–Treiman discrepancy arises at N^{3}LO.

We use $g_A = 1.290$ (instead of $g_A = 1.276$ [130]) to account for the Goldberger–Treiman discrepancy. Via the Goldberger–Treiman relation, $g_{\pi NN} = g_A M_N/f_\pi$, our value for g_A together with $f_\pi = 92.4$ MeV and $M_N = 938.918$ MeV implies $g^2_{\pi NN}/4\pi = 13.67$ which is consistent with the empirical value $g^2_{\pi NN}/4\pi = 13.65 \pm 0.08$ obtained from πN and NN data analysis [131,132]. The renormalizations of f_π, m_π, and M_N are taken care of by working with their physical vales.

In summary, the familiar expression for 1PE, Eq. (4.5), is appropriate to at least fourth order.

4.1.2. Two-pion exchange

The exchange of two or more pions always involves loop diagrams, which implies that we are faced with a non-trivial problem. To conduct such calculations, a scheme of field-theoretic perturbation theory as well as regularization and renormalization methods for dealing with divergent loop integrals must be adopted. Ordóñez et al. [53,54], who were the first to calculate chiral 2π-exchange to NNLO, used time-ordered perturbation theory and a Gaussian cutoff function for regularization. The Juelich group [107] developed a method involving unitary transformations (to get rid of the energy dependence of time-ordered perturbation theory) and applied so-called spectral function regularization. Both, the Brazil [62,63] and the

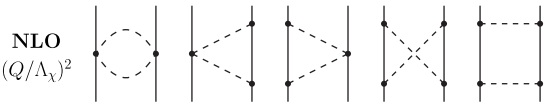

Fig. 3. Leading two-pion-exchange contributions to the *NN* interaction. Notation as in Fig. 1.

Munich [55,60,61] groups use covariant perturbation theory and dimensional regularization, but nevertheless, their works differ substantially in detail. We will follow here the method chosen by the Munich group since we believe it to be the most efficient and elegant one. In this approach, one starts with the relativistic versions of the πN Lagrangians (cf. Section 2.2) and sets up four-dimensional (covariant) loop integrals. Relativistic vertices and nucleon propagators are then expanded in powers of $1/M_N$. The divergences that occur in conjunction with the four-dimensional loop integrals are treated by means of dimensional regularization, a prescription which is consistent with chiral symmetry and power counting. The results derived in this way are the same obtained when starting right away with the HB versions of the πN Lagrangians. However, as it turns out, the method used by the Munich group is more efficient in dealing with the rather tedious calculations and particularly useful in conjunction with the planar box diagram. To give the reader a taste of the rather involved calculations, we present in Appendix B the explicit evaluation of the NLO diagrams shown in Fig. 3.

The results will be stated in terms of contributions to the momentum-space *NN* amplitude in the CMS, which takes the general form

$$\begin{aligned} V(\vec{p}\,',\vec{p}) &= V_C + \boldsymbol{\tau}_1\cdot\boldsymbol{\tau}_2\, W_C + [\, V_S + \boldsymbol{\tau}_1\cdot\boldsymbol{\tau}_2\, W_S\,]\,\vec{\sigma}_1\cdot\vec{\sigma}_2 + [\, V_{LS} + \boldsymbol{\tau}_1\cdot\boldsymbol{\tau}_2\, W_{LS}\,]\,(-i\vec{S}\cdot(\vec{q}\times\vec{k})) \\ &\quad + [V_T + \boldsymbol{\tau}_1\cdot\boldsymbol{\tau}_2\, W_T\,]\,\vec{\sigma}_1\cdot\vec{q}\,\vec{\sigma}_2\cdot\vec{q} + [\, V_{\sigma L} + \boldsymbol{\tau}_1\cdot\boldsymbol{\tau}_2\, W_{\sigma L}\,]\,\vec{\sigma}_1\cdot(\vec{q}\times\vec{k})\vec{\sigma}_2\cdot(\vec{q}\times\vec{k}), \end{aligned} \tag{4.7}$$

where $\vec{p}\,'$ and $\vec{p}$ denote the final and initial nucleon momenta in the CMS, respectively; moreover,

$$\begin{aligned} &\vec{q} \equiv \vec{p}\,' - \vec{p} \quad \text{is the momentum transfer,} \\ &\vec{k} \equiv \frac{1}{2}(\vec{p}\,' + \vec{p}) \quad \text{the average momentum,} \\ &\vec{S} \equiv \frac{1}{2}(\vec{\sigma}_1 + \vec{\sigma}_2) \quad \text{the total spin,} \end{aligned} \tag{4.8}$$

and $\vec{\sigma}_{1,2}$ and $\boldsymbol{\tau}_{1,2}$ are the spin and isospin operators, respectively, of nucleon 1 and 2. For on-energy-shell scattering, V_α and W_α ($\alpha = C, S, LS, T, \sigma L$) can be expressed as functions of q and k (with $q \equiv |\vec{q}|$ and $k \equiv |\vec{k}|$), only.

Our notation and conventions are similar to the ones used by the Munich group [55,60,61] except for two differences: our spin–orbit potentials, V_{LS} and W_{LS}, differ by a factor of $(+2)$ and all other potentials differ by a factor of (-1) from the Munich amplitudes. Our definitions are more in tune with what is commonly used in nuclear physics.

In all expressions given below, we will state only the *nonpolynomial* contributions to the *NN* amplitude. Note, however, that dimensional regularization typically generates also polynomial terms which are, in part, infinite or scale dependent (cf. Appendix B). These polynomials are absorbed by the contact interactions to be discussed in a later section.

Next-to-leading order (NLO). The leading two-pion exchange appears at second order ($\nu = 2$, next-to-leading order, NLO) and is shown in Fig. 3. Since a loop creates already $\nu = 2$ [cf. Eq. (3.5)], the vertices involved at this order have index $\Delta_i = 0$, i.e., they are from the leading order Lagrangian $\widehat{\mathcal{L}}^{\Delta=0}$, Eq. (2.65), where the πN vertices carry only one derivative. These vertices are denoted by small dots in the figures. The rather complicated evaluation of these diagrams is presented in Appendix B.

Concerning the planar box diagram in Fig. 3, we should note that we include only the non-iterative part of this diagram which is obtained by subtracting the iterated 1PE contribution Eq. (4.25) or (4.26), below, but using $M_N^2/E_p \approx M_N^2/E_{p''} \approx M_N$ at this order (NLO). Summarizing all contributions from irreducible two-pion exchange at second order, one obtains:

$$W_C = -\frac{L(q)}{384\pi^2 f_\pi^4}\left[4m_\pi^2(5g_A^4 - 4g_A^2 - 1) + q^2(23g_A^4 - 10g_A^2 - 1) + \frac{48g_A^4 m_\pi^4}{w^2}\right], \tag{4.9}$$

$$V_T = -\frac{1}{q^2}V_S = -\frac{3g_A^4 L(q)}{64\pi^2 f_\pi^4}, \tag{4.10}$$

where

$$L(q) \equiv \frac{w}{q}\ln\frac{w+q}{2m_\pi} \tag{4.11}$$

and

$$w \equiv \sqrt{4m_\pi^2 + q^2}. \tag{4.12}$$

As will be demonstrated in Section 4.2, below; this part of the 2PE is rather weak and insufficient to properly describe the *NN* interaction at intermediate range.

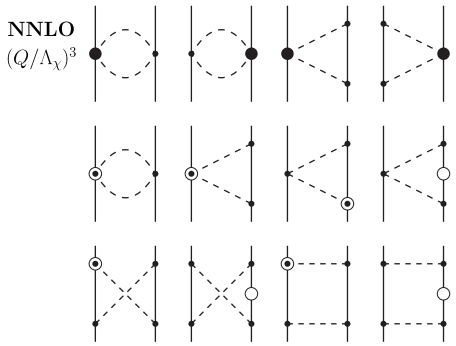

Fig. 4. Two-pion-exchange contributions to the *NN* interaction at order three in small momenta (NNLO). Basic notation as in Fig. 1. Large solid dots denote vertices from the Lagrangian $\widehat{\mathcal{L}}^{\Delta=1}$, Eq. (2.66), proportional to the LECs c_i. Symbols with an open circles are relativistic $1/M_N$ corrections which are also part of $\widehat{\mathcal{L}}^{\Delta=1}$. Only a few representative examples of $1/M_N$ corrections are shown. Note that all football diagrams shown in this figure vanish.

Next-to-next-to-leading order (NNLO). The two-pion-exchange diagrams of order three ($\nu = 3$, next-to-next-to-leading order, NNLO) are very similar to the ones of order two, except that they contain one insertion from $\widehat{\mathcal{L}}^{\Delta=1}$, Eq. (2.66). The resulting contributions are typically either proportional to one of the low-energy constants c_i or they contain a factor $1/M_N$. Notice that relativistic $1/M_N$ corrections derive from vertices and nucleon propagators. In Fig. 4, we show in row one the diagrams with one vertex proportional to c_i (large solid dot), and in row two and three a few representative graphs with a $1/M_N$ correction (symbols with an open circle). The number of $1/M_N$ correction graphs is large and not all are shown. Note that all football diagrams vanish at this order, because the loop integrals involve odd powers of the time component of the loop momentum. Again, the planar box diagram is corrected for a contribution from the iterated 1PE. If the iterative 2PE of Eq. (4.25), below, is used, the expansion of the factor $M_N^2/E_p = M_N - p^2/2M_N + \cdots$ is applied and the term proportional to $(-p^2/2M_N)$ is subtracted from the third order box diagram contribution. Then, one obtains for the full third order [55]:

$$V_C = \frac{3g_A^2}{16\pi f_\pi^4}\left\{\frac{g_A^2 m_\pi^5}{16M_N w^2} - \left[2m_\pi^2(2c_1 - c_3) - q^2\left(c_3 + \frac{3g_A^2}{16M_N}\right)\right]\widetilde{w}^2 A(q)\right\}, \tag{4.13}$$

$$W_C = \frac{g_A^2}{128\pi M_N f_\pi^4}\left\{3g_A^2 m_\pi^5 w^{-2} - \left[4m_\pi^2 + 2q^2 - g_A^2(4m_\pi^2 + 3q^2)\right]\widetilde{w}^2 A(q)\right\}, \tag{4.14}$$

$$V_T = -\frac{1}{q^2}V_S = \frac{9g_A^4\widetilde{w}^2 A(q)}{512\pi M_N f_\pi^4}, \tag{4.15}$$

$$W_T = -\frac{1}{q^2}W_S = -\frac{g_A^2 A(q)}{32\pi f_\pi^4}\left[\left(c_4 + \frac{1}{4M_N}\right)w^2 - \frac{g_A^2}{8M_N}(10m_\pi^2 + 3q^2)\right], \tag{4.16}$$

$$V_{LS} = \frac{3g_A^4\widetilde{w}^2 A(q)}{32\pi M_N f_\pi^4}, \tag{4.17}$$

$$W_{LS} = \frac{g_A^2(1 - g_A^2)}{32\pi M_N f_\pi^4}w^2 A(q), \tag{4.18}$$

with

$$A(q) \equiv \frac{1}{2q}\arctan\frac{q}{2m_\pi} \tag{4.19}$$

and

$$\widetilde{w} \equiv \sqrt{2m_\pi^2 + q^2}. \tag{4.20}$$

This contribution to the 2PE is the crucial one, because it provides an intermediate-range attraction of proper strength (Section 4.2). The isoscalar central potential, V_C, is strong and attractive due to the LEC c_3, which is negative and of large magnitude (cf. Table 2). Via resonance saturation, c_3 is associated with π–π correlations ('σ meson') and virtual Δ-isobar excitations, which create the most crucial contributions to 2PE in the frame work of conventional meson theory [11,20]. The configuration-space expressions, which correspond to the above momentum-space potentials, are given in Ref. [55], where also a detailed comparison with meson-exchange potentials is conducted.

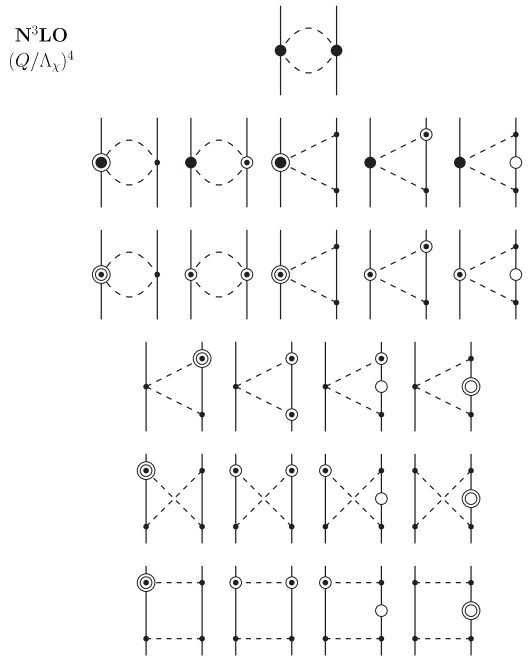

Fig. 5. One-loop 2π-exchange contributions to the *NN* interaction at order four. Notation as in Fig. 4. Moreover, symbols with a large solid dot and an open circle denote $1/M_N$ corrections of vertices proportional to c_i. Symbols with two open circles mark relativistic $1/M_N^2$ corrections. Both corrections are part of the Lagrangian $\widehat{\mathcal{L}}^{\Delta=2}$, Eq. (2.67). Representative examples for all types of one-loop graphs that occur at this order are shown.

If the iterative 2PE defined in Eq. (4.26), below, is applied, the $1/M_N$ terms are slightly different. As derived in Appendix C, the changes are taken care of by adding to Eqs. (4.13)–(4.16) the following terms:

$$V_C = -\frac{3g_A^4}{256\pi f_\pi^4 M_N}(m_\pi w^2 + \widetilde{w}^4 A(q)), \tag{4.21}$$

$$W_C = \frac{g_A^4}{128\pi f_\pi^4 M_N}(m_\pi w^2 + \widetilde{w}^4 A(q)), \tag{4.22}$$

$$V_T = -\frac{1}{q^2}V_S = \frac{3g_A^4}{512\pi f_\pi^4 M_N}(m_\pi + w^2 A(q)), \tag{4.23}$$

$$W_T = -\frac{1}{q^2}W_S = -\frac{g_A^4}{256\pi f_\pi^4 M_N}(m_\pi + w^2 A(q)). \tag{4.24}$$

Next-to-next-to-next-to-leading order (N^3LO). This order ($\nu = 4$) is very involved. The contributions can be subdivided into two groups, one-loop graphs, Fig. 5, and two-loop diagrams, Fig. 6. Applying Eq. (3.5), it is easy to verify that all contributions result in $\nu = 4$. We have relegated the comprehensive mathematical expressions of this order to Appendix D. The net effect of this contribution is small indicating a trend towards convergence (cf. Section 4.2).

Iterated one-pion exchange. Besides all the irreducible 2PE contributions presented above, there is also the reducible 2PE which is generated from iterated 1PE. This "iterative 2PE" is the only 2PE contribution which produces an imaginary part. Thus, one wishes to formulate this contribution such that relativistic elastic unitarity is satisfied. There are several ways to achieve this.

Kaiser et al. [55] define the iterative 2PE contribution as follows,

$$V_{2\pi,\mathrm{it}}^{(\mathrm{KBW})}(\vec{p}\,',\vec{p}) = \frac{M_N^2}{E_p}\int \frac{d^3p''}{(2\pi)^3}\frac{V_{1\pi}(\vec{p}\,',\vec{p}\,'')V_{1\pi}(\vec{p}\,'',\vec{p})}{p^2 - p''^2 + i\epsilon} \tag{4.25}$$

with $V_{1\pi}$ given in Eq. (4.5).

As it will turn out (cf. Section 4.4), in the development of a chiral *NN* potential, it is useful to adopt the relativistic scheme by Blankenbecler and Sugar [133] (BbS). In this approach, the iterated 1PE has the following form:

$$V_{2\pi,\mathrm{it}}^{(\mathrm{EM})}(\vec{p}\,',\vec{p}) = \int \frac{d^3p''}{(2\pi)^3}\frac{M_N^2}{E_{p''}}\frac{V_{1\pi}(\vec{p}\,',\vec{p}\,'')V_{1\pi}(\vec{p}\,'',\vec{p})}{p^2 - p''^2 + i\epsilon}. \tag{4.26}$$

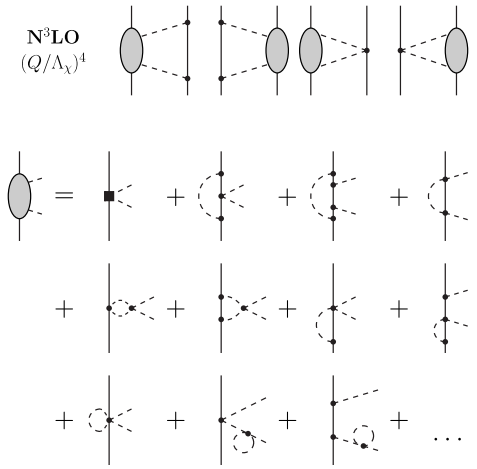

Fig. 6. Two-loop 2π-exchange contributions at order four. Basic notation as in Fig. 1. The oval stands for all one-loop πN graphs some of which are shown in the lower part of the figure. The solid square represents vertices proportional to the LECs d_i introduced in $\mathcal{L}^{(3)}_{\pi N}$ which is part of $\widehat{\mathcal{L}}^{\Delta=2}$, Eq. (2.67). More explanations are given in Appendix D.

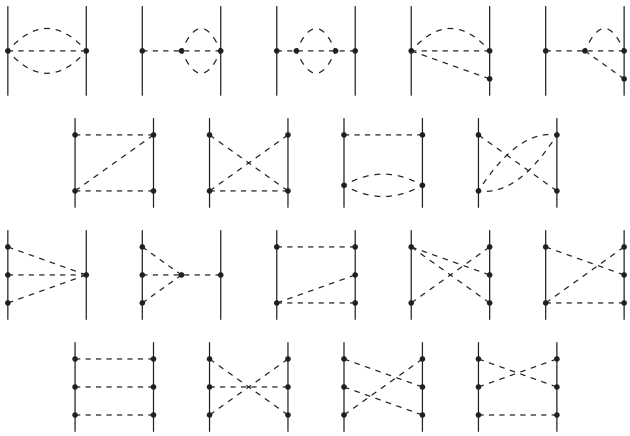

Fig. 7. Leading three-pion-exchange contributions to the *NN* interaction. Notation as in Fig. 1. Diagrams that result from interchange of nucleon lines and/or time reversal are not shown.

Eqs. (4.25) and (4.26) state the iterative 2PE to all orders. On the other hand, the covariant box diagram is calculated order by order and, therefore, requires a subtraction of the iterative 2PE order by order. For this, the expansion $M_N^2/E_p = M_N - p^2/2M_N + \cdots$ is applied in Eq. (4.25) and $M_N^2/E_{p''} = M_N - p''^2/2M_N + \cdots$ in Eq. (4.26). At NLO, both choices for the iterative 2PE collapse to the same, while at NNLO there are differences which give rise to the correction terms, Eqs. (4.21)–(4.24) when Eq. (4.26) is used (see Appendix C).

4.1.3. Three-pion exchange

Since the exchange of three pions involves two loops, three-pion exchange (3PE) starts at order four (N^3LO). Two loops generate $\nu = 4$ and, therefore, at this order, all vertices have to be from the leading order Lagrangian $\widehat{\mathcal{L}}^{\Delta=0}$, Eq. (2.65). One can distinguish between three groups of diagrams, namely, diagrams proportional to g_A^2 (first and second row of Fig. 7), g_A^4 (third row of the figure), and g_A^6 (fourth row). The graphs in the first row involve the $3\pi NN$ contact vertex from the leading πN Lagrangian and the 4π vertex from the leading $\pi\pi$ Lagrangian (both belong to $\widehat{\mathcal{L}}^{\Delta=0}$). Note that these vertices contain the unphysical parameter α which was introduced to parametrize the interpolating pion fields, Eq. (2.29). Therefore, this group of graphs has to be calculated together such that the parameter α drops out, as it should, since measurable quantities must not depend on α.

The 3PE contributions at N^3LO have been calculated by the Munich group and found to be negligible [57,58]. This is not surprising since only the leading vertices are involved which are known to be weak. As discussed, for similar reasons, the leading 2PE also turned out to be rather small (even though not negligible). Note, however, that the subleading 3PE contributions which involve one vertex from the Lagrangian $\widehat{\mathcal{L}}^{\Delta=1}$, Eq. (2.66), proportional the LEC c_i, have been found to

Table 2
Hadron masses and low-energy constants (LECs). $m_{\pi^\pm}$ and m_{π^0} denote the charged- and neutral-pion masses, and M_p and M_n are the proton and neutron masses, respectively, in units of MeV. g_A is the axial-vector coupling constant (dimensionless) and f_π the pion decay constant (in units of MeV). The c_i belong to the dimension-two πN Lagrangian, Eqs. (2.57) and (2.66), and are in units of GeV^{-1}, whereas the $\bar{d}_i$ are associated with the dimension-three Lagrangian, Eqs. (2.58) and (2.67), and are in units of GeV^{-2}. Column "*NN* Potential" lists the values used for a *NN* potential at N^{3}LO presented in Section 4.6.3, while column "Peripheral perturbative *NN*" shows the parameters applied in the peripheral *NN* scattering calculations of Section 4.2. Finally, the last column displays values from empirical determinations (see text for comments).

	NN potential (Section 4.6.3)	Peripheral perturbative *NN* (Section 4.2)	Empirical
$m_{\pi^\pm}$	139.5702	139.5702	139.57018(35) [115]
m_{π^0}	134.9766	134.9766	134.9766(6) [115]
M_p	938.2720	938.2720	938.272013(23) [115]
M_n	939.5653	939.5653	939.565346(23) [115]
g_A	1.29[a]	1.29[a]	1.2759(45) [130]
f_π	92.4	92.4	92.2 ± 0.2 [115]
c_1	−0.81	−0.81	−0.81 ± 0.15[b]
c_2	2.80	3.28	3.28 ± 0.23[c]
c_3	−3.20	−3.40	−4.69 ± 1.34[b]
c_4	5.40	3.40	3.40 ± 0.04[b]
$\bar{d}_1 + \bar{d}_2$	3.06	3.06	3.06 ± 0.21[c]
$\bar{d}_3$	−3.27	−3.27	−3.27 ± 0.73[c]
$\bar{d}_5$	0.45	0.45	0.45 ± 0.42[c]
$\bar{d}_{14} - \bar{d}_{15}$	−5.65	−5.65	−5.65 ± 0.41[c]

[a] Confer discussion of Goldberger–Treiman discrepancy in Section 4.1.1.
[b] Table 1, Fit 1 of Ref. [138].
[c] Table 2, Fit 1 of Ref. [123].

be sizable [59]. They contribute at fifth order (N^{4}LO). Our current analysis is restricted to N^{3}LO where only the leading 3PE contributes which we will ignore because of its negligible strength.

4.2. Perturbative NN scattering in peripheral partial waves

Nucleon–nucleon scattering in peripheral partial waves is of special interest—for several reasons. First, these partial waves probe the long and intermediate range of the nuclear force. Due to the centrifugal barrier, there is only small sensitivity to short-range contributions and, in fact, the N^{3}LO contact terms make no contributions for orbital angular momenta $L \geq 3$ (cf. Section 4.3). Thus, for F and higher waves and energies below the pion-production threshold, we have a window in which the *NN* interaction is governed by chiral symmetry alone (chiral one- and two-pion exchanges), and we can conduct a relatively clean test of how well the theory works. Using values for the LECs from πN analysis, the *NN* predictions are even parameter free. Moreover, the smallness of the phase shifts in peripheral partial waves suggests that the calculation can be done perturbatively. This avoids the complications and the possible model dependence that the nonperturbative treatment of the Schroedinger equation, necessary for low partial waves (Section 4.5), is beset with. Because of the importance of peripheral *NN* scattering, many calculations based upon chiral dynamics can be found in the literature [55,56,62,67,134–136]. We will follow Ref. [67].

Since we will compare the predictions with neutron–proton (*np*) phase shifts, we will specifically calculate *np* scattering in this subsection. Defining,

$$V_{1\pi}(m_\pi) \equiv -\frac{g_A^2}{4f_\pi^2}\frac{\vec{\sigma}_1\cdot\vec{q}\vec{\sigma}_2\cdot\vec{q}}{q^2+m_\pi^2}, \tag{4.27}$$

the correct 1PE for *np* scattering is given by

$$V_{1\pi}^{(np)}(\vec{p}\,',\vec{p}) = -V_{1\pi}(m_{\pi^0}) + (-1)^{I+1}\,2\,V_{1\pi}(m_{\pi^\pm}), \tag{4.28}$$

where I denotes the isospin of the two-nucleon system. We use the pion masses given in Table 2 and

$$M_N = \frac{2M_pM_n}{M_p+M_n} = 938.9182\ \text{MeV}. \tag{4.29}$$

Also in the iterative 2PE, we apply the correct *np* 1PE, i.e., in Eq. (4.25) we replace $V_{1\pi}$ with $V_{1\pi}^{(np)}$. Thus, the perturbative relativistic T-matrix for *np* scattering, taking the exchange of up to two pions into account, is calculated in the following way,

$$\begin{aligned} T(\vec{p}\,',\vec{p}) &= V_{1\pi}^{(np)}(\vec{p}\,',\vec{p}) + V_{2\pi}^{(np)}(\vec{p}\,',\vec{p}) \\ &= V_{1\pi}^{(np)}(\vec{p}\,',\vec{p}) + V_{2\pi,\text{it}}^{(\text{KBW},np)}(\vec{p}\,',\vec{p}) + V'_{2\pi}(\vec{p}\,',\vec{p}). \end{aligned} \tag{4.30}$$

As discussed, the expression for $V_{1\pi}^{(np)}$ is good to any order we will consider in this article (cf. Section 4.1.1) and $V_{2\pi,\text{it}}^{(\text{KBW},np)}$ includes all orders. There is no need to break the latter term up into orders, because the admixture of (very small) higher

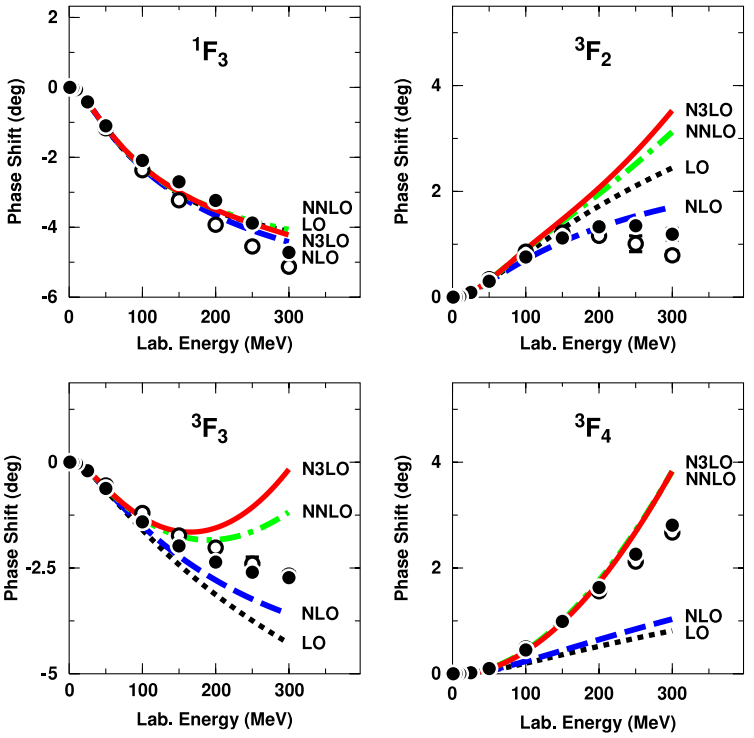

Fig. 8. F-wave phase shifts of neutron–proton scattering for laboratory kinetic energies below 300 MeV. We show the predictions from chiral pion exchange to leading order (LO), next-to-leading order (NLO), next-to-next-to-leading order (NNLO), and next-to-next-to-next-to-leading order (N3LO). Note that in $^3F_4$, the NNLO and N3LO curves cannot be distinguished on the scale of the figure. The solid dots and open circles are the results from the Nijmegen multi-energy *np* phase shift analysis [139] and the VPI/GWU single-energy *np* analysis SM99 [140], respectively.

order contributions from $V_{2\pi,\mathrm{it}}^{(\mathrm{KBW},np)}$ will not affect the accuracy we are working at. The most important term in the above equation is $V'_{2\pi}$, *the irreducible 2PE contributions*, for which we have the low-momentum expansion,

$$V'_{2\pi} = V'^{(2)}_{2\pi} + V'^{(3)}_{2\pi} + V'^{(4)}_{2\pi} + \cdots, \tag{4.31}$$

with the various $V'^{(\nu)}_{2\pi}$ given in Section 4.1.2. In the calculation of $V'_{2\pi}$, we use the average pion mass $m_\pi = 138.039$ MeV and, thus, neglect the charge dependence due to pion-mass splitting in irreducible diagrams. The charge dependence that emerges from irreducible 2π exchange was investigated in Ref. [137] and found to be negligible for partial waves with $L \geq 3$.

For the T-matrix given in Eq. (4.30), we calculate phase shifts for partial waves with $L \geq 3$ and $T_{lab} \leq 300$ MeV (see Ref. [67] for the details of this calculation). The LECs used in this calculation are shown in Table 2, column "Peripheral perturbative *NN*". Note that many determinations of the LECs, c_i and $\bar{d}_i$, can be found in the literature. The most reliable way to determine the LECs from empirical πN information is to extract them from the πN amplitude inside the Mandelstam triangle (unphysical region) which can be constructed with the help of dispersion relations from empirical πN data. This method was used by Büttiker and Meißner [138]. Unfortunately, the values for c_2 and all $\bar{d}_i$ parameters obtained in Ref. [138] carry uncertainties, so large that the values cannot provide any guidance. Therefore, in Table 2, only c_1, c_3, and c_4 are from Ref. [138], while the other LECs are taken from Ref. [123] where the πN amplitude in the physical region was considered. To establish a link between πN and *NN*, we apply the values from the above determinations in our calculations of the *NN* peripheral phase shifts. In general, we use the central values; the only exception is c_3, where we choose a value that is, in terms of magnitude, about one standard deviation below the one from Ref. [138]. With the exception of c_3, phase shift predictions do not depend sensitively on variations of the LECs within the quoted uncertainties.

In Figs. 8 and 9, we show the phase shift predictions for neutron–proton scattering in F and G waves, respectively, for laboratory kinetic energies below 300 MeV. The orders displayed are defined as follows:

- Leading order (LO) is just 1PE, first term on the r.h.s. of Eq. (4.30).
- Next-to-leading order (NLO) includes the first two terms on the r.h.s. of Eq. (4.30) (1PE & iterative 2PE) plus $V'^{(2)}_{2\pi}$ [Section 4.1.2, Eqs. (4.9) and (4.10)].
- Next-to-next-to-leading order (NNLO) consists of NLO plus $V'^{(3)}_{2\pi}$ [Section 4.1.2, Eqs. (4.13)–(4.18)].
- Next-to-next-to-next-to-leading order (denoted by N3LO in the figures) is made up of NNLO plus $V'^{(4)}_{2\pi}$ [Appendix D, Eqs. (D.1)–(D.15) and (D.18)–(D.27)].

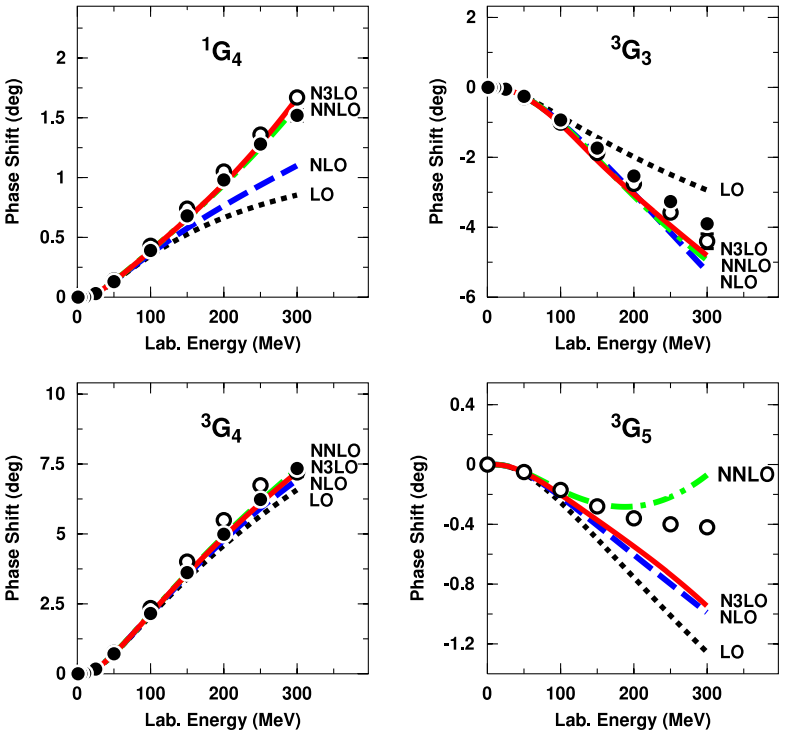

Fig. 9. Same as Fig. 8, but for *G* waves.

It is clearly seen in Figs. 8 and 9 that the leading 2π exchange (NLO) is, in general, rather small, insufficient to explain the empirical facts in most partial waves. In contrast, the next order (NNLO) is very large; in some cases, several times NLO. This is due to the $\pi\pi NN$ contact interactions proportional to the LECs c_i that are introduced in the subleading Lagrangian $\mathcal{L}^{\Delta=1}$, Eq. (2.66). These contacts are supposed to simulate the contributions from intermediate Δ-isobars and correlated 2π exchange which are known to be large and crucial for a realistic model for the *NN* interaction at intermediate ranges (see, e. g., Ref. [20]).

At N^{3}LO a clearly identifiable trend towards convergence emerges. In *G* waves (except for $^3G_5$, see Appendix D.3 for a discussion of this issue), N^{3}LO differs very little from NNLO implying that we have reached convergence. Also $^1F_3$ and $^3F_4$ appear fully converged. However, in $^3F_2$ and $^3F_3$, N^{3}LO differs noticeably from NNLO, but the difference is much smaller than the one between NNLO and NLO. This is what we perceive as a trend towards convergence. Individual N^{3}LO contributions to peripheral phase shifts are shown in Appendix D.3.

In Figs. 10 and 11, we conduct a comparison between the predictions from chiral one- and two-pion exchange at N^{3}LO and the corresponding predictions from conventional meson theory (curve 'Bonn'). As representative for conventional meson theory, we choose the Bonn meson-exchange model for the *NN* interaction [20], since it contains a comprehensive and thoughtfully constructed model for 2π exchange. This 2π model includes box and crossed box diagrams with *NN*, $N\Delta$, and $\Delta\Delta$ intermediate states as well as direct $\pi\pi$ interaction in *S* and *P* waves (of the $\pi\pi$ system) consistent with empirical information from πN and $\pi\pi$ scattering. Besides this the Bonn model also includes (repulsive) ω meson exchange and irreducible diagrams of π and ρ exchange (which are also repulsive). However, note that in the phase shift predictions displayed in Figs. 10 and 11, the "Bonn" curve includes only the 1π and 2π contributions from the Bonn model; the short-range contributions are left out since the purpose of the figure is to compare different models/theories for $\pi + 2\pi$. In all waves shown (with the usual exception of $^3G_5$) we see, in general, good agreement between N^{3}LO and Bonn. In $^3F_2$ and $^3F_3$ above 150 MeV and in $^3F_4$ above 250 MeV the chiral model to N^{3}LO is more attractive than the Bonn 2π model. Note, however, that the Bonn model is relativistic and, thus, includes relativistic corrections up to infinite orders. Thus, one may speculate that higher orders in ChPT may create some repulsion, moving the Bonn and the chiral predictions even closer together [141].

The 2π exchange contribution to the *NN* interaction can also be derived from *empirical* πN and $\pi\pi$ input using dispersion theory, which is based upon unitarity, causality (analyticity), and crossing symmetry. The amplitude $N\bar{N} \to \pi\pi$ is constructed from $\pi N \to \pi N$ and $\pi N \to \pi\pi N$ data using crossing properties and analytic continuation; this amplitude is then 'squared' to yield the $N\bar{N}$ amplitude which is related to *NN* by crossing symmetry [16]. The Paris group [17,18] pursued this path and calculated *NN* phase shifts in peripheral partial waves. Naively, the dispersion-theoretic approach is the ideal one, since it is based exclusively on empirical information. Unfortunately, in practice, quite a few uncertainties enter. First, there are ambiguities in the analytic continuation and, second, the dispersion integrals have to be cut off at a

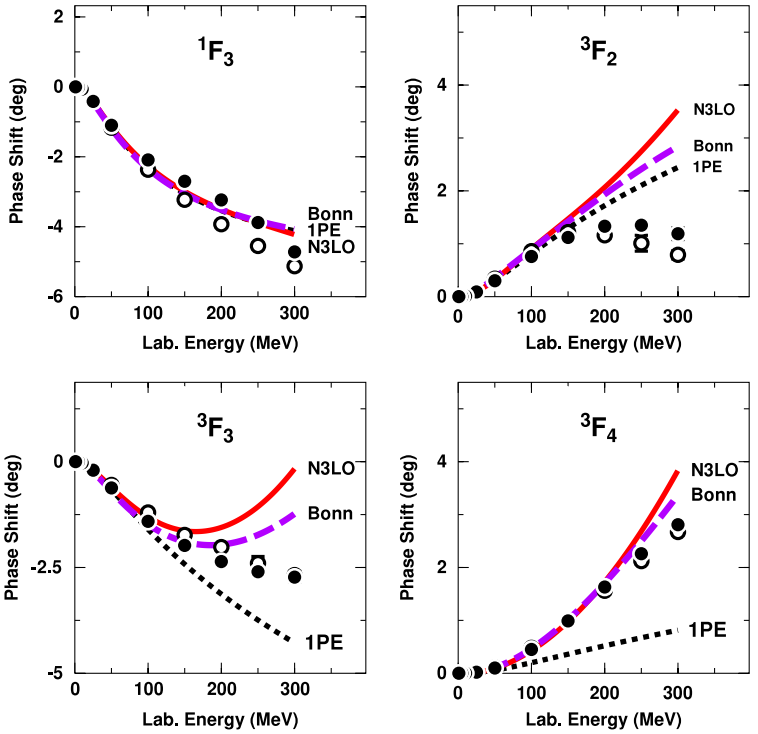

Fig. 10. F-wave phase shifts of neutron–proton scattering for laboratory kinetic energies below 300 MeV. We show the results from one-pion exchange (1PE), and one- plus two-pion exchange as predicted by ChPT at next-to-next-to-next-to-leading order (N3LO) and by the Bonn Full Model [20] (Bonn). Note that the "Bonn" curve does not include the repulsive ω and $\pi\rho$ exchanges of the full model, since this figure serves the purpose to compare just predictions by different models/theories for the $\pi + 2\pi$ contribution to the NN interaction. Empirical phase shifts (solid dots and open circles) as in Fig. 8.

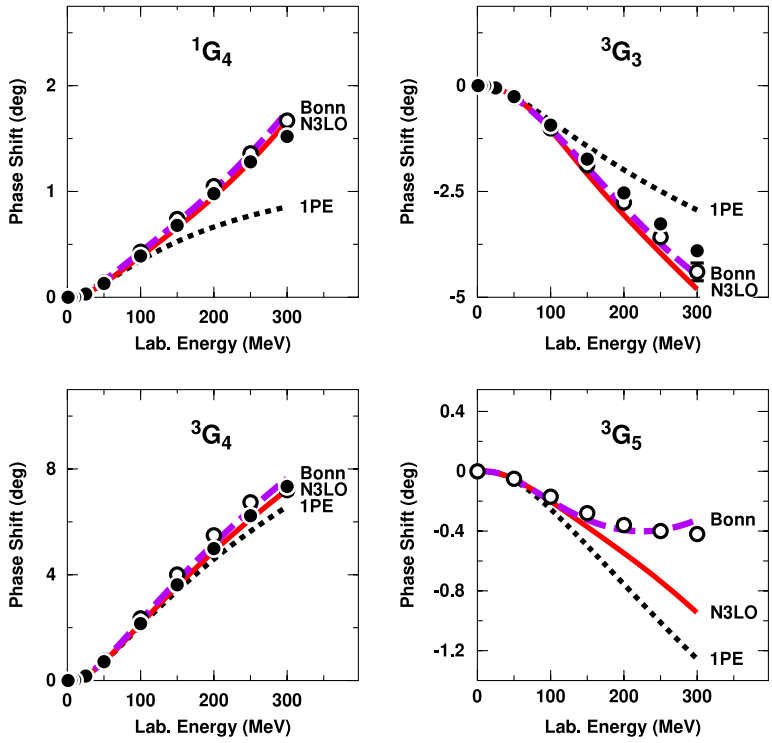

Fig. 11. Same as Fig. 10, but for G waves.

certain momentum to ensure reasonable results. In Ref. [20], a thorough comparison was conducted between the predictions by the Bonn model and the Paris approach and it was demonstrated that the Bonn predictions always lie comfortably within the range of uncertainty of the dispersion-theoretic results. Therefore, there is no need to perform a separate comparison of our chiral N^{3}LO predictions with dispersion theory, since it would not add anything that we cannot conclude from Figs. 10 and 11.

Finally, we need to compare the predictions with the empirical phase shifts. In F waves the N^{3}LO predictions above 200 MeV are, in general, too attractive. Note, however, that this is also true for the predictions by the Bonn $\pi + 2\pi$ model. In the *full* Bonn model, besides $\pi + 2\pi$, (repulsive) ω and $\pi\rho$ exchanges are included which move the predictions right on top of the data. The exchange of a ω meson or combined $\pi\rho$ exchange are 3π exchanges. Three-pion exchange occurs first at chiral order four. It has been investigated by Kaiser [57,58] and found to be negligible, at this order. However, 3π exchange at order five appears to be sizable [59] and may have impact on F waves. Besides this, there is the usual short-range phenomenology. In ChPT, this short-range interaction is parametrized in terms of four-nucleon contact terms (since heavy mesons do not have a place in that theory). Contact terms of order four (N^{3}LO) do not contribute to F waves, but order six does. In summary, the remaining small discrepancies between the N^{3}LO predictions and the empirical phase shifts may be straightened out in fifth or sixth order of ChPT.

4.3. NN contact terms

The successful test of the chiral pion-exchange contributions in peripheral partial waves in the previous section has shown that we got the long- and intermediate-range parts of the nuclear force right. However, for a "complete" nuclear force, we have to describe correctly all partial waves, including the lower ones. In fact, in calculations of *NN* observables at low energies (cross sections, analyzing powers, etc.), the lower partial waves with $L \leq 2$ are the most important ones, generating the largest contributions. The same is true for microscopic nuclear structure calculations. These lower partial waves are dominated by the dynamics at short distances. Therefore, we need to look now into the short-range part of the *NN* potential.

In conventional meson theory, the short-range nuclear force is described by the exchange of heavy mesons, notably the $\omega(782)$. Qualitatively, the short-distance behavior of the *NN* potential is obtained by Fourier transform of the propagator of a heavy meson,

$$\int d^3q \frac{e^{i\vec{q}\cdot\vec{r}}}{m_\omega^2 + \vec{q}^2} \sim \frac{e^{-m_\omega r}}{r}. \tag{4.32}$$

ChPT is an expansion in small momenta Q, too small to resolve structures like a $\rho(770)$ or $\omega(782)$ meson, because $Q \ll \Lambda_\chi \approx m_{\rho,\omega}$. But the latter relation allows us to expand the propagator of a heavy meson into a power series,

$$\frac{1}{m_\omega^2 + Q^2} \approx \frac{1}{m_\omega^2}\left(1 - \frac{Q^2}{m_\omega^2} + \frac{Q^4}{m_\omega^4} - + \cdots\right), \tag{4.33}$$

where the ω is representative for any heavy meson of interest. The above expansion suggests that it should be possible to describe the short-distance part of the nuclear force simply in terms of powers of Q/m_ω, which fits in well with our over-all power expansion since $Q/m_\omega \approx Q/\Lambda_\chi$.

A second purpose of contact terms is renormalization. Dimensional regularization of the loop integrals that occur in multi-pion-exchange diagrams typically generates polynomial terms with coefficients that are, in part, infinite or scale dependent (cf. Appendix B). Contact terms pick up infinities and remove scale dependences, which is why they are also known as counterterms.

The partial-wave decomposition of a power Q^ν has an interesting property. First note that Q can only be either the momentum transfer between the two interacting nucleons q or the average momentum k [cf. Eq. (4.8) for their definitions]. In any case, for even ν,

$$Q^\nu = f_{\frac{\nu}{2}}(\cos\theta), \tag{4.34}$$

where f_m stands for a polynomial of degree m and θ is the CMS scattering angle. The partial-wave decomposition of Q^ν for a state of orbital angular momentum L involves the integral

$$I_L^{(\nu)} = \int_{-1}^{+1} Q^\nu P_L(\cos\theta) d\cos\theta = \int_{-1}^{+1} f_{\frac{\nu}{2}}(\cos\theta) P_L(\cos\theta) d\cos\theta, \tag{4.35}$$

where P_L is a Legendre polynomial. Due to the orthogonality of the P_L,

$$I_L^{(\nu)} = 0 \quad \text{for } L > \frac{\nu}{2}. \tag{4.36}$$

Consequently, contact terms of order zero contribute only in S waves, while order two terms contribute up to P waves, order four terms up to D waves, etc.

Due to parity, only even powers of Q are allowed. Thus, the expansion of the contact potential is formally given by

$$V_{\rm ct} = V_{\rm ct}^{(0)} + V_{\rm ct}^{(2)} + V_{\rm ct}^{(4)} + \cdots, \tag{4.37}$$

where the superscript denotes the power or order.

We will now present, one by one, the various orders of *NN* contact terms which result from the contact Lagrangians presented in Section 2.3.

4.3.1. Zeroth order (LO)

The contact Lagrangian $\widehat{\mathcal{L}}_{NN}^{(0)}$, Eq. (2.61), which is part of $\widehat{\mathcal{L}}^{\Delta=0}$, Eq. (2.65), leads to the following *NN* contact potential,

$$V_{\rm ct}^{(0)}(\vec{p}\,',\vec{p}) = C_S + C_T\,\vec{\sigma}_1\cdot\vec{\sigma}_2, \tag{4.38}$$

and, in terms of partial waves, we have

$$\begin{aligned} V_{\rm ct}^{(0)}({}^1S_0) &= \widetilde{C}_{{}^1S_0} = 4\pi\,(C_S - 3\,C_T) \\ V_{\rm ct}^{(0)}({}^3S_1) &= \widetilde{C}_{{}^3S_1} = 4\pi\,(C_S + C_T). \end{aligned} \tag{4.39}$$

4.3.2. Second order (NLO)

The contact Lagrangian $\widehat{\mathcal{L}}_{NN}^{(2)}$, Eq. (2.62), which is part of $\widehat{\mathcal{L}}^{\Delta=2}$, Eq. (2.67), generates the following *NN* contact potential

$$\begin{aligned} V_{\rm ct}^{(2)}(\vec{p}\,',\vec{p}) \,=\, & C_1\,q^2 + C_2\,k^2 + \left(C_3\,q^2 + C_4\,k^2\right)\vec{\sigma}_1\cdot\vec{\sigma}_2 + C_5\left(-i\vec{S}\cdot(\vec{q}\times\vec{k})\right) \\ & + C_6\,(\vec{\sigma}_1\cdot\vec{q})\,(\vec{\sigma}_2\cdot\vec{q}) + C_7\,(\vec{\sigma}_1\cdot\vec{k})\,(\vec{\sigma}_2\cdot\vec{k}). \end{aligned} \tag{4.40}$$

The coefficients C_i used here in the contact potential are, of course, related to the coefficients C_i' that occur in the Lagrangian $\widehat{\mathcal{L}}_{NN}^{(2)}$, Eq. (2.62). The relation, which is unimportant for our purposes, can be found in Refs. [54,64].

There are many ways to perform the partial-wave decomposition of the above potential. We perceive the method presented by Erkelenz et al. [142] as the most elegant one. Thus, one obtains

$$\begin{aligned} V_{\rm ct}^{(2)}({}^1S_0) &= C_{{}^1S_0}(p^2+p'^2) \\ V_{\rm ct}^{(2)}({}^3P_0) &= C_{{}^3P_0}\,pp' \\ V_{\rm ct}^{(2)}({}^1P_1) &= C_{{}^1P_1}\,pp' \\ V_{\rm ct}^{(2)}({}^3P_1) &= C_{{}^3P_1}\,pp' \\ V_{\rm ct}^{(2)}({}^3S_1) &= C_{{}^3S_1}(p^2+p'^2) \\ V_{\rm ct}^{(2)}({}^3S_1-{}^3D_1) &= C_{{}^3S_1-{}^3D_1}p^2 \\ V_{\rm ct}^{(2)}({}^3D_1-{}^3S_1) &= C_{{}^3S_1-{}^3D_1}p'^2 \\ V_{\rm ct}^{(2)}({}^3P_2) &= C_{{}^3P_2}\,pp' \end{aligned} \tag{4.41}$$

with

$$\begin{aligned} C_{{}^1S_0} &= 4\pi\left(C_1 + \frac{1}{4}C_2 - 3C_3 - \frac{3}{4}C_4 - C_6 - \frac{1}{4}C_7\right) \\ C_{{}^3P_0} &= 4\pi\left(-\frac{2}{3}C_1 + \frac{1}{6}C_2 - \frac{2}{3}C_3 + \frac{1}{6}C_4 - \frac{2}{3}C_5 + 2C_6 - \frac{1}{2}C_7\right) \\ C_{{}^1P_1} &= 4\pi\left(-\frac{2}{3}C_1 + \frac{1}{6}C_2 + 2C_3 - \frac{1}{2}C_4 + \frac{2}{3}C_6 - \frac{1}{6}C_7\right) \\ C_{{}^3P_1} &= 4\pi\left(-\frac{2}{3}C_1 + \frac{1}{6}C_2 - \frac{2}{3}C_3 + \frac{1}{6}C_4 - \frac{1}{3}C_5 - \frac{4}{3}C_6 + \frac{1}{3}C_7\right) \\ C_{{}^3S_1} &= 4\pi\left(C_1 + \frac{1}{4}C_2 + C_3 + \frac{1}{4}C_4 + \frac{1}{3}C_6 + \frac{1}{12}C_7\right) \\ C_{{}^3S_1-{}^3D_1} &= 4\pi\left(-\frac{2\sqrt{2}}{3}C_6 - \frac{\sqrt{2}}{6}C_7\right) \\ C_{{}^3P_2} &= 4\pi\left(-\frac{2}{3}C_1 + \frac{1}{6}C_2 - \frac{2}{3}C_3 + \frac{1}{6}C_4 + \frac{1}{3}C_5\right). \end{aligned} \tag{4.42}$$

4.3.3. Fourth order (N^3LO)

The contact potential of order four reads

$$V_{\rm ct}^{(4)}(\vec{p}',\vec{p}) = D_1\,q^4 + D_2\,k^4 + D_3\,q^2k^2 + D_4\,(\vec{q}\times\vec{k})^2 + \Big(D_5\,q^4 + D_6\,k^4 + D_7\,q^2k^2 + D_8\,(\vec{q}\times\vec{k})^2\Big)\,\vec{\sigma}_1\cdot\vec{\sigma}_2 + \big(D_9\,q^2 + D_{10}\,k^2\big)\Big(-i\vec{S}\cdot(\vec{q}\times\vec{k})\Big) + \big(D_{11}\,q^2 + D_{12}\,k^2\big)\,(\vec{\sigma}_1\cdot\vec{q})\,(\vec{\sigma}_2\cdot\vec{q}) + \big(D_{13}\,q^2 + D_{14}\,k^2\big)\,(\vec{\sigma}_1\cdot\vec{k})\,(\vec{\sigma}_2\cdot\vec{k}) + D_{15}\Big(\vec{\sigma}_1\cdot(\vec{q}\times\vec{k})\vec{\sigma}_2\cdot(\vec{q}\times\vec{k})\Big)\,. \tag{4.43}$$

The rather lengthy partial-wave expressions of this order are relegated to Appendix E.

4.4. Definition of NN potential

We have now rounded up everything needed for a realistic nuclear force – long, intermediate, and short-ranged components – and so we can finally proceed to the lower partial waves. However, here we encounter another problem. The two-nucleon system at low angular momentum, particularly, in S waves, is characterized by the presence of a shallow bound state (the deuteron) and large scattering lengths. Thus, perturbation theory does not apply. In contrast to π–π and π–N, the interaction between nucleons is not suppressed in the chiral limit ($Q \to 0$). Weinberg [50,51] showed that the strong enhancement of the scattering amplitude arises from purely nucleonic intermediate states ("infrared enhancement"). He therefore suggested to use perturbation theory to calculate the *NN* potential (i.e., the irreducible graphs) and to apply this potential in a scattering equation to obtain the *NN* amplitude. We will follow this prescription and discuss potential problems in the next subsection.

Since the irreducible diagrams that make up the potential are calculated using covariant perturbation theory (cf. Section 4.1), it is consistent to start from the covariant Bethe–Salpeter (BS) equation [143] describing two-nucleon scattering. In operator notation, the BS equation reads

$$T = \mathcal{V} + \mathcal{V}\,\mathcal{G}\,T \tag{4.44}$$

where T denotes the invariant T-matrix ($T = i\mathcal{M}$ with $\mathcal{M}$ the invariant amplitude) for the two-nucleon scattering process, $\mathcal{V}$ the sum of all connected two-particle irreducible diagrams, and $\mathcal{G}$ is $(-i)$ times the relativistic two-nucleon propagator. The BS equation is equivalent to a set of two equations

$$T = V + V\,g\,T \tag{4.45}$$

$$V = \mathcal{V} + \mathcal{V}\,(\mathcal{G} - g)\,V \tag{4.46}$$

$$= \mathcal{V} + \mathcal{V}_{1\pi}\,(\mathcal{G} - g)\,\mathcal{V}_{1\pi} + \cdots, \tag{4.47}$$

where g is a covariant three-dimensional propagator which preserves relativistic elastic unitarity. We choose the propagator g proposed by Blankenbecler and Sugar (BbS) [133] (for more details on relativistic three-dimensional reductions of the BS equation, see Ref. [11]). The ellipsis in Eq. (4.47) stands for terms of irreducible 3π and higher pion exchanges which we neglect.

Note that when we speak of covariance in conjunction with (heavy baryon) ChPT, we are not referring to manifest covariance. Relativity and relativistic off-shell effects are accounted for in terms of a Q/M_N expansion up to the given order and up to the number of pions we take into consideration. Thus, Eq. (4.47) is evaluated in the following way,

$$V \approx \mathcal{V}(\text{on-shell}) + \mathcal{V}_{1\pi}\,\mathcal{G}\,\mathcal{V}_{1\pi} - V_{1\pi}\,g\,V_{1\pi} \tag{4.48}$$

$$\approx V_{1\pi} + \widetilde{V}_{2\pi} + \mathcal{V}_{1\pi}\,\mathcal{G}\,\mathcal{V}_{1\pi} - V_{1\pi}\,g\,V_{1\pi} \tag{4.49}$$

$$= V_{1\pi} + V'_{2\pi}, \tag{4.50}$$

where $\mathcal{V}_{1\pi}$ denotes the relativistic (off-shell) 1PE, while $V_{1\pi}$ is the on-shell 1PE given in Eq. (4.5). $\widetilde{V}_{2\pi}$ stands for the irreducible 2π exchanges calculated (on-shell) in Section 4.1.2, *but without the covariant planar box diagram*, which in the above equations is given by $\mathcal{V}_{1\pi}\,\mathcal{G}\,\mathcal{V}_{1\pi}$. Furthermore, $V_{1\pi}\,g\,V_{1\pi}$ is the iterated 1PE discussed in Section 4.1.2. Thus, the term $(\mathcal{V}_{1\pi}\,\mathcal{G}\,\mathcal{V}_{1\pi} - V_{1\pi}\,g\,V_{1\pi})$ represents the irreducible part of the box diagram contribution. Finally, $V'_{2\pi}$ subsumes all 2π exchanges without the iterated $V_{1\pi}$ and is, therefore, also known as the irreducible 2PE. Since all contributions are calculated on-shell, the potential has no energy dependence.

Adding the short-range contact terms $V_{\rm ct}$ to the above, yields the full *NN* potential,

$$V = V_{1\pi} + V'_{2\pi} + V_{\rm ct}. \tag{4.51}$$

Notice that the pion-exchange part of this potential differs from the perturbative amplitude, Eq. (4.30), by the absence of the iterative 2PE. The latter is generated automatically when the potential is inserted into a Schroedinger or Lippmann–Schwinger equation (see below). We also note that adding the contact interactions to the pion interactions will generate loop corrections of the contact terms. This leads to a m_π-dependent renormalization of the contact parameters and can be ignored if m_π dependence is not an issue.

As discussed, the irreducible 2PE, $V'_{2\pi}$, is organized according to increasing orders,

$$V'_{2\pi} = V'^{(2)}_{2\pi} + V'^{(3)}_{2\pi} + V'^{(4)}_{2\pi} + \cdots, \tag{4.52}$$

and was calculated in Section 4.1.2: $V'^{(2)}_{2\pi}$ is given by the contributions of Eqs. (4.9) and (4.10), $V'^{(3)}_{2\pi}$ is made up from Eqs. (4.13)–(4.24), and $V'^{(4)}_{2\pi}$ is contained in Appendix D.

The contact potentials come in even orders,

$$V_{\rm ct} = V^{(0)}_{\rm ct} + V^{(2)}_{\rm ct} + V^{(4)}_{\rm ct} + \cdots, \tag{4.53}$$

and were presented in Section 4.3.

In summary, the *NN* potential V, calculated to certain orders, is given by:

$$V_{\rm LO} = V_{1\pi} + V^{(0)}_{\rm ct} \tag{4.54}$$

$$V_{\rm NLO} = V_{\rm LO} + V'^{(2)}_{2\pi} + V^{(2)}_{\rm ct} \tag{4.55}$$

$$V_{\rm NNLO} = V_{\rm NLO} + V'^{(3)}_{2\pi} \tag{4.56}$$

$$V_{\rm N^3LO} = V_{\rm NNLO} + V'^{(4)}_{2\pi} + V^{(4)}_{\rm ct}. \tag{4.57}$$

The potential V satisfies the relativistic BbS equation, Eq. (4.45), which reads explicitly,

$$T(\vec{p}\,',\vec{p}) = V(\vec{p}\,',\vec{p}) + \int \frac{d^3p''}{(2\pi)^3} V(\vec{p}\,',\vec{p}\,'') \frac{M_N^2}{E_{p''}} \frac{1}{p^2 - p''^2 + i\epsilon} T(\vec{p}\,'',\vec{p}) \tag{4.58}$$

with $E_{p''} \equiv \sqrt{M_N^2 + p''^2}$. The advantage of using a relativistic scattering equation is that it automatically includes relativistic corrections to all orders. Thus, in the scattering equation, no propagator modifications are necessary when raising the order to which the calculation is conducted.

Defining

$$\widehat{V}(\vec{p}\,',\vec{p}) \equiv \frac{1}{(2\pi)^3} \sqrt{\frac{M_N}{E_{p'}}} V(\vec{p}\,',\vec{p}) \sqrt{\frac{M_N}{E_p}} \tag{4.59}$$

and

$$\widehat{T}(\vec{p}\,',\vec{p}) \equiv \frac{1}{(2\pi)^3} \sqrt{\frac{M_N}{E_{p'}}} T(\vec{p}\,',\vec{p}) \sqrt{\frac{M_N}{E_p}}, \tag{4.60}$$

where the factor $1/(2\pi)^3$ is added for convenience, the BbS equation collapses into the usual, nonrelativistic Lippmann–Schwinger (LS) equation,

$$\widehat{T}(\vec{p}\,',\vec{p}) = \widehat{V}(\vec{p}\,',\vec{p}) + \int d^3p'' \widehat{V}(\vec{p}\,',\vec{p}\,'') \frac{M_N}{p^2 - p''^2 + i\epsilon} \widehat{T}(\vec{p}\,'',\vec{p}). \tag{4.61}$$

Since $\widehat{V}$ satisfies Eq. (4.61), it can be used like a usual nonrelativistic potential, and $\widehat{T}$ may be perceived as the conventional nonrelativistic T-matrix. In applications, it is more convenient to use the K-matrix instead of the T-matrix and to have the LS equation decomposed into partial waves: all these technical issues are explained in detail in Appendix A of Ref. [13] where also the formulas for the calculation of *np* and *pp* (the latter with Coulomb) phase shifts are provided. The partial-wave decomposition of the operators by which the potential is represented can be found in Section 4 of Ref. [142], and numerical methods for solving the LS equation are explained in Ref. [144].

4.5. Renormalization

4.5.1. Regularization and nonperturbative renormalization

Iteration of $\widehat{V}$ in the LS equation, Eq. (4.61), requires cutting $\widehat{V}$ off for high momenta to avoid infinities. This is consistent with the fact that ChPT is a low-momentum expansion which is valid only for momenta $Q \ll \Lambda_\chi \approx 1$ GeV. Therefore, the potential $\widehat{V}$ is multiplied with the regulator function $f(p', p)$,

$$\widehat{V}(\vec{p}\,',\vec{p}) \longmapsto \widehat{V}(\vec{p}\,',\vec{p}) f(p', p) \tag{4.62}$$

with

$$f(p', p) = \exp[-(p'/\Lambda)^{2n} - (p/\Lambda)^{2n}], \tag{4.63}$$

such that

$$\widehat{V}(\vec{p}\,',\vec{p})\,f(p',p) \approx \widehat{V}(\vec{p}\,',\vec{p})\left\{1-\left[\left(\frac{p'}{\Lambda}\right)^{2n}+\left(\frac{p}{\Lambda}\right)^{2n}\right]+\cdots\right\}. \tag{4.64}$$

Typical choices for the cutoff parameter Λ that appears in the regulator are $\Lambda \approx 0.5$ GeV $\ll \Lambda_\chi \approx 1$ GeV.

Eq. (4.64) provides an indication of the fact that the exponential cutoff does not necessarily affect the given order at which the calculation is conducted. For sufficiently large n, the regulator introduces contributions that are beyond the given order. Assuming a good rate of convergence of the chiral expansion, such orders are small as compared to the given order and, thus, do not affect the accuracy at the given order. In calculations, one uses, of course, the exponential form, Eq. (4.63), and not the expansion, Eq. (4.64). On a similar note, we also do not expand the square-root factors in Eqs. (4.59)–(4.60) because they are kinematical factors which guarantee relativistic elastic unitarity.

It is pretty obvious that results for the T-matrix may depend sensitively on the regulator and its cutoff parameter. This is acceptable if one wishes to build models. For example, the meson models of the past [11,20] always depended sensitively on the choices for the cutoff parameters which, in fact, were important for the fit of the *NN* data. However, the EFT approach wishes to be fundamental in nature and not just another model.

In field theories, divergent integrals are not uncommon and methods have been developed for how to deal with them. One regulates the integrals and then removes the dependence on the regularization parameters (scales, cutoffs) by renormalization. In the end, the theory and its predictions do not depend on cutoffs or renormalization scales.

So-called renormalizable quantum field theories, like QED, have essentially one set of prescriptions that takes care of renormalization through all orders. In contrast, EFTs are renormalized order by order.

The renormalization of *perturbative* EFT calculations is not a problem. *The problem is nonperturbative renormalization.* This problem typically occurs in *nuclear* EFT because nuclear physics is characterized by bound states which are nonperturbative in nature. EFT power counting may be different for nonperturbative processes as compared to perturbative ones. Such difference may be caused by the infrared enhancement of the reducible diagrams generated in the LS equation.

Weinberg's implicit assumption [47,50] was that the counterterms introduced to renormalize the perturbatively calculated potential, based upon naive dimensional analysis ("Weinberg counting"), are also sufficient to renormalize the nonperturbative resummation of the potential in the LS equation. In 1996, Kaplan et al. (KSW) [145] pointed out that there are problems with the Weinberg scheme if the LS equation is renormalized by minimally subtracted dimensional regularization. This criticism resulted in a flurry of publications on the renormalization of the nonperturbative *NN* problem [146–162]. The literature is too comprehensive to discuss all contributions. Let us just mention some of the work that has particular relevance for our present discussion.

If the potential V consists of contact terms only (a.k.a. pion-less theory), then the nonperturbative summation (4.61) can be performed analytically and the power counting is explicit. However, when pion exchange is included, then (4.61) can be solved only numerically and the power counting is less transparent. Perturbative ladder diagrams of arbitrarily high order, where the rungs of the ladder represent a potential made up from irreducible pion exchange, suggest that an infinite number of counterterms is needed to achieve cutoff independence for all the terms of increasing order generated by the iterations. For that reason, Kaplan et al. (KSW) [145] proposed to sum the leading order contact interaction to all orders (analytically) and to add higher order contacts and pion exchange perturbatively up to the given order. Unfortunately, it turned out that the order-by-order convergence of 1PE is poor in the ${}^3S_1$–${}^3D_1$ state [146]. The failure was triggered by the $1/r^3$ singularity of the 1PE tensor force when iterated to second order. Therefore, KSW counting is no longer taken into consideration (see, however, [160]). A balanced discussion of possible solutions is provided in [150].

Some researchers decided to take a second look at Weinberg's original proposal. A systematic investigation of Weinberg counting in leading order has been conducted by Nogga, Timmermans, and van Kolck [152] in momentum space, and by Valderrama and Arriola at LO and higher orders in configuration space [151,153,154]. A comprehensive discussion of both approaches and their equivalence can be found in Refs. [157,161].

The LO *NN* potential is given in (4.54) and consists of 1PE plus two non-derivative contact terms that contribute only in S waves. Nogga et al. [152] find that the given counterterms renormalize the S waves (i.e., stable results are obtained for $\Lambda \to \infty$) and the naively expected infinite number of counterterms is not needed. This means that Weinberg power counting does actually work in S waves at LO (ignoring the m_π dependence of the contact interaction discussed in Refs. [145,150]). However, there are problems with a particular class of higher partial waves, namely those in which the tensor force from 1PE is attractive. The first few cases of this kind of low angular momentum are ${}^3P_0$, ${}^3P_2$, and ${}^3D_2$, which need a counterterm for cutoff independence. The leading (non-derivative) counterterms do not contribute in P and higher waves, which is why Weinberg counting fails in these cases. But the second order contact potential provides counterterms for P waves. Therefore, the promotion of, particularly, the ${}^3P_0$ and ${}^3P_2$ contacts from NLO to LO would fix the problem in P waves. To take care of the ${}^3D_2$ problem, a N^{3}LO contact, i.e. a term from $V_{\rm ct}^{(4)}$, needs to be promoted to LO. Partial waves with orbital angular momentum $L \geq 3$ may be calculated in Born approximation with sufficient accuracy and, therefore, do not pose renormalization problems. In this way, one arrives at a scheme of 'modified Weinberg counting' [152] for the leading order two-nucleon interaction.

4.5.2. Renormalization beyond leading order

As shown below, for a quantitative chiral *NN* potential one needs to advance all the way to N^{3}LO. Thus, the renormalization issue needs to be discussed beyond LO. Naively, the most perfect renormalization procedure is the one where the cutoff

parameter Λ is carried to infinity while stable results are maintained. This was done successfully at LO in the work by Nogga et al. [152] described above. At NNLO, the infinite-cutoff renormalization procedure has been investigated in [158] for partial waves with total angular momentum $J \leq 1$ and in [154] for all partial waves with $J \leq 5$. At N^{3}LO, an investigation of the $^1S_0$ state exists [157]. From all of these works, it is evident that no counterterm is effective in partial waves with short-range repulsion and only a single counterterm can effectively be used in partial waves with short-range attraction. Thus, for the $\Lambda \to \infty$ renormalization prescription, even at N^{3}LO, we have either one or no counterterm per partial-wave state. This is inconsistent with any reasonable power counting scheme and, therefore, defies the principals of an EFT.

A possible way out of this dilemma was proposed already in [152] and reiterated in a recent paper by Long and van Kolck [159]. In the latter reference, the authors examine the renormalization of an attractive $1/r^2$ potential perturbed by a $1/r^4$ correction. Generalizing their findings, they come to the conclusion that, for any attractive $1/r^n$ potential (with $n \geq 2$), partial waves with low angular momentum L must be summed to all orders and one contact term is needed for each L to renormalize the LO contribution. However, there exists an angular momentum L_p ($L_p \approx 3$ for the nuclear case, cf. Ref. [152]), above which the leading order can be calculated perturbatively. In short, naive dimensional analysis (NDA) does not apply at LO below L_p. However, once this failure of NDA is corrected at LO, higher order corrections can be added in perturbation theory using counterterm that follow NDA [159].

Ref. [159] used just a toy model and, therefore, a full investigation using the chiral expansion is needed to answer the question if this renormalization approach will work for the realistic nuclear force. A first calculation of this kind for the S waves was recently performed by Valderrama [163]. The author renormalizes the LO interaction nonperturbatively and then uses the LO distorted wave to calculate the 2PE contributions at NLO and NNLO perturbatively. It turns out that perturbative renormalizability requires the introduction of three counterterms in $^1S_0$ and six in the coupled $^3S_1$–$^3D_1$ channels. Thus, the number of counterterms required in this scheme is larger than in the Weinberg scheme, which reduces the predictive power. For a final evaluation of this approach, also the results for P and D waves are needed, which are not yet published.

However, even if such a project turns out to be successful for *NN* scattering, there is doubt if the interaction generated in this approach is of any use for applications in nuclear few- and many-body problems. In applications, one would first have to solve the many-body problem with the renormalized LO interaction, and then add higher order corrections in perturbation theory. However, it was shown in a recent paper [164] that the renormalized LO interaction is characterized by a very large tensor force from 1PE. This is no surprise since LO is renormalized with $\Lambda \to \infty$ implying that the 1PE, particularly its tensor force, is totally uncut. As a consequence of this, the wound integral in nuclear matter, κ, comes out to be about 40%. The hole-line and coupled cluster expansions are know to converge $\propto \kappa^{n-1}$ with n the number of hole-lines or particles per cluster [165–167]. For conventional nuclear forces, the wound integral is typically between 5% and 10% and the inclusion of three-body clusters (or three hole-lines) are needed to obtain converged results in the many-body system [85, 87,168]. Thus, if the wound integral is 40%, probably, up to six hole-lines need to be included for approximate convergence. Such calculations are not feasible even with the most powerful computers of today and will not be feasible any time soon. Therefore, even if the renormalization procedure proposed in [159] will work for *NN* scattering, the interaction produced will be highly impractical (to say the least) in applications in few- and many-body problems because of convergence problems with the many-body energy and wave functions.

4.5.3. Back to the beginnings

The various problems with the renormalization procedures discussed above may have a simple common reason: An EFT that has validity only for momenta $Q < \Lambda_\chi$ is applied such that momenta $Q \gg \Lambda_\chi$ are heavily involved (because the regulator cutoff $\Lambda \to \infty$). A recent paper by Epelbaum and Gegelia [169] illustrates the point: The authors construct an exactly solvable toy model that simulates a pionful EFT and yields finite results for $\Lambda \to \infty$. However, as it turns out, these finite results are incompatible with the underlying EFT, while for cutoffs in the order of the hard scale consistency is maintained. In simple terms, the point to realize is this: *If an EFT calculation produces (accidentally) a finite result for $\Lambda \to \infty$, then that does not automatically imply that this result is also meaningful.*

This matter is further elucidated in the lectures by Lepage of 1997 [170]. Lepage points out that it makes little sense to take the momentum cutoff beyond the range of validity of the effective theory. By assumption, our data involves energies that are too low – wave lengths that are too long – to probe the true structure of the theory at very short distances. When one goes beyond the hard scale of the theory, structures are seen that are almost certainly wrong. Thus, results cannot improve and, in fact, they may degrade or, in more extreme cases, the theory may become unstable or untunable. In fact, in the *NN* case, this is what is happening in several partial waves (as reported above). Therefore, Lepage suggests to take the following three steps when building an effective theory:

1. Incorporate the correct long-range behavior: The long-range behavior of the underlying theory must be known, and it must be built into the effective theory. In the case of nuclear forces, the long-range theory is, of course, well known and given by one- and multi-pion exchanges.
2. Introduce an ultraviolet cutoff to exclude high-momentum states, or, equivalent, to soften the short-distance behavior: The cutoff has two effects: First it excludes high-momentum states, which are sensitive to the unknown short-distance dynamics; only states that we understand are retained. Second it makes all interactions regular at $r = 0$, thereby avoiding the infinities that beset the naive approach.

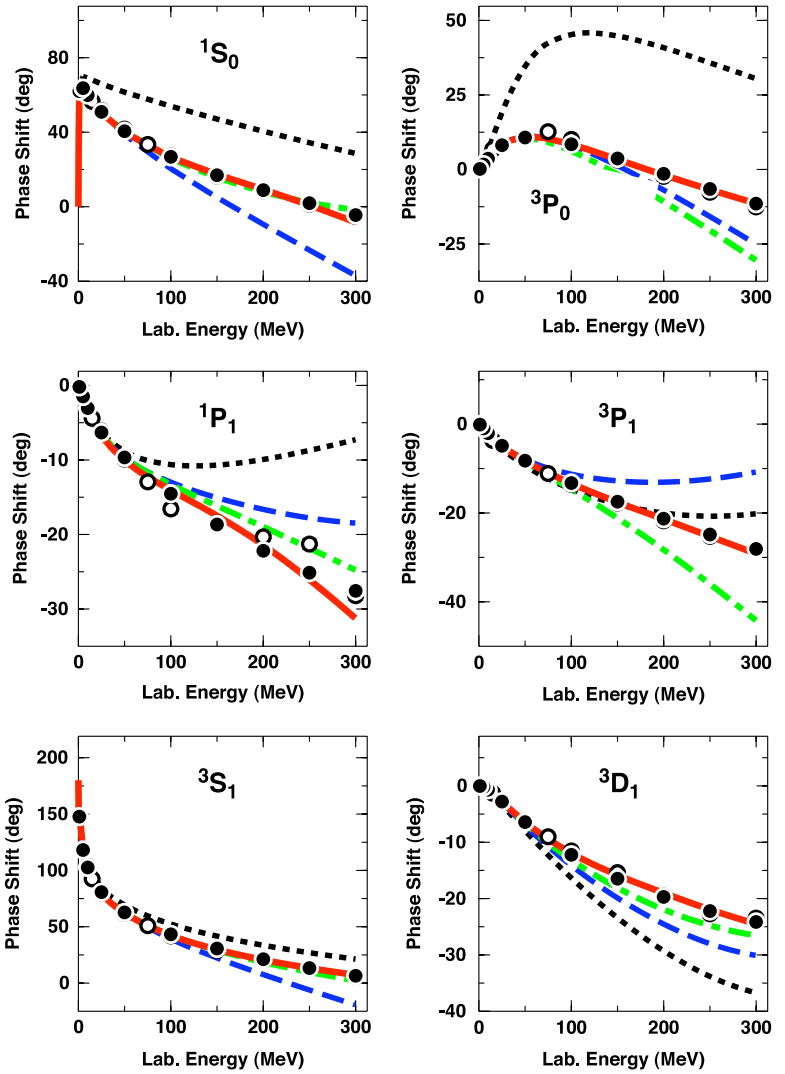

Fig. 12. Phase shifts of *np* scattering as calculated from *NN* potentials at different orders of ChPT. The black dotted line is LO (500), the blue dashed is NLO (550/700) [172], the green dash-dotted NNLO (600/700) [172], and the red solid N^{3}LO (500) [68], where the numbers in parentheses denote the cutoffs in MeV. Partial waves with total angular momentum $J \leq 1$ are displayed. Empirical phase shifts (solid dots and open circles) as in Fig. 8.

3. Add local correction terms (also known as contact or counterterms) to the effective Hamiltonian. These mimic the effects of the high-momentum states excluded by the cutoff introduced in the previous step. In the meson-exchange picture, the short-range nuclear force is described by heavy meson exchange, like the $\rho(770)$ and $\omega(782)$. However, at low energy, such structures are not resolved. Since we must include contact terms anyhow, it is most efficient to use them to account for any heavy meson exchange as well. The correction terms systematically remove dependence on the cutoff.

A first investigation in the above spirit has been conducted by Epelbaum and Meißner [155] in 2006. The authors stress that there is no point in taking the cutoff Λ beyond the breakdown scale of the EFT, $\Lambda_\chi \approx m_\rho \approx 1$ GeV, since the error of the calculation is not expected to decrease in that regime. Any value for the cutoff parameter Λ is acceptable if the error associated with its finite value is within the theoretical uncertainty at the given order. The authors conduct an investigation at LO (including only the counterterms implied by Weinberg counting) and find that, starting from $\Lambda \approx 3$ fm^{-1}, the error in the *NN* phase shifts due to keeping Λ finite stays within the theoretical uncertainty at LO.

4.5.4. Concluding the renormalization issue

Crucial for an EFT are regulator independence (within the range of validity of the EFT) and a power counting scheme that allows for order-by-order improvement with decreasing truncation error. The purpose of renormalization is to achieve this regulator independence while maintaining a functional power counting scheme. After the comprehensive tries and errors of the past, it appears that there are two renormalization schemes which have the potential to achieve the above goals and, therefore, should be investigated systematically in the near future.

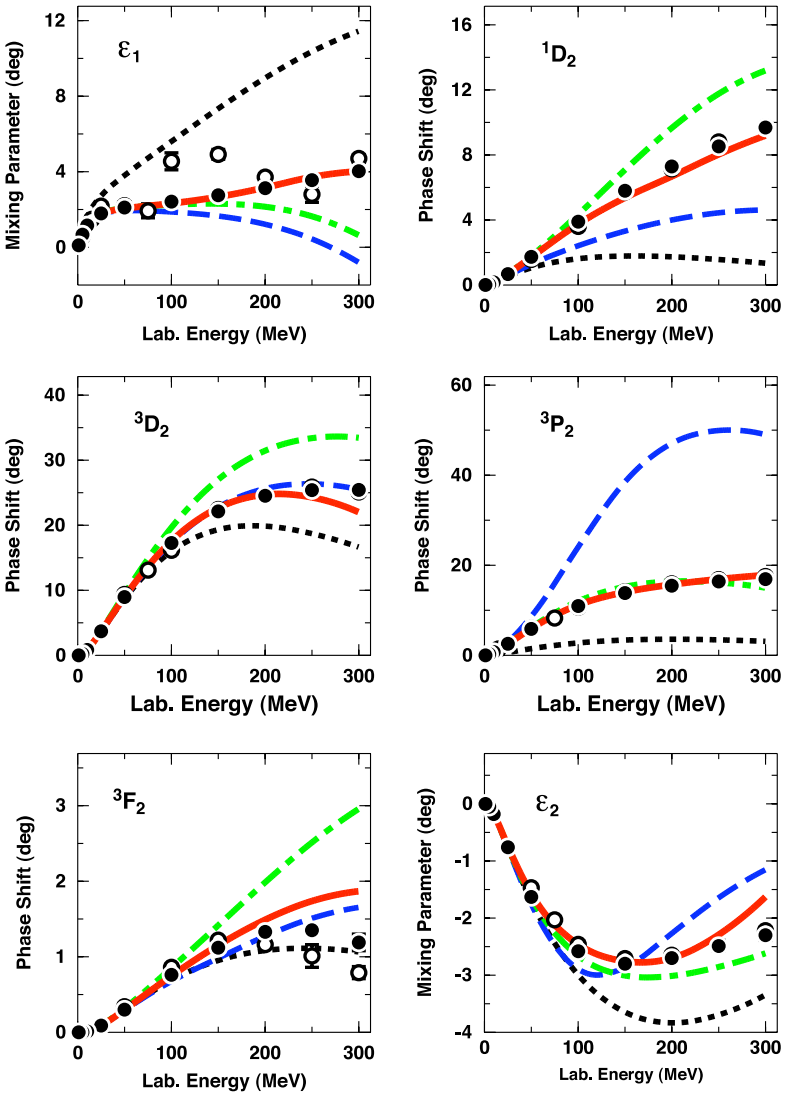

Fig. 13. Same as Fig. 12, but $J = 2$ phase shifts and $J \leq 2$ mixing parameters are shown.

In *scheme one*, the LO calculation is conducted nonperturbatively (with $\Lambda \to \infty$ as in [152]) and subleading orders are added perturbatively in distorted wave Born approximation. As mentioned above, Valderrama has started this in S waves [163], but results in higher partial waves are needed to fully assess this approach. Even though at this early stage any judgment is speculative, we take the liberty to predict that this approach will be only of limited success and utility—for the following reasons. First, it will probably require about twice as many counterterms as Weinberg counting and, therefore, will have less predictive power. Second, this scheme may converge badly, because the largest portion of the nuclear force, namely, the intermediate-range attraction appears at NNLO. Third, as discussed in Ref. [164], this force may be problematic (and, therefore, impractical) in applications in nuclear few- and many-body systems, because of a pathologically strong tensor force that will cause bad convergence of energy and wave functions. Finally, in the work that has been conducted so far within this scheme by Valderrama, it is found that only rather soft cutoffs can be used.

The latter point (namely, soft cutoffs) suggests that one may then as well conduct the calculation nonperturbatively at all orders (up to N^{3}LO) using Weinberg counting, which is no problem with soft cutoffs. This is *scheme two* that we propose to investigate systematically. In the spirit of Lepage, the cutoff independence should be examined for cutoffs below the hard scale and not beyond. Ranges of cutoff independence within the theoretical error are to be identified using 'Lepage plots' [170]. A very systematic investigation of this kind does not exist at this time and is therefore needed. However, there is comprehensive circumstantial evidence from the numerous chiral *NN* potentials constructed over the past decade [53,65–69,171] (see Figs. 14 and 15, below) indicating that this investigation will most likely be a success. The potentials discussed in the following section are all based upon Weinberg counting.

Table 3
Columns three and four show the χ^2/datum for the reproduction of the 1999 *np* database [173] (subdivided into energy intervals) by families of *np* potentials at NLO and NNLO constructed by the Juelich group [172]. The χ^2/datum is stated in terms of ranges which result from a variation of the cutoff parameters used in the regulator functions. The values of these cutoff parameters in units of MeV are given in parentheses. $T_{\rm lab}$ denotes the kinetic energy of the incident neutron in the laboratory system.

$T_{\rm lab}$ bin (MeV)	# of *np* data	Juelich *np* potentials	
		NLO (550/700–400/500)	NNLO (600/700–450/500)
0–100	1058	4–5	1.4–1.9
100–190	501	77–121	12–32
190–290	843	140–220	25–69
0–290	2402	67–105	12–27

4.6. Constructing quantitative chiral NN potentials

4.6.1. What order?

As discussed, the *NN* potential can be calculated up to various orders, cf. Eqs. (4.54)–(4.57), and the accuracy increases as the order increases. That triggers the obvious question: To what order do we have to go for an accuracy that we would perceive as necessary and sufficient for, e. g., reliable microscopic nuclear structure calculations? We had a first look at the order-by-order evolvement in Section 4.2 where we compared phase shift predictions with empirical values in peripheral partial waves. But that was only a small part of the story. The most important partial waves are the lower ones, since they generate the largest contributions in most applications. Now we have potentials at hand that are defined through all partial waves, and so we can investigate the issue of how well ChPT converges in the important lower partial waves. This is demonstrated in Figs. 12 and 13, where we show the $J \leq 2$ phase parameters for potentials constructed at LO, NLO, NNLO, and N^{3}LO. These figures clearly reveal substantial improvements in the reproduction of the empirical phase shifts as the orders go up.

There is an even better way to confront theory with experiment. We can calculate observables of *NN* scattering and compare to the experimental data. It is customary to state the result of such a comparison in terms of the χ^2/datum where a value around unity would signify a perfect fit.

Let us start with potentials developed to NLO and NNLO. In Table 3, we show the χ^2/datum for the fit of the world *np* data below 290 MeV for families of *np* potentials at NLO and NNLO constructed by the Juelich group [172]. The NLO potentials produce the very large χ^2/datum between 67 and 105, and the NNLO are between 12 and 27. The rate of improvement from one order to the other is very encouraging, but the quality of the reproduction of the *np* data at NLO and NNLO is obviously insufficient for reliable predictions.

Based upon these facts, it has been pointed out in 2002 by Entem and Machleidt [66,67] that one has to proceed to N^{3}LO. Consequently, the first N^{3}LO potential was published in 2003 [68].

At N^{3}LO, there are a total of 24 contact terms (24 parameters) which contribute to the partial waves with $L \leq 2$ (cf. Section 4.3 and Appendix E). These 24 LECs are essentially free constants which parametrize the short-ranged phenomenological part of the interaction. In Table 4, column 'Q^4/N^{3}LO', we show how these terms are distributed over the partial waves. Most important for the improved reproduction of the *NN* phase shifts (and *NN* observables) at N^{3}LO is the fact that contacts appear for the first time in *D* waves. *D* waves are not truly peripheral and, therefore, 1PE plus 2PE alone do not describe them well (Fig. 13). The *D*-wave contacts provide the necessary short-range corrections to get the *D*-phases right. Besides this, at N^{3}LO, another contact is added to each *P*-wave, which leads to substantial improvements, particularly, in $^3P_0$ and $^3P_1$ above 100 MeV (cf. Fig. 12).

In Table 4, we also show the number of parameters used in the Nijmegen partial-wave analysis (PWA93) [139] and in the high-precision CD-Bonn potential [13]. The table reveals that, for *S* and *P* waves, the number of parameters used in high-precision phenomenology and in EFT at N^{3}LO are about the same. **Thus, the EFT approach provides retroactively a justification for the phenomenology used in the 1990's to obtain high-precision fits.**

At NLO and NNLO, the number of contact parameters is substantially smaller than for PWA93 and CD-Bonn, which explains why these orders are insufficient for a quantitative potential. The 24 parameters of N^{3}LO are close to the 30+ used in PWA93 and high-precision potentials. Consequently (see following sections for details), at N^{3}LO, a fit of the *NN* data is possible that is of about the same quality as the one by the high-precision *NN* potentials [12,13,174,175]. Thus, one may perceive N^{3}LO as the order of ChPT that is necessary and sufficient for a reliable *NN* potential.

4.6.2. Charge dependence

So far we considered only neutron–proton scattering. However, as stressed repeatedly by the Nijmegen group [139,176], for a precise reproduction of the *NN* data, i.e., the *np* and the *pp* data, it is crucial to take charge dependence into account and to construct separate *np*, *pp*, and *nn* potentials which differ by the subtleties of charge dependence.

By definition, *charge independence* (or isospin symmetry) is invariance under any rotation in isospin space. A violation of this symmetry is referred to as charge dependence or charge independence breaking (CIB). *Charge symmetry* is invariance under a rotation by 180° about the *y*-axis in isospin space if the positive *z*-direction is associated with the positive charge.

Table 4
Number of parameters needed for fitting the *np* data in phase shift analysis and by a high-precision *NN* potential *versus* the total number of *NN* contact terms of EFT based potentials to different orders.

	Nijmegen partial-wave analysis [139]	CD-Bonn high-precision potential [13]	Contact potentials		
			Q^0 LO	Q^2 NLO/NNLO	Q^4 N^3LO
$^1S_0$	3	4	1	2	4
$^3S_1$	3	4	1	2	4
$^3S_1$–$^3D_1$	2	2	0	1	3
$^1P_1$	3	3	0	1	2
$^3P_0$	3	2	0	1	2
$^3P_1$	2	2	0	1	2
$^3P_2$	3	3	0	1	2
$^3P_2$–$^3F_2$	2	1	0	0	1
$^1D_2$	2	3	0	0	1
$^3D_1$	2	1	0	0	1
$^3D_2$	2	2	0	0	1
$^3D_3$	1	2	0	0	1
$^3D_3$–$^3G_3$	1	0	0	0	0
$^1F_3$	1	1	0	0	0
$^3F_2$	1	2	0	0	0
$^3F_3$	1	2	0	0	0
$^3F_4$	2	1	0	0	0
$^3F_4$–$^3H_4$	0	0	0	0	0
$^1G_4$	1	0	0	0	0
$^3G_3$	0	1	0	0	0
$^3G_4$	0	1	0	0	0
$^3G_5$	0	1	0	0	0
Total	35	38	2	9	24

The violation of this symmetry is known as charge symmetry breaking (CSB). Obviously, CSB is a special case of charge dependence.

CIB of the strong *NN* interaction means that, in the isospin $I = 1$ state, the proton–proton ($I_z = +1$), neutron–proton ($I_z = 0$), or neutron–neutron ($I_z = -1$) interactions are (slightly) different, after electromagnetic effects have been removed. CSB of the *NN* interaction refers to a difference between proton–proton (*pp*) and neutron–neutron (*nn*) interactions, only. For reviews, see Refs. [11,104,137,177–180].

CIB is seen most clearly in the $^1S_0$ *NN* scattering lengths. The latest empirical values for the singlet scattering length a and effective range r are:

$$a_{pp}^N = -17.3 \pm 0.4 \text{ fm [178]}, \qquad r_{pp}^N = 2.85 \pm 0.04 \text{ fm [178]}; \tag{4.65}$$

$$a_{nn}^N = -18.95 \pm 0.40 \text{ fm [181,182]}, \qquad r_{nn}^N = 2.75 \pm 0.11 \text{ fm [178]}; \tag{4.66}$$

$$a_{np} = -23.740 \pm 0.020 \text{ fm [13]}, \qquad r_{np} = 2.77 \pm 0.05 \text{ fm [13]}. \tag{4.67}$$

The values given for *pp* and *nn* scattering refer to the nuclear part of the interaction as indicated by the superscript N; i. e., electromagnetic effects have been removed from the experimental values.

The above values imply that charge symmetry is broken by

$$\Delta a_{CSB} \equiv a_{pp}^N - a_{nn}^N = 1.65 \pm 0.60 \text{ fm}, \tag{4.68}$$

$$\Delta r_{CSB} \equiv r_{pp}^N - r_{nn}^N = 0.10 \pm 0.12 \text{ fm}; \tag{4.69}$$

and the following CIB is observed:

$$\Delta a_{CIB} \equiv \frac{1}{2}(a_{pp}^N + a_{nn}^N) - a_{np} = 5.6 \pm 0.6 \text{ fm}, \tag{4.70}$$

$$\Delta r_{CIB} \equiv \frac{1}{2}(r_{pp}^N + r_{nn}^N) - r_{np} = 0.03 \pm 0.13 \text{ fm}. \tag{4.71}$$

In summary, the *NN* singlet scattering lengths show a small amount of CSB and a clear signature of CIB.

The current understanding is that – on a fundamental level – charge dependence ('isospin violation') is due to a difference between the up and down quark masses and electromagnetic interactions. As first discussed in Refs. [183–185], EFT is a

Table 5
Isospin breaking contributions to the *NN* interaction.

Order	Contributions
NLØ ($\nu = 2$)	Pion-mass splitting in 1PE, Static Coulomb potential.
NNLØ ($\nu = 3$)	CSB contacts without derivatives, Charge dependence of the pion–nucleon coupling constant in 1PE ($\sim \epsilon\, m_\pi^2/\Lambda_\chi^2$).
N^{3}LØ ($\nu = 4$)	CIB contacts without derivatives, Charge dependence of the pion–nucleon coupling constant in 1PE [$\sim e^2/(4\pi)^2$], Pion-mass splitting in NLO 2PE, Nucleon-mass splitting in NLO 2PE and LS equation, $\pi\gamma$ exchange, Relativistic corrections to the Coulomb potential ($\sim e^2\, Q^2/M_N^2$), Further electromagnetic corrections.

suitable tool to also deal with isospin violations. In the two-flavor case, the mass term in the QCD Lagrangian, Eq. (2.1), can be written as [cf. Eq. (2.25)]

$$\begin{aligned} -\bar{q}\,\mathcal{M}\,q &= -\frac{1}{2}\bar{q}\,(m_u + m_d) I q - \frac{1}{2}\bar{q}\,(m_u - m_d)\tau_3\, q \\ &= -\frac{1}{2}\bar{q}\,(m_u + m_d)(I - \epsilon\,\tau_3)\, q \end{aligned} \tag{4.72}$$

with

$$\epsilon = \frac{m_d - m_u}{m_u + m_d} \sim \frac{1}{3}, \tag{4.73}$$

cf. Eqs. (2.4) and (2.5). The first term of Eq. (4.72) conserves isospin but breaks chiral symmetry. It is responsible for the non-vanishing pion mass and leads to terms $\propto (m_\pi^2)^n$ (with $n \geq 1$) in the effective Lagrangian. The second term breaks isospin symmetry and generates terms proportional to $(\epsilon m_\pi^2)^n$. Note that the isospin breaking effects are much smaller than the value for ϵ suggests, because the relevant scale is Λ_χ rather than $(m_u + m_d)$.

For isospin violating effects caused by the electromagnetic interaction, the small parameter $e^2 = 4\pi\alpha \sim 1/10$ can be used (where $\alpha = 1/137.036$ denotes the fine-structure constant). It is then suggestive to consider

$$\epsilon \sim e \sim \frac{Q}{\Lambda_\chi} \tag{4.74}$$

as the general expansion parameter. For photon loops, one may further assume

$$\frac{e^2}{(4\pi)^2} \sim \frac{Q^4}{\Lambda_\chi^4}. \tag{4.75}$$

We will now briefly discuss various isospin violating contributions to the *NN* interaction listed in Table 5. For a more comprehensive and systematic study, the interested reader is referred to Ref. [186].

It is well known that the pion-mass difference is mainly due to electromagnetic interactions among the quarks and, thus, according to Eq. (4.75), of order $\nu = 4$. Therefore, the effect of pion-mass difference on 1PE can be estimated to be

$$\frac{\Delta m_\pi^2}{m_\pi^2} = \frac{\Delta m_\pi^2}{\Lambda_\chi^2}\,\frac{\Lambda_\chi^2}{m_\pi^2} \sim \frac{e^2}{(4\pi)^2}\,\frac{\Lambda_\chi^2}{m_\pi^2} \sim \frac{Q^2}{\Lambda_\chi^2}. \tag{4.76}$$

So, it is of order $\nu = 2$ or NLØ (cf. Table 5) with the slash signifying that the extended power counting scheme, Eqs. (4.74) and (4.75), is applied. This CIB effect is taken care of by replacing the $I = 1$ isospin-symmetric 1PE potential, Eq. (4.5), by

$$V_{1\pi}^{(pp)} = V_{1\pi}^{(nn)} = V_{1\pi}(m_{\pi^0}) \tag{4.77}$$

for *pp* and *nn* scattering and

$$V_{1\pi}^{(np,I=1)} = -V_{1\pi}(m_{\pi^0}) + 2\,V_{1\pi}(m_{\pi^\pm}) \tag{4.78}$$

for $I = 1$ *np* scattering, with $V_{1\pi}(m_\pi)$ defined in Eq. (4.27). If the pion masses were all the same, the above potentials would be identical. However, due to their mass splitting (Table 2), the $I = 1$ *np* potential is more attractive than the *pp* one, and this effect is known to explain about one half of the CIB scattering length difference, Eq. (4.70). For completeness, we also give the $I = 0$ *np* 1PE potential which is

$$V_{1\pi}^{(np,I=0)} = -V_{1\pi}(m_{\pi^0}) - 2\,V_{1\pi}(m_{\pi^\pm}). \tag{4.79}$$

Due to the smallness of the pion mass, 1PE is also a sizable contribution in all partial waves with $L > 0$; and due to the pion's relatively large mass splitting (3.4%), 1PE creates relatively large charge-dependent effects in all partial waves (cf. Tables V, and VI and Fig. 4 of Ref. [13]). Therefore, all modern phase shift analyses [139,140] and all modern *NN* potentials [12,13,174] include the CIB effect created by 1PE.

The other NLØ contribution (Table 5) is due to the static Coulomb interaction which is $\sim e^2$ and, therefore, also of order two. The Coulomb potential has considerable impact on the $^1S_0$ phase shifts at low energies and creates CIB effects of similar size as 1PE in *P* and *D* waves (cf. Tables V and VI and Fig. 5 of Ref. [13]). The calculation of phase shifts in the presence of the Coulomb potential is explained in Appendix A.3 of Ref. [13].

At NNLØ ($\nu = 3$), CSB contributions to the charge dependence of the pion–nucleon coupling constant ($\sim \epsilon\, m_\pi^2/\Lambda_\chi^2$) occur. However, since empirically there is no clear evidence for such charge dependence [104,132], this contribution is ignored. Moreover, at NNLØ, there is a non-derivative CSB contact term

$$\propto \epsilon\, m_\pi^2 (\bar N \tau_3 N)(\bar N N), \tag{4.80}$$

which is crucial for the fit of the CSB splitting of the $^1S_0$ scattering length, Eq. (4.68).

The leading CIB contact interactions are of electromagnetic origin and have the structure

$$\propto \frac{e^2}{(4\pi)^2} (\bar N \tau_3 N)(\bar N \tau_3 N). \tag{4.81}$$

They are obviously of order $\nu = 4$ ($\mathrm{N^3LØ}$) and needed for the fit of the CIB splitting of the $^1S_0$ scattering length, Eq. (4.70). Besides this, there are numerous other $\mathrm{N^3LØ}$ contributions (cf. Table 5). One-loop electromagnetic corrections to the pion–nucleon coupling constant create effects of order $e^2/(4\pi)^2$ in the 1PE, which will be ignored for the reasons given above. Corrections due to pion-mass difference in the NLO 2PE can be estimated to be

$$\frac{\Delta m_\pi^2}{m_\pi^2}\,\frac{Q^2}{\Lambda_\chi^2} \sim \frac{Q^4}{\Lambda_\chi^4}. \tag{4.82}$$

As explained in Refs. [187,188], these corrections can be calculated most conveniently by separating the NLO 2PE as given in Eqs. (4.9) and (4.10) into an isoscalar and an isovector piece:

$$V_{2\pi} = V_{2\pi}^0 + \boldsymbol{\tau}_1 \cdot \boldsymbol{\tau}_2\, V_{2\pi}^1. \tag{4.83}$$

The isoscalar part $V_{2\pi}^0$ is given by [187]

$$V_{2\pi}^0 = \frac{2}{3} V_{2\pi}^0(m_{\pi^\pm}, m_{\pi^\pm}) + \frac{1}{3} V_{2\pi}^0(m_{\pi^0}, m_{\pi^0}) \approx V_{2\pi}^0(\bar m_\pi, \bar m_\pi), \tag{4.84}$$

where the arguments represent the masses of the two exchanged pions, which are given in Table 2, and with $\bar m_\pi$ denoting the average pion masses defined by

$$\bar m_\pi \equiv \frac{2}{3} m_{\pi^\pm} + \frac{1}{3} m_{\pi^0} = 138.0390\ \mathrm{MeV}. \tag{4.85}$$

For the isovector part $V_{2\pi}^1$ one obtains [187,188]

$$V_{2\pi}^1 = \begin{cases} V_{2\pi}^1(m_{\pi^\pm}, m_{\pi^\pm}) & \text{for } pp \text{ and } nn, \\ 2\, V_{2\pi}^1(m_{\pi^\pm}, m_{\pi^0}) - V_{2\pi}^1(m_{\pi^\pm}, m_{\pi^\pm}) \approx V_{2\pi}^1(m_{\pi^0}, m_{\pi^0}) & \text{for } np,\ I = 1; \end{cases} \tag{4.86}$$

and for np, $I = 0$, we have $V_{2\pi} = V_{2\pi}(\bar m_\pi, \bar m_\pi)$. In conjunction with the work performed in Ref. [68], it was found that the CIB effects due to pion-mass splitting in the NLO 2PE potential are negligibly small in *P* and higher partial waves when also the pion-mass dependence of the polynomial terms is included (cf. discussion in Appendix A of Ref. [188]). However, in the $^1S_0$ state, this effect is non-negligible (causing $\Delta a_{CIB} \approx -0.5$ fm), but can be absorbed by the non-derivative CIB contact. Thus, from a procedural point of view, the CIB effect from pion-mass splitting in the NLO 2PE can simply be ignored (which is the procedure applied in Ref. [68]).

Nucleon-mass splitting in intermediate states of 2PE diagrams creates CSB as discussed in detail in Refs. [189,190]. When derived just for the NLO 2PE diagrams, this effect is $\mathrm{N^3LØ}$. Accurate calculations conducted within the framework of conventional meson theory [179] have shown that this effect is very small in *P* and higher partial waves for diagrams with only nucleon intermediate states and moderate when single Δ excitation is taken into account (which corresponds to order $\mathrm{N^4LØ}$ in Δ-less ChPT). The effect in $^1S_0$ is non-negligible, but can be absorbed by the non-derivative CSB contact term. All existing models for the *NN* interaction at $\mathrm{N^3LO}$ ignore this CSB. However, it would be worthwhile to calculate this effect accurately for chiral 2PE and compare to the comprehensive results obtained from conventional meson models [179] where it was found that the CSB splitting of the singlet scattering length can be explained by nucleon-mass difference alone.

Nucleon masses also enter the outer legs of *NN* scattering diagrams and the *LS* equation. Here, practitioners use, in general, the accurate proton and neutron masses and the proper relativistic formula for the relation between the on-shell CM momentum and the kinetic energy of the incident nucleon in the laboratory system (cf. Appendix A.3 of Ref. [13]).

Table 6
Columns three to five display the χ^2/datum for the reproduction of the 1999 ***np* database** [173] (subdivided into energy intervals) by various *np* potentials. For the chiral potentials, the χ^2/datum is stated in terms of ranges which result from a variation of the cutoff parameters used in the regulator functions. The values of these cutoff parameters in units of MeV are given in parentheses. $T_{\rm lab}$ denotes the kinetic energy of the incident nucleon in the laboratory system.

$T_{\rm lab}$ bin (MeV)	# of **np** data	Idaho N^{3}LO [68] (500–600)	Juelich N^{3}LO [171] (600/700–450/500)	Argonne V_{18} [174]
0–100	1058	1.0–1.1	1.0–1.1	0.95
100–190	501	1.1–1.2	1.3–1.8	1.10
190–290	843	1.2–1.4	2.8–20.0	1.11
0–290	2402	1.1–1.3	1.7–7.9	1.04

Irreducible $\pi\gamma$ exchange [191] causes CIB of order N^{3}LØ ($\sim e^2/(4\pi)^2$). It is a moderate effect in $^1S_0$ ($\Delta a_{CIB} \approx -0.35$ fm) and small in P and higher partial waves (cf. Ref. [13]). Some N^{3}LO potentials [68] do include this $\pi\gamma$ contribution. Corrections to the $\pi\gamma$ graphs (which are N^{4}LØ) and even $2\pi\gamma$ diagrams (N^{6}LØ) have recently been calculated by Kaiser [192–194] and found to be astonishingly large. No *NN* calculation has yet included them.

Finally, at N^{3}LØ, several corrections to the long-range electromagnetic interaction occur. The leading relativistic correction to the static Coulomb potential [176,195] is most conveniently included by replacing the fine-structure constant α by

$$\alpha' = \alpha \frac{E_p^2 + p^2}{M_p\, E_p}. \tag{4.87}$$

Other electromagnetic contributions to *pp* scattering are two-photon exchange, the Darwin–Foldy term, vacuum polarization, and the magnetic moment interaction [139,174]. In the case of *np* scattering, the electromagnetic interaction consists only of the magnetic moment contribution. The electromagnetic interactions are important contributions to the scattering amplitude. Note, however, that in the calculation of the strong nuclear phase shifts the electromagnetic interaction is only of relevance when its distortion of the wave functions affects the nuclear phase shifts in a non-negligible way. It is well known that this effect is large for the Coulomb potential in essentially all partial waves, but it is negligible for all other electromagnetic interactions in all partial waves, except $^1S_0$ below 30 MeV, where the effect can be calculated fairly model-independently and has been tabulated in Ref. [176]. Thus, in practice, it is sufficient to calculate *pp* phase shifts with only the Coulomb effect and *np* phase shifts without any electromagnetic effects (which is the way the phase shifts published in Refs. [12,13] and shown in the tables of Appendix F are calculated).

4.6.3. A quantitative NN potential at N^{3}LO

After previous sections have thoroughly prepared the terrain, we will now present a quantitative *NN* potential at N^{3}LO, including details of construction and results. We choose the Idaho N^{3}LO potential [68] as example. The isospin-symmetric part of the chiral *NN* potential at N^{3}LO is defined in Eq. (4.57) and the isospin violating terms were discussed in the previous section. Numerous parameters are involved which can be subdivided into three groups: πN LECs, *NN* contact parameters, and the cutoff parameter Λ of the regulator Eq. (4.63). For Λ we choose initially 500 MeV. Within a certain reasonable range, results should not depend sensitively on Λ (cf. discussion in Section 4.5). Therefore, we have also made a second fit for $\Lambda = 600$ MeV.

Data fitting and results for NN scattering. The fitting procedure starts with the peripheral partial waves because they involve fewer and more fundamental parameters. Partial waves with $L \geq 3$ are exclusively determined by 1PE and 2PE because the N^{3}LO contacts contribute to $L \leq 2$ only. 1PE and 2PE at N^{3}LO depend on the axial-vector coupling constant, g_A (we use $g_A = 1.29$), the pion decay constant, $f_\pi = 92.4$ MeV, and eight low-energy constants (LECs) that appear in the dimension-two and dimension-three πN Lagrangians, Eqs. (2.57) and (2.58). The LECs are listed in Table 2, where column '*NN* Potential' shows the values used for the present N^{3}LO potential. In the fitting process, we varied three of them, namely, c_2, c_3, and c_4. We found that the other LECs are not very effective in the *NN* system and, therefore, we left them at their central values as determined in πN analysis. The most influential constant is c_3, which – in terms of magnitude – has to be chosen on the low side (slightly more than one standard deviation below its πN determination), otherwise there is too much central attraction. Concerning c_4, our choice $c_4 = 5.4$ GeV^{-1} lowers the $^3F_2$ phase shift (and slightly the $^1F_3$) bringing it into closer agreement with the phase shift analysis—as compared to using the πN value $c_4 = 3.4$ GeV^{-1}. The other F waves and the higher partial waves are essentially unaffected by this variation of c_4. Finally, the change of c_2 from its πN value of 3.28 GeV^{-1} to 2.80 GeV^{-1} (our choice) brings about some subtle improvements of the fit, but it is not essential. Overall, the fit of all $J \geq 3$ waves is very good. The F-wave phase shifts are, in fact, described better than in the perturbative calculation shown in Fig. 8 because the regulator moderates the attractive surplus, thus, simulating correctly higher order contributions beyond the present order.

We turn now to the lower partial waves. Here, the most important fit parameters are the ones associated with the 24 contact terms that contribute to the partial waves with $L \leq 2$ (cf. Section 4.3 and Table 4). In addition, we have two charge-dependent contacts which are used to fit the three different $^1S_0$ scattering lengths, a_{pp}, a_{nn}, and a_{np}.

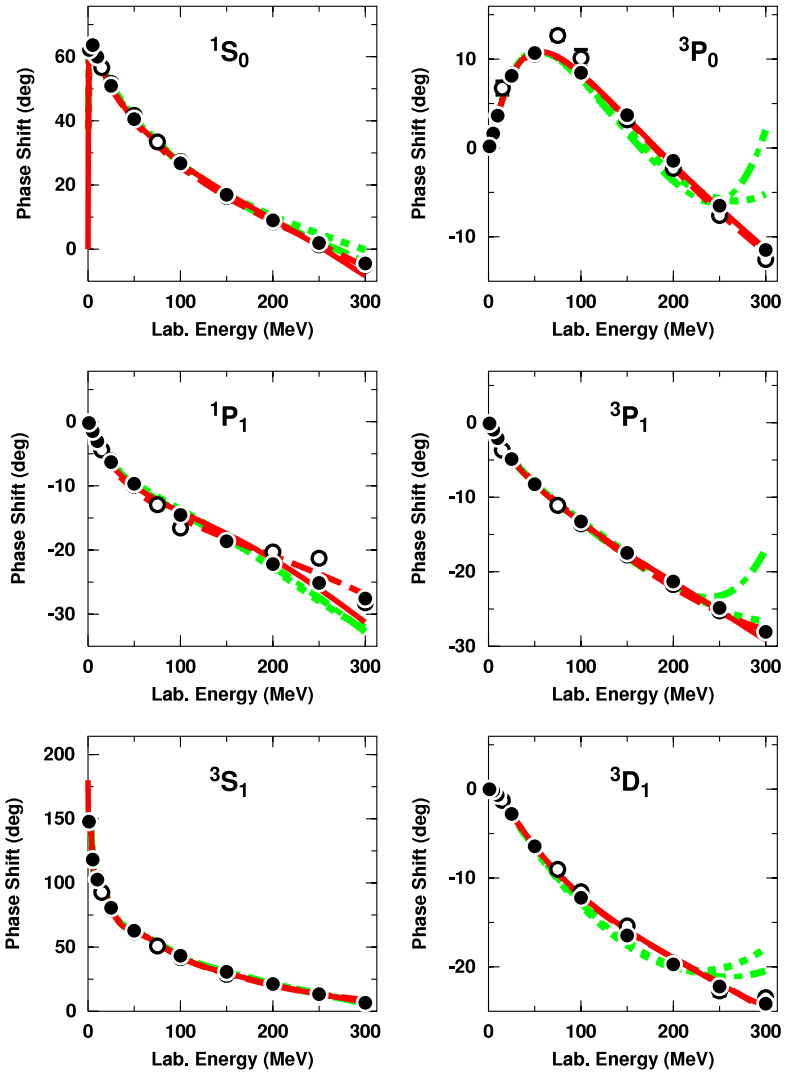

Fig. 14. Neutron–proton phase parameters as described by various chiral potentials at N^{3}LO. The (red) solid and the dashed curves are calculated from Idaho N^{3}LO potentials [68] with $\Lambda = 500$ and 600 MeV, respectively; while the (green) dash-dotted and the dotted curves are based upon Juelich N^{3}LO potentials [171] with cutoff combinations 600/700 and 450/500 MeV, respectively. Partial waves with total angular momentum $J \leq 1$ are displayed. Empirical phase shifts (solid dots and open circles) as in Fig. 8.

In the optimization procedure, we fit first phase shifts, and then we refine the fit by minimizing the χ^2 obtained from a direct comparison with the data. We start with *pp*, since the *pp* phase shifts and data are more accurate than the *np* ones. The *pp* fit fixes essentially the $I = 1$ potential. The $I = 1$ *np* potential is just the *pp* one modified by charge dependence due to nucleon-mass difference, pion-mass splitting in 1PE, $\pi\gamma$ exchange, and omission of Coulomb (as discussed in Section 4.6.2). In addition to this, the non-derivative contact in the $^1S_0$ state is changed such as to reproduce the *np* scattering length. The *nn* potential is the *pp* one without Coulomb, using neutron masses, and fitting the *nn* scattering length in the $^1S_0$ state with the non-derivative contact.

The χ^2/datum for the fit of the *np* data below 290 MeV are shown in Table 6, and the corresponding ones for *pp* are given in Table 7. These tables reveal that at N^{3}LO a χ^2/datum comparable to the high-precision Argonne V_{18} [174] potential can, indeed, be achieved. The Idaho N^{3}LO potential [68] with $\Lambda = 500$ MeV produces a χ^2/datum $= 1.1$ for the world *np* data below 290 MeV which compares well with the χ^2/datum $= 1.04$ by the Argonne potential. In 2005, also the Juelich group produced several N^{3}LO *NN* potentials [171], the best of which fits the *np* data with a χ^2/datum $= 1.7$ and the worse with 7.9 (Table 6).

Turning to *pp*, the χ^2 for *pp* data are typically larger than for *np* because of the higher precision of *pp* data. Thus, the Argonne V_{18} produces a χ^2/datum $= 1.4$ for the world *pp* data below 290 MeV and the best Idaho N^{3}LO *pp* potential obtains 1.5. The fit by the best Juelich N^{3}LO *pp* potential results in a χ^2/datum $= 2.9$ and the worst produces 22.3.

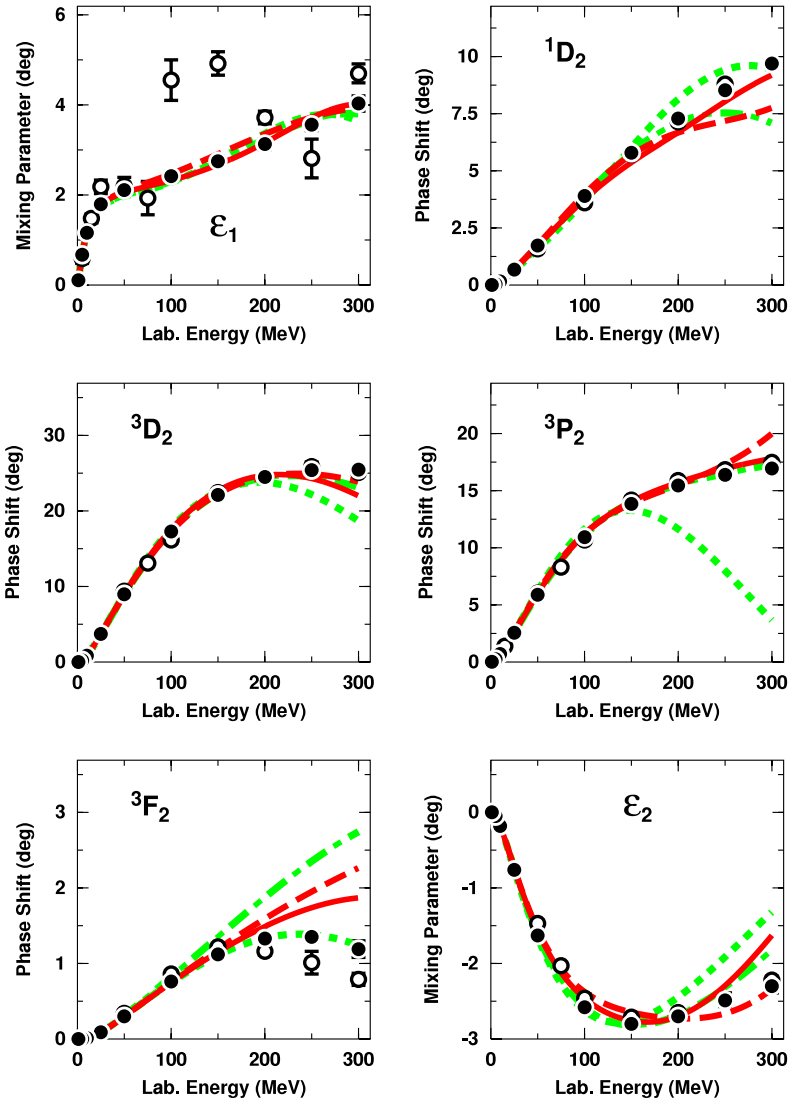

Fig. 15. Same as Fig. 14 but $J = 2$ phase shifts and $J \leq 2$ mixing parameters are shown.

Table 7
Same as Table 6 but for ***pp***.

T_{lab} bin (MeV)	# of **pp** data	Idaho N^{3}LO [68] (500–600)	Juelich N^{3}LO [171] (600/700–450/500)	Argonne V_{18} [174]
0–100	795	1.0–1.7	1.0–3.8	1.0
100–190	411	1.5–1.9	3.5–11.6	1.3
190–290	851	1.9–2.7	4.3–44.4	1.8
0–290	2057	1.5–2.1	2.9–22.3	1.4

Phase shifts of *np* scattering from two Idaho (solid and dashed lines) and two Juelich (dash-dotted and dotted lines) N^{3}LO *np* potentials are shown in Figs. 14 and 15. The phase shifts confirm what the corresponding χ^2 have already revealed. Low-energy scattering parameters are listed in Table 8. A few more technical details and tables with numerical values for contact and phase parameters are provided in Appendix F.

The deuteron. The reproduction of the deuteron parameters is shown in Table 9. We present results for two N^{3}LO potentials, namely, Idaho [68] with $\Lambda = 500$ MeV and Juelich [171] with cutoff combination 550/600 MeV. Remarkable are the predictions by the chiral potentials for the deuteron radius which are in good agreement with the latest empirical value obtained by the isotope-shift method [197]. All *NN* potentials of the past (Table 9 includes two representative examples, namely, CD-Bonn [13] and AV18 [174]) fail to reproduce this very precise new value for the deuteron radius.

Table 8
Scattering lengths (a) and effective ranges (r) in units of fm. (a_{pp}^C and r_{pp}^C refer to the pp parameters in the presence of the Coulomb force. a^N and r^N denote parameters determined from the nuclear force only and with all electromagnetic effects omitted.)

	Idaho N^{3}LO [68] (500)	Juelich N^{3}LO [171] (550/600)	CD-Bonn [13]	AV18 [174]	Empirical
$^1S_0$					
a_{pp}^C	−7.8188	−7.8003	−7.8154	−7.8138	−7.8196(26) [176] −7.8149(29) [196]
r_{pp}^C	2.795	2.737	2.773	2.787	2.790(14) [176] 2.769(14) [196]
a_{pp}^N	−17.083	−16.423	−17.460	−17.164	
r_{pp}^N	2.876	2.828	2.845	2.865	
a_{nn}^N	−18.900	−18.900	−18.968	−18.818	−18.95(40) [181,182]
r_{nn}^N	2.838	2.770	2.819	2.834	2.75(11) [178]
a_{np}	−23.732	−23.613	−23.738	−23.732	−23.740(20) [13]
r_{np}	2.725	2.651	2.671	2.697	[2.77(5)] [13]
$^3S_1$					
a_t	5.417	5.417	5.420	5.419	5.419(7) [13]
r_t	1.752	1.742	1.751	1.753	1.753(8) [13]

Table 9
Deuteron properties as predicted by various NN potentials are compared to empirical information. (Deuteron binding energy B_d, asymptotic S state A_S, asymptotic D/S state η, deuteron radius r_d, quadrupole moment Q, D-state probability P_D; the calculated r_d and Q are without meson-exchange current contributions and relativistic corrections.)

	Idaho N^{3}LO [68] (500)	Juelich N^{3}LO [171] (550/600)	CD-Bonn [13]	AV18 [174]	Empirical[a]
B_d (MeV)	2.224575	2.218279	2.224575	2.224575	2.224575(9)
A_S (fm$^{-1/2}$)	0.8843	0.8820	0.8846	0.8850	0.8846(9)
η	0.0256	0.0254	0.0256	0.0250	0.0256(4)
r_d (fm)	1.975	1.977	1.966	1.967	1.97535(85)
Q (fm^2)	0.275	0.266	0.270	0.270	0.2859(3)
P_D (%)	4.51	3.28	4.85	5.76	

[a] See Table XVIII of Ref. [13] for references; the empirical value for r_d is from Ref. [197].

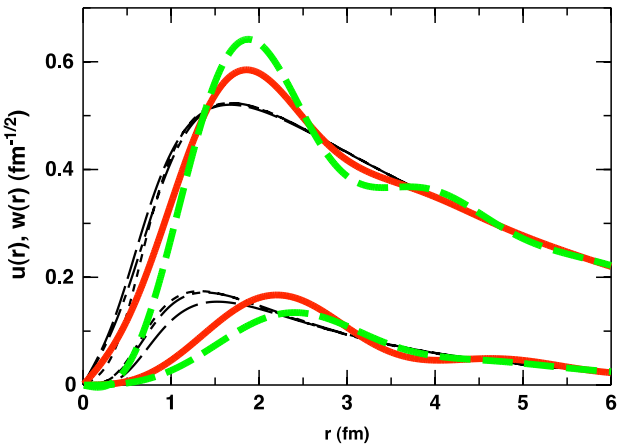

Fig. 16. Deuteron wave functions: the family of larger curves are S waves, the smaller ones D waves. The thick colored lines represent the wave functions derived from chiral NN potentials at order N^{3}LO (red solid: Idaho (500) [68], green dashed: Juelich (550/600) [171]). The thin dashed, dash-dotted, and dotted lines refer to the wave functions of the CD-Bonn [13], Nijm-I [12], and AV18 [174] potentials, respectively.

In Fig. 16, we display the deuteron wave functions derived from the N^{3}LO potentials and compare them with wave functions based upon conventional NN potentials from the recent past. Characteristic differences are noticeable; in particular, the chiral wave functions are shifted towards larger r due to softer cutoffs and the effect of the contact terms, which explains the larger deuteron radius.

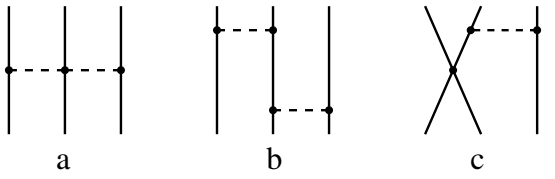

Fig. 17. Three-nucleon force diagrams at NLO. Notation as in Fig. 1.

5. Nuclear many-body forces

The chiral 2NF discussed in the previous section has been applied in microscopic calculations of nuclear structure with, in general, a great deal of success [75–88]. However, from high-precision studies conducted in the 1990s, it is well known that certain few-nucleon reactions and nuclear structure issues require 3NFs for their microscopic explanation. Outstanding examples are the A_y puzzle of N–d scattering [198,199] and the ground state of ^{10}B [200]. As noted before, an important advantage of the EFT approach to nuclear forces is that it creates two- and many-nucleon forces on an equal footing (cf. the overview given in Fig. 1). In this section, we will explain in some detail chiral three- and four-nucleon forces. We will limit our presentation to the isospin-symmetric case; isospin violating 3NFs are discussed in Ref. [201].

5.1. Three-nucleon forces

Nuclear three-body forces in ChPT were initially discussed by Weinberg [52] and the 3NF at NNLO was first derived by van Kolck [70].

For a 3NF, we have $A = 3$ and $C = 1$ and, thus, Eq. (3.4) implies

$$\nu = 2 + 2L + \sum_i \Delta_i. \tag{5.1}$$

We will use this equation to analyze 3NF contributions order by order.

5.1.1. Next-to-leading order

The lowest possible power is obviously $\nu = 2$ (NLO), which is obtained for no loops ($L = 0$) and only leading vertices ($\sum_i \Delta_i = 0$). We display typical graphs in Fig. 17. As discussed by Weinberg [52], the contributions from these diagrams vanish at NLO. To see this, let us first look at graph (a), which contains a Weinberg–Tomozawa vertex, Eq. (A.43), that includes a time-derivative of a pion field. Since this diagram does not involve reducible topologies, it can be treated as a Feynman diagram in which energy is conserved at each vertex, so that the time-derivative yields a difference of nucleon kinetic energies $\sim Q^2/M_N$ instead of $\sim Q$. Thus, the contribution from this graph is suppressed by a factor Q/M_N and demoted to NNLO. Graphs (b) and (c) of Fig. 17 are best discussed in terms of time-ordered perturbation theory. Weinberg [52] and van Kolck [70] showed that, at NLO, the irreducible topologies of these graphs cancel against the recoil corrections from the reducible ones, leaving no net irreducible 3N contribution. What remains is just the iteration of the static 2N potentials. In fact, this had been pointed out already by Yang and Glöckle [127] and Coon and Friar [128] in the 1980's.

The bottom line is that there is no genuine 3NF contribution at NLO. The first non-vanishing 3NF appears at NNLO.

5.1.2. Next-to-next-to-leading order

The power $\nu = 3$ (NNLO) is obtained when there are no loops ($L = 0$) and $\sum_i \Delta_i = 1$, i.e., $\Delta_i = 1$ for one vertex while $\Delta_i = 0$ for all other vertices. There are three topologies which fulfill this condition, known as the two-pion exchange (2PE), 1PE, and contact graphs [70,71] (Fig. 18).

Using the subleading vertices equations (A.51) and (A.52), it is straightforward to derive the 2PE 3N potential to be

$$V_{\rm 2PE}^{\rm 3NF} = \left(\frac{g_A}{2f_\pi}\right)^2 \frac{1}{2} \sum_{i\neq j\neq k} \frac{(\vec\sigma_i\cdot\vec q_i)(\vec\sigma_j\cdot\vec q_j)}{(q_i^2+m_\pi^2)(q_j^2+m_\pi^2)}\, F_{ijk}^{ab}\, \tau_i^a \tau_j^b \tag{5.2}$$

with $\vec q_i \equiv \vec p_i{}' - \vec p_i$, where $\vec p_i$ and $\vec p_i{}'$ are the initial and final momenta of nucleon i, respectively, and

$$F_{ijk}^{ab} = \delta^{ab}\left[-\frac{4c_1 m_\pi^2}{f_\pi^2} + \frac{2c_3}{f_\pi^2}\,\vec q_i\cdot\vec q_j\right] + \frac{c_4}{f_\pi^2}\sum_c \epsilon^{abc}\,\tau_k^c\,\vec\sigma_k\cdot[\vec q_i\times\vec q_j]\,. \tag{5.3}$$

There are great similarities between this force and earlier derivations of 2PE 3NFs, notably the 50-year-old Fujita–Miyazawa [202], the Tucson-Melbourne (TM) [203], and the Brazil [204] forces. A thorough comparison between various 2PE 3NFs is conducted in Ref. [205] resulting in the recommendation to drop the so-called "c-term" from the TM force, since it does not have an equivalent in the ChPT derived force, Eqs. (5.2) and (5.3), giving rise to the construction of the TM' (or TM99) force [206].

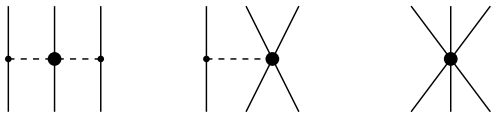

Fig. 18. The three-nucleon force at NNLO. From left to right: 2PE, 1PE, and contact diagrams. Notation as in Fig. 1.

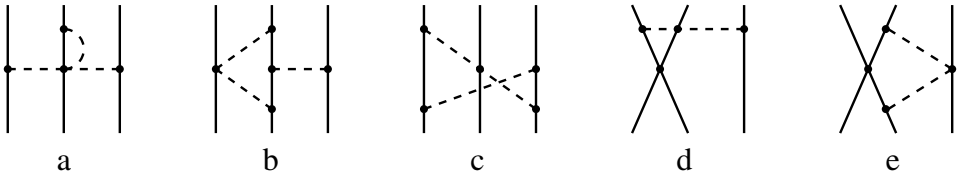

Fig. 19. Leading one-loop 3NF diagrams at N^{3}LO. We show one representative example for each of five topologies, which are: (a) 2PE, (b) 1PE–2PE, (c) ring, (d) contact-1PE, (e) contact-2PE. Notation as in Fig. 1.

Notice that Eq. (5.3) does not include a c_2-term. Due to two time-derivatives, the contribution from the c_2 vertex is $(Q/M_N)^2$ suppressed and demoted by two orders. Note also that the 2PE 3NF does not contain any new parameters, because the LECs c_1, c_3, and c_4 appear already in the 2PE 2NF (Section 4.1.2) and are fixed by πN and/or NN data.

The other two 3NF contributions shown in Fig. 18 are easily derived by taking the last two terms of the $\Delta = 1$ Lagrangian, Eq. (2.66), into account. The 1PE contribution is

$$V_{\rm 1PE}^{\rm 3NF} = -D\,\frac{g_A}{8f_\pi^2}\sum_{i\neq j\neq k}\frac{\vec\sigma_j\cdot\vec q_j}{q_j^2+m_\pi^2}(\boldsymbol\tau_i\cdot\boldsymbol\tau_j)(\vec\sigma_i\cdot\vec q_j) \tag{5.4}$$

and the 3N contact potential reads

$$V_{\rm ct}^{\rm 3NF} = E\,\frac{1}{2}\sum_{j\neq k}\boldsymbol\tau_j\cdot\boldsymbol\tau_k. \tag{5.5}$$

These 3NF terms involve the two new parameters D and E, which do not appear in the 2N problem. There are many ways to pin these two parameters down. In Ref. [71], the triton binding energy and the nd doublet scattering length $^2a_{nd}$ were used. One may also choose the binding energies of ^{3}H and ^{4}He [98] or an optimal over-all fit of the properties of light nuclei [99]. Exploiting the consistency of interactions and currents in ChPT [207], the parameter D of the $\pi NNNN$ vertex involved in the 1PE 3NF can be constrained by p-wave pion-production data [208] or electroweak processes like the tritium β-decay [209] or proton–proton fusion ($p\,p\,\rightarrow\,d\,e^+\,\nu_e$) [210]. Once D and E are fixed, the results for other 3N, 4N, etc. observables are predictions.

The 3NF at NNLO has been applied in calculations of few-nucleon reactions [71,89–97], structure of light- and medium-mass nuclei [98–101], and nuclear and neutron matter [102,103] with a good deal of success. Yet, the famous 'A_y puzzle' of nucleon–deuteron scattering is not resolved [71,94]. When only 2NFs are applied, the analyzing power in p–^{3}He scattering is even more underpredicted than in p–d [74,211]. However, when the NNLO 3NF is added, the p–^{3}He A_y substantially improves (more than in p–d) [97]—but a discrepancy remains. Furthermore, the spectra of light nuclei leave room for improvement [99].

We note that there are further 3NF contributions at NNLO, namely, the $1/M_N$ corrections of the NLO 3NF diagrams (Fig. 17). Some of these terms involve the vertices equations (A.49) and (A.50), and the $1/M_N$ correction of the c_4 vertex, Eq. (A.52); others are due to higher order recoil corrections. Several of those contributions have been calculated by Coon and Friar in 1986 [128]. These corrections are believed to be very small.

To summarize, the 3NF at NNLO is a remarkable contribution: It represents the leading many-body force within the scheme of ChPT; it includes terms that were advocated already some 50 years ago; and it produces noticeable improvements in few-nucleon reactions and the structure of light nuclei. But unresolved problems remain. Moreover, in the case of the 2NF, we have seen that one has to proceed to N^{3}LO to achieve sufficient accuracy. Therefore, the 3NF at N^{3}LO is needed for at least two reasons: for consistency with the 2NF and to hopefully resolve outstanding problems in microscopic structure and reactions.

5.1.3. Next-to-next-to-next-to-leading order

According to Eq. (5.1), the value $\nu = 4$, which corresponds to N^{3}LO, is obtained for the following classes of diagrams.

3NF loop diagrams at N^{3}LO. For this group of graphs, we have $L = 1$ and, therefore, all Δ_i have to be zero to ensure $\nu = 4$. Thus, these one-loop 3NF diagrams can include only leading vertices, the parameters of which are fixed from πN and NN analysis. We show five representative examples of this very large class of diagrams in Fig. 19. One sub-group of these diagrams (2PE graphs) has been calculated by Ishikawa and Robilotta [72], and two other topologies (1PE–2PE and ring

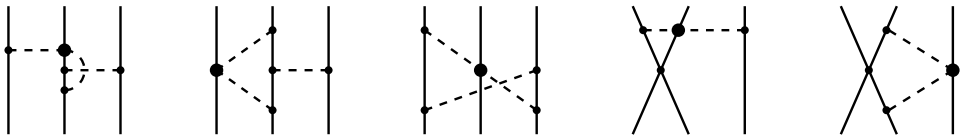

Fig. 20. Subleading one-loop 3NF diagrams which appear at N^{4}LO. Notation as in Fig. 1.

diagrams) have been evaluated by the Bonn–Jülich group [73]. The remaining topologies, which involve a leading four-nucleon contact term [diagrams (d) and (e) of Fig. 19], are under construction by the Bonn–Jülich group. The N^{3}LO 2PE 3NF has been applied in the calculation of nucleon–deuteron observables in Ref. [72] producing very small effects.

The smallness of the 2PE loop 3NF at N^{3}LO is not unexpected. It is consistent with experience with corresponding 2NF diagrams: the NLO 2PE contribution to the *NN* potential, which involves one loop and only leading vertices (Fig. 3), is also relatively small (Fig. 8).

By the same token, one may expect that also all the other N^{3}LO 3NF loop topologies will produce only small effects.

3NF tree diagrams at N^{3}LO. The order $\nu = 4$ is also obtained for the combination $L = 0$ (no loops) and $\sum_i \Delta_i = 2$. Thus, either two vertices have to carry $\Delta_i = 1$ or one vertex has to be of the $\Delta_i = 2$ kind, while all other vertices are $\Delta_i = 0$. This is achieved if in the NNLO 3NF graphs of Fig. 18 the power of one vertex is raised by one. The latter happens if a relativistic $1/M_N$ correction is applied. A closer inspection reveals that all $1/M_N$ corrections of the NNLO 3NF vanish and the first non-vanishing corrections are proportional to $1/M_N^2$ and appear at N^{4}LO. However, there are non-vanishing $1/M_N^2$ corrections of the NLO 3NF and there are so-called drift corrections [212] which contribute at N^{3}LO (some drift corrections are claimed to contribute even at NLO [212]). We do not expect these contributions to be sizable. Moreover, there are contributions from the $\Delta_i = 2$ Lagrangian [123] proportional to the low-energy constants d_i. As it turns out, these terms have at least one time-derivative, which causes them to be Q/M_N suppressed and demoted to N^{4}LO.

Thus, besides some minor $1/M_N^2$ corrections, there are no tree contributions to the 3NF at N^{3}LO.

Summarizing the 3NF at N^{3}LO: For the reasons discussed, we anticipate that this 3NF is weak and will not solve any of the outstanding problems. In view of this expectation, we have to look for more sizable 3NF contributions elsewhere.

5.1.4. *The 3NF at* N^{4}LO

The obvious step to take is to proceed to the next order, N^{4}LO or $\nu = 5$. Some of the tree diagrams that appear at this order were mentioned already: the $1/M_N^2$ corrections of the NNLO 3NF and the trees with one d_i vertex which are $1/M_N$ suppressed. Because of the suppression factors, we do not expect sizable effects from these graphs. Moreover, there are also tree diagrams with one vertex from the $\Delta_i = 3$ πN-Lagrangian [122,213] proportional to the LECs e_i. Because of the high dimension of these vertices and assuming reasonable convergence, we do not anticipate much from these trees either.

However, we believe that the loop contributions that occur at this order are truly important. They are obtained by replacing in the N^{3}LO loops (Fig. 19) one vertex by a $\Delta_i = 1$ vertex. We show five examples of this large group of diagrams in Fig. 20. This 3NF is presumably large and, thus, what we are looking for.

The reasons, why these graphs are large, can be argued as follows. Corresponding 2NF diagrams are the three-pion-exchange (3PE) contributions to the *NN* interaction. In analogy to Figs. 19 and 20, there are 3PE 2NF diagrams with only leading vertices (Fig. 7) and the ones with one (subleading) c_i vertex (and the rest leading). These diagrams have been evaluated by Kaiser in Refs. [57–59], respectively. Kaiser finds that the 3PE contributions with one subleading vertex are about an order magnitude larger than the leading ones.

5.1.5. *3NF summary*

To make a complicated story short, this is the bottom line concerning 3NF [162]:

- The leading chiral 3NF (that appears at NNLO) is sizable, improves predictions, but also leaves unresolved problems. Therefore, additional *sizable* 3NF contributions are needed.
- The chiral 3NF at N^{3}LO involves only leading vertices and most likely does *not* produce sizable contributions.
- Sizable contributions are expected from the subleading one-loop 3NF diagrams that occur at N^{4}LO. *These 3NF contributions may turn out to be the missing pieces in the 3NF puzzle and have the potential to solve the outstanding problems in microscopic nuclear structure.*

5.2. *Four-nucleon forces*

Formally, the lowest order four-nucleon force (4NF) occurs for two separately interacting nucleon pairs with leading vertices and no loops, Fig. 21. This scenario is characterized by $A = 4, C = 2, L = 0$, and $\sum_i \Delta_i = 0$ and therefore, according to Eq. (3.4), has the power $\nu = 2$ (NLO). However, similar to the NLO 3NF [Fig. 17 (b) and (c)], the 4NF diagrams of Fig. 21 cancel against the recoil corrections from corresponding iterative diagrams [70]. The disconnected 4NF diagrams of order

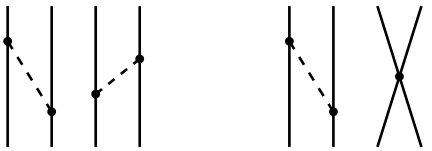

Fig. 21. Disconnected four-nucleon force diagrams at NLO, which cancel against the recoil corrections from corresponding iterative diagrams.

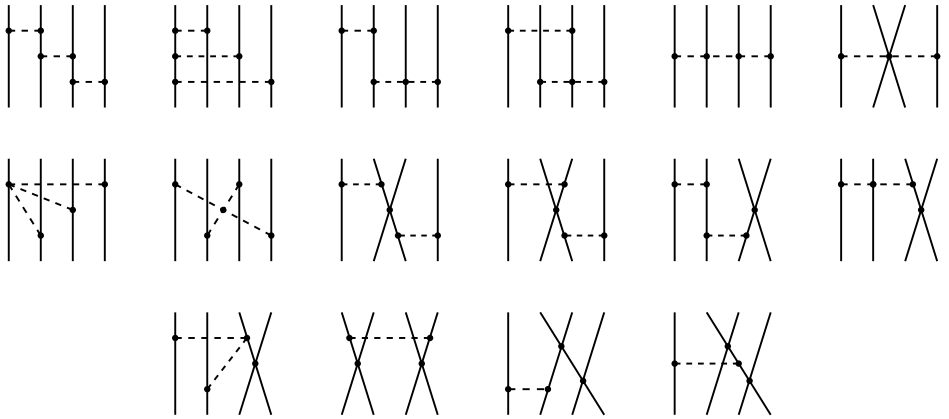

Fig. 22. Leading four-nucleon force at N^{3}LO.

four, which are obtained for either $L = 1$ or $\sum_i \Delta_i = 2$, also cancel [214]. Thus, we are left with just the connected ($C = 1$) $A = 4$ diagrams for which Eq. (3.4) yields

$$\nu = 4 + 2L + \sum_i \Delta_i. \tag{5.6}$$

Therefore, a connected 4NF appears for the first time at $\nu = 4$ (N^{3}LO), with no loops and only leading vertices, Fig. 22. This 4NF includes no new parameters and does not vanish [214,215]. Some graphs in Fig. 22 appear to be reducible (iterative). Note, however, that these are Feynman diagrams, which are best analyzed in terms of time-ordered perturbation theory. The various time-orderings include also some irreducible topologies (which are, by definition, 4NFs). Or, in other words, the Feynman diagram minus the reducible part of it yields the (irreducible) contribution to the 4NF. The reducible part depends on the two-, three-, and four-body scattering equations used.

Assuming a good rate of convergence, a contribution of order $(Q/\Lambda_\chi)^4$ is expected to be rather small. Thus, ChPT predicts 4NF to be essentially insignificant, consistent with experience. Still, nothing is fully proven in physics unless we have performed explicit calculations. Recently, the leading 4NF (Fig. 22) has been applied in a calculation of the ^{4}He binding energy, where it contributes a few 100 keV [216]. It should be noted that this preliminary calculation involves many approximations, but it certainly provides the right order of magnitude of the result, which is indeed very small as compared to the full ^{4}He binding energy of 28.3 MeV.

6. Introducing Δ-isobar degrees of freedom

The lowest excited state of the nucleon is the $\Delta(1232)$ resonance or isobar (a π–N P-wave resonance with both spin and isospin 3/2) with an excitation energy of $\Delta M = M_\Delta - M_N = 293$ MeV. Because of its strong coupling to the π–N system and low excitation energy, it is an important ingredient for models of pion–nucleon scattering in the Δ-region and pion production from the two-nucleon system at intermediate energies, where the particle production proceeds prevailingly through the formation of Δ isobars [11]. At low energies, the more sophisticated conventional models for the 2π-exchange contribution to the NN interaction include the virtual excitation of Δ's, which in these models accounts for about 50% of the intermediate-range attraction of the nuclear force—as demonstrated by the Bonn potential [20,217].

Because of its relatively small excitation energy, it is not clear from the outset if, in an EFT, the Δ should be taken into account explicitly or integrated out as a "heavy" degree of freedom. If it is included, then $\Delta M \sim m_\pi$ is considered as another small expansion parameter, besides the pion mass and small external momenta. This scheme has become known as the small scale expansion (SSE) [218]. Note, however, that this extension is of phenomenological character, since ΔM does not vanish in the chiral limit.

In the chiral EFT discussed so far in this report (also known as the "Δ-less" theory), the effects due to Δ isobars are taken into account implicitly. Note that the dimension-two LECs, the c_i, have unnaturally large values (cf. Table 2). The reason for this is that the Δ-isobar (and some meson resonances) contribute considerably to the c_i—a mechanism that has become

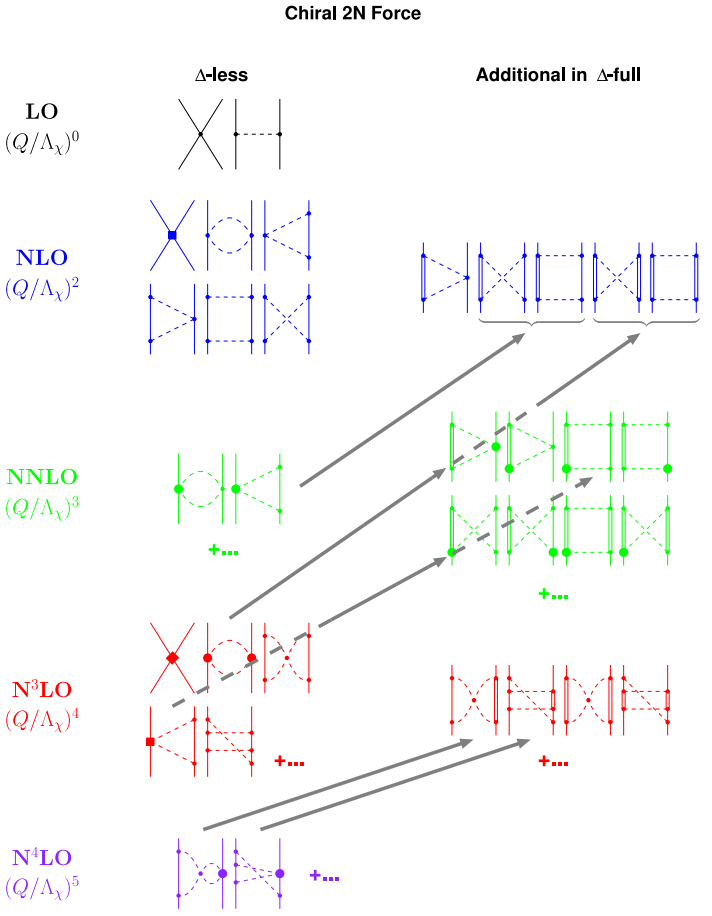

Fig. 23. Chiral 2NF without and with Δ-isobar degrees of freedom. Arrows indicate the shift of strength when explicit Δ's are added to the theory. Note that the Δ-full theory consists of the diagrams involving Δ's *plus* the Δ-less ones. Double lines represent Δ-isobars; remaining notation as in Fig. 1.

known as resonance saturation [219]. Therefore, the explicit inclusion of the Δ ("Δ-full" theory) will take strength out of these LECs and move this strength to a lower order [53,56,220–222]. As a consequence, the convergence of the expansion improves, which is another motivation for introducing explicit Δ-degrees of freedom. We observed that, in the Δ-less theory, the subleading 2PE and 3PE contributions to the 2NF are larger than the leading ones. The promotion of large contributions by one order in the Δ-full theory fixes this problem.

In the heavy baryon formalism, the leading Lagrangian involving Δ's reads [54,70] (listing only terms relevant to our present discussion)

$$\widehat{\mathcal{L}}_{\Delta}^{\Delta_i=0} = \bar{\Delta}(i\partial_0 - \Delta M)\Delta - \frac{h_A}{2f_\pi}\left(\bar{N}\mathbf{T}\vec{S}\Delta + \text{h.c.}\right)\cdot\nabla\boldsymbol{\pi} - D_T\,\bar{N}\boldsymbol{\tau}\vec{\sigma}N\cdot\left(\bar{N}\mathbf{T}\vec{S}\Delta + \text{h.c.}\right), \tag{6.1}$$

where Δ is a four-component spinor in both spin and isospin space representing the Δ-isobar and h_A and D_T are LECs.[5] Moreover, S^i are 2×4 spin transition matrices which satisfy $S^iS^{i\dagger} = (2\delta^{ij} - i\epsilon^{ijk}\sigma^k)/3$ and T^a are similar isospin matrices with $T^aT^{b\dagger} = (2\delta^{ab} - i\epsilon^{abc}\tau^c)/3$. Notice that, due to the heavy baryon expansion, the mass of the Δ-isobar, M_Δ, has disappeared and only the small mass difference ΔM enters.

The LECs of the πN Lagrangian are usually extracted in the analysis of π–N scattering data and clearly come out differently in the Δ-full theory as compared to the Δ-less one. While in the Δ-less theory, the magnitude of the LECs c_3 and c_4 is about 3–5 GeV^{-1} (cf. Table 2), they turn out to be around 1 GeV^{-1} in the Δ-full theory [221].

In the 2NF, the virtual excitation of Δ-isobars requires at least one loop and, thus, the contribution occurs first at $\nu = 2$ (NLO), see Fig. 23. The Δ contributions to the 2PE were first evaluated in Refs. [53,54,220] using time-ordered perturbation theory and later by Kaiser et al. [56] in covariant perturbation theory. Recently, also the NNLO contributions have been worked out [221]. Krebs et al. [221] verified the consistency between the Δ-full and Δ-less theories by showing that the

[5] Our convention for h_A is consistent with Refs. [54,56,70,107] and differs by a factor of two from Refs. [218,221,223].

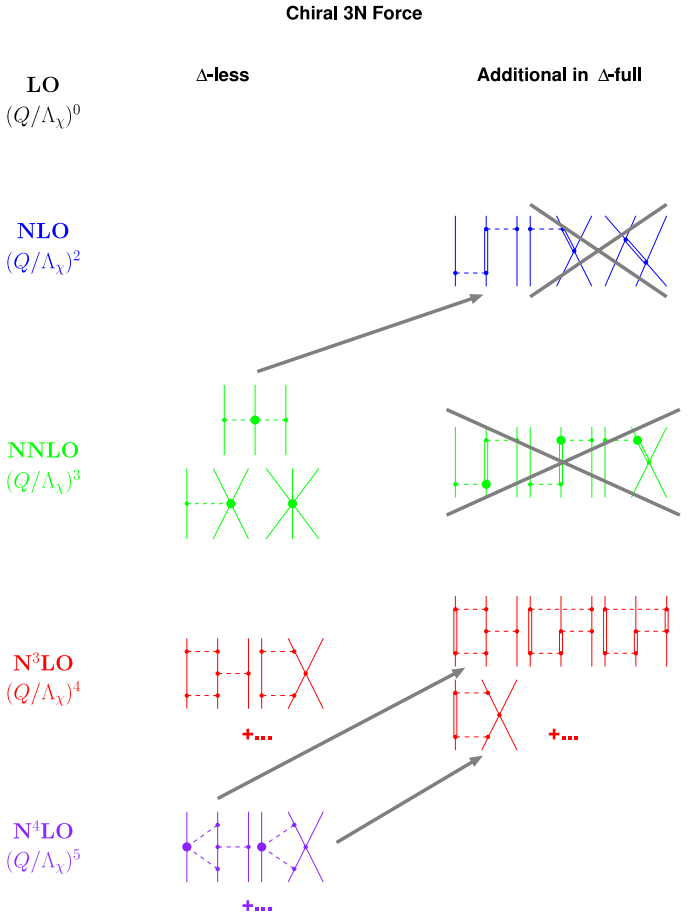

Fig. 24. The 3NF without and with Δ-isobar degrees of freedom. Arrows indicate the shift of strength when explicit Δ's are added to the theory. Note that the Δ-full theory consists of the diagrams involving Δ's *plus* the Δ-less ones. Double lines represent Δ-isobars; remaining notation as in Fig. 1.

contributions due to intermediate Δ-excitations, expanded in powers of $1/\Delta M$, can be absorbed into a redefinition of the LECs of the Δ-less theory. The corresponding shift of the LECs c_3, c_4 is given by

$$c_3 = -2c_4 = -\frac{h_A^2}{9\Delta M}. \tag{6.2}$$

Using $h_A = 3g_A/\sqrt{2}$ (large N_c value), almost all of c_3 and an appreciable part of c_4 is explained by the Δ resonance.

The studies of Refs. [56,221] confirm that a large amount of the intermediate-range attraction of the 2NF is shifted from NNLO to NLO with the explicit introduction of the Δ-isobar. However, it is also found that the NNLO 2PE potential of the Δ-less theory provides a very good approximation to the NNLO potential in the Δ-full theory.

The Δ isobar also changes the 3NF scenario, see Fig. 24. The leading 2PE 3NF is promoted to NLO. In the Δ-full theory, this term has the same mathematical form as the corresponding term in the Δ-less theory, Eqs. (5.2) and (5.3), provided one chooses $c_1 = 0$ and c_3, c_4 according to Eq. (6.2). Note that the other two NLO 3NF terms involving Δ's vanish [222] as a consequence of the antisymmetrization of the 3N states. The Δ contributions to the 3NF at NNLO [222] vanish at this order, because the subleading $N\Delta\pi$ vertex contains a time-derivative, which demotes the contributions by one order. However, substantial 3NF contributions are expected at N^{3}LO from one-loop diagrams with one, two, or three intermediate Δ-excitations, which correspond to diagrams of order N^{4}LO, N^{5}LO, and N^{6}LO, respectively, in the Δ-less theory. 3NF loop diagrams with one and two Δ's are included in the Illinois force [224] in a simplified way.

To summarize, the inclusion of explicit Δ degrees of freedom does certainly improve the convergence of the chiral expansion by shifting sizable contributions from NNLO to NLO. On the other hand, at NNLO the results for the Δ-full and Δ-less theory are essentially the same. Note that the Δ-full theory consists of the diagrams involving Δ's plus all diagrams of the Δ-less theory. Thus, the Δ-full theory is much more involved. Moreover, in the Δ-full theory, $1/M_N$ 2NF corrections appear at NNLO (not shown in Fig. 23), which were found to be uncomfortably large by Kaiser et al. [56]. Thus, it appears that up to NNLO, the Δ-less theory is more manageable.

The situation could, however, change at N^{3}LO where potentially large contributions enter the picture. It may be more efficient to calculate these terms in the Δ-full theory, because in the Δ-less theory they are spread out over N^{3}LO, N^{4}LO

and, in part, N^{5}LO. These higher order contributions are a crucial test for the convergence of the chiral expansion of nuclear forces and represent a challenging topic for the future.

7. Conclusions

The past 15 years have seen great progress in our understanding of nuclear forces in terms of low-energy QCD. Key to this development was the realization that low-energy QCD is equivalent to an effective field theory (EFT) which allows for a perturbative expansion that has become know as chiral perturbation theory (ChPT). In this framework, two- and many-body forces emerge on an equal footing and the empirical fact that nuclear many-body forces are substantially weaker than the two-nucleon force is explained naturally.

In this review, we have shown in detail how the two-nucleon force is derived from ChPT and demonstrated that, at N^{3}LO, the accuracy can be achieved that is necessary and sufficient for reliable microscopic nuclear structure predictions. First calculations applying the N^{3}LO *NN* potential [68] in the conventional shell model [75–77], the *ab initio* no-core shell model [78,79], the coupled cluster formalism [80–86], and the unitary-model-operator approach [87,88] have produced promising results.

We also discussed nuclear many-body forces based upon chiral EFT. The 3NF at NNLO has been known for a while [70,71] and applied in few-nucleon reactions [71,89–97], structure of light- and medium-mass nuclei [98–101], and nuclear and neutron matter [102,103] with some success. However, the famous 'A_y puzzle' of nucleon–deuteron scattering is not resolved by the 3NF at NNLO. Thus, one important open issue are the few-nucleon forces beyond NNLO ("subleading few-nucleon forces") which, besides the A_y puzzle, may also resolve some important outstanding nuclear structure problems. As explained, this may require going even beyond N^{3}LO.

Another open question is the convergence of the chiral expansion (of the two- as well as the three-nucleon potentials) at orders beyond N^{3}LO, for which the inclusion of Δ-isobar degrees of freedom may be useful. Furthermore, the nonperturbative renormalizations of the chiral potentials require more work and a better understanding.

Finally, we note that topics of interest we did not discuss include parity-violating nuclear forces and consistent electroweak currents.

Having identified some of the open issues, we hope that this review will be helpful towards future progress.

If the outstanding problems are resolved within the next few years, then, after 80 years of desperate struggle, we may finally claim that the nuclear force problem is essentially under control. The greatest beneficiary of such progress will be the field of *ab initio* nuclear structure physics.

Acknowledgements

The work by R.M. was supported in part by the US Department of Energy under Grant No. DE-FG02-03ER41270. The work of D.R.E. was funded by the Ministerio de Ciencia y Tecnología under Contract No. FPA2007-65748, the Junta de Castilla y León under Contract No. GR12, and the European Community-Research Infrastructure Integrating Activity "Study of Strongly Interacting Matter" (HadronPhysics2 Grant No. 227431).

Appendix A. Notation, conventions, and Feynman rules

A.1. Notation and conventions

The contravariant space-time four-vector is given by

$$x^\mu = (t, \vec{x}) \tag{A.1}$$

and the four-momentum vector reads

$$p^\mu = (E, \vec{p}). \tag{A.2}$$

We use units such that $\hbar = c = 1$.

Greek indices μ, ν, etc. run over the four space-time coordinate labels 0, 1, 2, 3, with $x^0 = t$ the time coordinate. Latin indices i, j, k, and so on run over the three space coordinate labels 1, 2, 3. The metric is diagonal with

$$g^{\mu\nu} = g_{\mu\nu} = \begin{pmatrix} 1 & & & 0 \\ & -1 & & \\ & & -1 & \\ 0 & & & -1 \end{pmatrix} \tag{A.3}$$

and the covariant versions of the above-mentioned vectors are

$$x_\mu = g_{\mu\nu} x^\nu = (t, -\vec{x}), \qquad p_\mu = g_{\mu\nu} p^\nu = (E, -\vec{p}), \tag{A.4}$$

where summation over repeated indices is always understood; also

$$x^2 = x_\mu x^\mu = t^2 - \vec{x}^2. \tag{A.5}$$

While for an ordinary three-vector we have, in general, $\vec{x} = (x^1, x^2, x^3)$, there is caution in place with the (three-dimensional) nabla operator which is defined to be

$$\vec{\nabla} = (\nabla_1, \nabla_2, \nabla_3) = \left(\frac{\partial}{\partial x^i}\right) = (\partial_i) = \left(-\frac{\partial}{\partial x_i}\right) = (-\partial^i). \tag{A.6}$$

The four-momentum operator reads

$$p^\mu = i\frac{\partial}{\partial x_\mu} = i\partial^\mu = \left(i\partial^0, -i\vec{\nabla}\right) = \left(i\frac{\partial}{\partial t}, \vec{p}\right), \tag{A.7}$$

$$p_\mu = i\frac{\partial}{\partial x^\mu} = i\partial_\mu = \left(i\partial_0, i\vec{\nabla}\right) = \left(i\frac{\partial}{\partial t}, -\vec{p}\right). \tag{A.8}$$

The relativistic nucleon field satisfies the free Dirac equation

$$(\not{p} - M_N)\,\Psi(x) \equiv \left(\gamma^\mu p_\mu - M_N\right)\Psi(x) = 0 \tag{A.9}$$

where M_N denotes the nucleon mass and γ_μ the Dirac matrices which we apply in Dirac–Pauli representation

$$\gamma^0 = \begin{pmatrix} I & 0 \\ 0 & -I \end{pmatrix} \qquad \gamma^i = \begin{pmatrix} 0 & \sigma^i \\ -\sigma^i & 0 \end{pmatrix} \tag{A.10}$$

with I the two-dimensional identity matrix and σ^i the Pauli matrices

$$\sigma^1 = \begin{pmatrix} 0 & 1 \\ 1 & 0 \end{pmatrix} \qquad \sigma^2 = \begin{pmatrix} 0 & -i \\ i & 0 \end{pmatrix} \qquad \sigma^3 = \begin{pmatrix} 1 & 0 \\ 0 & -1 \end{pmatrix}. \tag{A.11}$$

$$\left[\sigma^i, \sigma^j\right] = \sigma^i\sigma^j - \sigma^j\sigma^i = 2i\epsilon^{ijk}\sigma^k, \qquad \{\sigma^i, \sigma^j\} = \sigma^i\sigma^j + \sigma^j\sigma^i = 2\delta^{ij}, \tag{A.12}$$

$$\sigma^i\sigma^j = i\epsilon^{ijk}\sigma^k + \delta^{ij}, \tag{A.13}$$

with

$$\epsilon^{ijk} = \begin{cases} +1 & \text{if } (i, j, k) \text{ even permutation of } (1, 2, 3) \\ -1 & \text{if odd permutation} \\ 0 & \text{otherwise.} \end{cases} \tag{A.14}$$

Following convention, we denote the Pauli matrices by τ^a $(a = 1, 2, 3)$ when operating in isospin space, with

$$\tau^a\tau^b = i\epsilon^{abc}\tau^c + \delta^{ab}. \tag{A.15}$$

Notice that, for isospin components, it does not make sense to distinguish between upper and lower indices and, therefore, subscripts and superscripts have the same meaning.

The Dirac matrices have the properties

$$\{\gamma^\mu, \gamma^\nu\} = 2\,g^{\mu\nu}, \qquad \gamma^{0\dagger} = \gamma^0\gamma^0\gamma^0 = \gamma^0, \qquad \gamma^{i\dagger} = \gamma^0\gamma^i\gamma^0 = -\gamma^i. \tag{A.16}$$

The γ_5-matrix is defined by

$$\gamma^5 = \gamma_5 = i\gamma^0\gamma^1\gamma^2\gamma^3 = \begin{pmatrix} 0 & I \\ I & 0 \end{pmatrix}. \tag{A.17}$$

$$\{\gamma^\mu, \gamma^5\} = 0, \qquad (\gamma^5)^2 = 1, \qquad \gamma^{5\dagger} = \gamma^5. \tag{A.18}$$

Commutator of γ matrices:

$$\sigma^{\mu\nu} = \frac{i}{2}\left[\gamma^\mu, \gamma^\nu\right], \qquad \gamma^\mu\gamma^\nu = g^{\mu\nu} - i\sigma^{\mu\nu}, \tag{A.19}$$

$$\sigma^{ij} = \epsilon^{ijk}\begin{pmatrix} \sigma^k & 0 \\ 0 & \sigma^k \end{pmatrix}, \qquad \sigma^{0i} = i\begin{pmatrix} 0 & \sigma^i \\ \sigma^i & 0 \end{pmatrix} = -\sigma^{i0} \tag{A.20}$$

The relativistic Dirac field for positive-energy nucleons is

$$\Psi(x) = \sum_{s,t}\int \frac{d^3p}{(2\pi)^{3/2}}\sqrt{\frac{M_N}{E_p}}\,u(\vec{p}, s)\,\xi_t\,e^{-ip\cdot x}\,b(\vec{p}, s, t) \tag{A.21}$$

with the Dirac spinor given by

$$u(\vec{p},s)=\sqrt{\frac{E_p+M_N}{2M_N}}\left(\begin{array}{c} I \\ \dfrac{\vec{\sigma}\cdot\vec{p}}{E_p+M_N}\end{array}\right)\chi_s \tag{A.22}$$

where $E_p = p^0 = \sqrt{\vec{p}^2+M_N^2}$. The Pauli spinors χ_s and ξ_t describe, respectively, the spin and isospin of the nucleon. Further, $b(\vec{p},s,t)$ and $b^\dagger(\vec{p},s,t)$ are destruction and creation operators for a nucleon with momentum $\vec{p}$, and spin and isospin quantum numbers s and t, respectively. They satisfy the anti-commutation relations

$$\left\{b(\vec{p},s,t),\, b^\dagger(\vec{p}\,',s',t')\right\}=\delta_{s,s'}\delta_{t,t'}\delta^3(\vec{p}-\vec{p}\,'), \tag{A.23}$$

$$\left\{b(\vec{p},s,t),\, b(\vec{p}\,',s',t')\right\}=\left\{b^\dagger(\vec{p},s,t),\, b^\dagger(\vec{p}\,',s',t')\right\}=0. \tag{A.24}$$

$$\bar{\Psi}\equiv\Psi^\dagger\gamma^0. \tag{A.25}$$

In the heavy baryon formalism, the free field equation for nucleons is, in leading order and using $v_\mu=(1,0,0,0)$,

$$iv_0N(x)=0 \tag{A.26}$$

and the nucleon field is

$$N(x)=\sum_{s,t}\int\frac{d^3l}{(2\pi)^{3/2}}\,\chi_s\,\xi_t\,e^{-il\cdot x}\,b(\vec{l},s,t) \tag{A.27}$$

where $l_0=0$ at leading order and $\vec{l}^2/2M_N$ at NLO.

$$\bar{N}\equiv N^\dagger\gamma^0=N^\dagger. \tag{A.28}$$

The pion fields are in terms of their cartesian components ($i=1,2,3$; no distinction between upper and lower index i)

$$\pi_i(x)=\int\frac{d^3q}{(2\pi)^{3/2}}\frac{1}{\sqrt{2\omega}}\left[e^{-iq\cdot x}a_i(\vec{q})+e^{iq\cdot x}a_i^\dagger(\vec{q})\right] \tag{A.29}$$

where $\omega=q^0=\sqrt{\vec{q}^2+m_\pi^2}$ and a_i and $a_i^\dagger$ are, respectively, the destruction and creation operators obeying the commutation relations

$$\left[a_i(\vec{q}),\, a_j^\dagger(\vec{q}\,')\right]=\delta_{ij}\delta^3(\vec{q}-\vec{q}\,'), \tag{A.30}$$

$$\left[a_i(\vec{q}),\, a_j(\vec{q}\,')\right]=\left[a_i^\dagger(\vec{q}),\, a_j^\dagger(\vec{q}\,')\right]=0. \tag{A.31}$$

The charged- and neutral-pion fields are given by

$$\pi_+=\frac{1}{\sqrt{2}}\left(\pi_1+i\pi_2\right), \tag{A.32}$$

$$\pi_-=\frac{1}{\sqrt{2}}\left(\pi_1-i\pi_2\right), \tag{A.33}$$

$$\pi_0=\pi_3. \tag{A.34}$$

Throughout this article, we state amplitudes in terms of the "potential" V which is defined by

$$V=i\,\mathcal{M} \tag{A.35}$$

where $\mathcal{M}$ is the invariant amplitude, calculated according to Feynman rules. The relation of $\mathcal{M}$ to the S-matrix is

$$\begin{aligned}\langle p_1'p_2'|S|p_1p_2\rangle &= \delta^3(\vec{p}_1-\vec{p}_1')\,\delta^3(\vec{p}_2-\vec{p}_2')+(2\pi)^4\,\delta^4(p_1+p_2-p_1'-p_2')\,\frac{1}{(2\pi)^6}\left(\frac{M_N^4}{E_1'E_2'E_1E_2}\right)^{\frac{1}{2}}\\ &\quad\times\mathcal{M}(p_1',p_2';p_1,p_2).\end{aligned} \tag{A.36}$$

A.2. Feynman rules

The basic formalism underlying the Feynman rules is the Dyson expansion of the S-matrix [cf. e.g., Eq. (6.1.1) of Ref. [225]]. Since we are applying *covariant* perturbation theory, we assume $\mathcal{H}_I=-\mathcal{L}_I$ (where $\mathcal{H}_I$ denotes the interaction Hamiltonian density and $\mathcal{L}_I$ the interaction Lagrangian density) and use the usual covariant Feynman propagators. From a procedural point of view, this is acceptable for the derivative couplings considered here (see, however, Ref. [226] for exceptions). For a discussion of the differences between covariant perturbation theory and time-ordered perturbation theory (also known as "old-fashioned" perturbation theory), see the evaluation of the football diagram, Appendix B.2.2 below.

In all *one-pion vertices* given below, q denotes the four-momentum of an outgoing pion of isospin component a. In all *two-pion vertices*, q_1 denotes the four-momentum of an ingoing pion with isospin component a and q_2 the four-momentum of an outgoing pion with isospin component b. Nucleon momenta are, in general, denoted by p and p'.

A.2.1. Leading order

The relativistic version of the leading order πN Lagrangian has been given in Eq. (2.41). We consider the axial-vector (AV) and the Weinberg–Tomozawa (WT) couplings, which involve one- and two-pion fields, respectively. The relativistic AV interaction Lagrangian is given by

$$\mathcal{L}_{AV} = -\frac{g_A}{2f_\pi}\,\bar{\Psi}\,\gamma^\mu\,\gamma_5\,\boldsymbol{\tau}\Psi\cdot\partial_\mu\boldsymbol{\pi}. \tag{A.37}$$

For simple Lagrangians like this one, the vertex is just i times the Lagrangian stripped off the fields which generates (q out)

$$\frac{g_A}{2f_\pi}\,\gamma_\mu\gamma_5\tau^a q^\mu. \tag{A.38}$$

In the heavy baryon formalism, the AV Lagrangian reads [cf. Eq. (2.53)]

$$\widehat{\mathcal{L}}_{AV} = -\frac{g_A}{2f_\pi}\,\bar{N}\,\boldsymbol{\tau}\cdot(\vec{\sigma}\cdot\vec{\nabla})\boldsymbol{\pi}\,N \tag{A.39}$$

with vertex (q out)

$$-\frac{g_A}{2f_\pi}\,\tau^a\vec{\sigma}\cdot\vec{q}. \tag{A.40}$$

The relativistic WT coupling term is

$$\mathcal{L}_{WT} = -\frac{1}{4f_\pi^2}\,\bar{\Psi}\,\gamma^\mu\,\boldsymbol{\tau}\cdot(\boldsymbol{\pi}\times\partial_\mu\boldsymbol{\pi})\,\Psi \tag{A.41}$$

implying the vertex (q_1 in, q_2 out)

$$\frac{1}{4f_\pi^2}\,\gamma_\mu\epsilon^{abc}\tau^c(q_1^\mu+q_2^\mu). \tag{A.42}$$

The Heavy Baryon version is

$$\widehat{\mathcal{L}}_{WT} = -\frac{1}{4f_\pi^2}\,\bar{N}\,\boldsymbol{\tau}\cdot(\boldsymbol{\pi}\times\partial_0\boldsymbol{\pi})\,N \tag{A.43}$$

with vertex (q_1 in, q_2 out)

$$\frac{1}{4f_\pi^2}\,\epsilon^{abc}\tau^c(q_1^0+q_2^0). \tag{A.44}$$

The relativistic nucleon propagator reads [cf. Eq. (A.9)]

$$\frac{i}{\not{p}-M_N+i\epsilon} = \frac{i(\not{p}+M_N)}{p^2-M_N^2+i\epsilon} \tag{A.45}$$

and the leading order heavy baryon version of the nucleon propagator is given by [cf. Eq. (A.26)]

$$\frac{i}{l^0+i\epsilon}. \tag{A.46}$$

The pion propagator is [cf. Eq. (2.32)]

$$\frac{i\delta^{ab}}{q^2-m_\pi^2+i\epsilon}. \tag{A.47}$$

A.2.2. Next-to-leading order

The "fixed" part of the dimension-two HB Lagrangian is given in Eq. (2.56). It leads to a nucleon kinetic energy correction

$$-i\,\frac{\vec{p}^{\,2}}{2M_N}, \tag{A.48}$$

and produces the one-pion vertex (q out)

$$\frac{g_A}{4M_Nf_\pi}\,\tau^a\,\vec{\sigma}\cdot(\vec{p}+\vec{p}\,')\,q^0 \tag{A.49}$$

and the two-pion vertex (q_1 in, q_2 out)

$$-\frac{1}{8M_N f_\pi^2}\,\epsilon^{abc}\,\tau^c\,(\vec{p}+\vec{p}\,')\cdot(\vec{q}_1+\vec{q}_2). \tag{A.50}$$

The vertices equations (A.49) and (A.50) are the first relativistic corrections of the vertices equations (A.40) and (A.44), respectively. These corrections can also be obtained by starting from the corresponding relativistic vertices equations (A.38) and (A.42), sandwiching them between Dirac spinors, and making a $1/M_N$ expansion.

The "contact" part of the dimension-two Lagrangian, Eq. (2.57), gives rise to the following two-pion vertices (q_1 in, q_2 out):

$$\frac{i\delta^{ab}}{f_\pi^2}\left[-4c_1m_\pi^2+\left(2c_2-\frac{g_A^2}{4M_N}\right)q_1^0q_2^0+2c_3q_{1\mu}q_2^\mu\right] \tag{A.51}$$

and

$$-\frac{i}{f_\pi^2}\left(c_4+\frac{1}{4M_N}\right)\epsilon^{ijk}\epsilon^{abc}\sigma^i\tau^c q_1^j q_2^k. \tag{A.52}$$

For more Feynman rules, see Appendix A of Ref. [119].

Appendix B. Two-pion-exchange contributions to the 2NF at NLO

An overview of the 2PE diagrams that contribute at NLO was shown in Fig. 3. We will now evaluate the various groups of diagrams one by one.

B.1. Triangle diagrams

B.1.1. The triangles in covariant perturbation theory

The triangle diagrams are shown in Fig. B.1. The contributions from diagram (a) and (b) will be denoted by $V_{\rm a}$ and $V_{\rm b}$, respectively. According to relativistic Feynman rules, one obtains

$$\begin{aligned} V_{\rm a} &= i\frac{g_A^2}{16f_\pi^4}\int\frac{d^4l}{(2\pi)^4}\,(2l^\mu+q^\mu)\epsilon^{abc}\tau_1^c\bar{u}_1(\vec{p}\,')\gamma_\mu u_1(\vec{p})\frac{i}{(l+q)^2-m_\pi^2+i\epsilon}\\ &\quad\times\frac{i}{l^2-m_\pi^2+i\epsilon}\bar{u}_2(-\vec{p}\,')(-l^\nu)\tau_2^b\gamma_\nu\gamma_5\frac{i(\not{k}_N+M_N)}{k_N^2-M_N^2+i\epsilon}(l^\rho+q^\rho)\tau_2^a\gamma_\rho\gamma_5u_2(-\vec{p}), \end{aligned}\tag{B.1}$$

$$\begin{aligned} V_{\rm b} &= i\frac{g_A^2}{16f_\pi^4}\int\frac{d^4l}{(2\pi)^4}\,(2l^\mu+q^\mu)\epsilon^{abc}\tau_2^c\bar{u}_2(-\vec{p}\,')\gamma_\mu u_2(-\vec{p})\frac{i}{(l+q)^2-m_\pi^2+i\epsilon}\\ &\quad\times\frac{i}{l^2-m_\pi^2+i\epsilon}\bar{u}_1(\vec{p}\,')(-l^\nu-q^\nu)\tau_1^b\gamma_\nu\gamma_5\frac{i(\bar{\not{k}}_N+M_N)}{\bar{k}_N^2-M_N^2+i\epsilon}(l^\rho)\tau_1^a\gamma_\rho\gamma_5u_1(\vec{p}), \end{aligned}\tag{B.2}$$

where the momenta are defined in Fig. B.1 and $q=(0,\vec{p}\,'-\vec{p})$. The sum over the isospin operators is $\epsilon^{abc}\tau_i^c\tau_j^b\tau_j^a=-i\,2\boldsymbol{\tau}_i\cdot\boldsymbol{\tau}_j$ and, for the intermediate nucleon, we have $\gamma_\nu\gamma_5(\not{k}_N+M_N)\gamma_\rho\gamma_5=\gamma_\nu(\not{k}_N-M_N)\gamma_\rho$. Thus,

$$\begin{aligned} V_{\rm a} &= -i\boldsymbol{\tau}_1\cdot\boldsymbol{\tau}_2\frac{g_A^2}{8f_\pi^4}\int\frac{d^4l}{(2\pi)^4}\,(2l^\mu+q^\mu)\bar{u}_1(\vec{p}\,')\gamma_\mu u_1(\vec{p})\frac{1}{(l+q)^2-m_\pi^2+i\epsilon}\\ &\quad\times\frac{1}{l^2-m_\pi^2+i\epsilon}\bar{u}_2(-\vec{p}\,')(-l^\nu)\gamma_\nu\frac{(\not{k}_N-M_N)}{k_N^2-M_N^2+i\epsilon}(l^\rho+q^\rho)\gamma_\rho u_2(-\vec{p}), \end{aligned}\tag{B.3}$$

$$\begin{aligned} V_{\rm b} &= -i\boldsymbol{\tau}_1\cdot\boldsymbol{\tau}_2\frac{g_A^2}{8f_\pi^4}\int\frac{d^4l}{(2\pi)^4}\,(2l^\mu+q^\mu)\bar{u}_2(-\vec{p}\,')\gamma_\mu u_2(-\vec{p})\frac{1}{(l+q)^2-m_\pi^2+i\epsilon}\\ &\quad\times\frac{1}{l^2-m_\pi^2+i\epsilon}\bar{u}_1(\vec{p}\,')(-l^\nu-q^\nu)\gamma_\nu\frac{(\bar{\not{k}}_N-M_N)}{\bar{k}_N^2-M_N^2+i\epsilon}(l^\rho)\gamma_\rho u_1(\vec{p}). \end{aligned}\tag{B.4}$$

At NLO, only the lowest order in the $1/M_N$ expansion is included. The nucleon-mass dependence comes from the Dirac spinors and the nucleon propagator and performing such an expansion, we find at lowest order

$$\bar{u}_i\gamma_\mu u_i\approx\delta_{\mu0} \tag{B.5}$$

$$\bar{u}_i\gamma_\nu(\not{k}_N-M_N)\gamma_\rho u_i\approx\delta_{\nu j}\delta_{\rho m}2M_N(\delta_{jm}+i\epsilon^{jmn}\sigma_i^n) \tag{B.6}$$

$$\frac{1}{k_N^2-M_N^2+i\epsilon}\approx\frac{1}{2M_N}\,\frac{1}{-l^0+i\epsilon}. \tag{B.7}$$

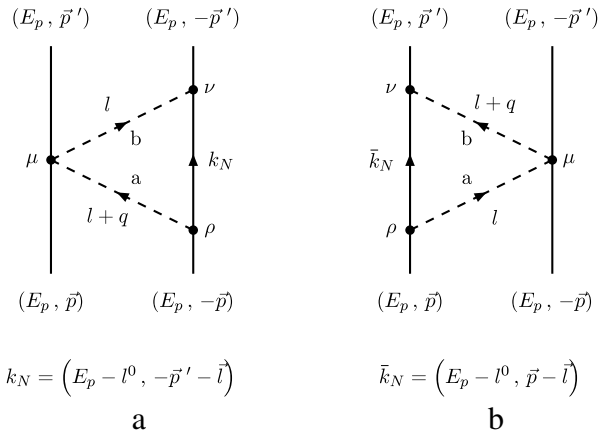

Fig. B.1. Two-pion-exchange triangle diagrams at NLO.

In this approximation, the amplitudes are

$$V_{\rm a} = -\,i\,\boldsymbol{\tau}_1\cdot\boldsymbol{\tau}_2\frac{g_A^2}{4f_\pi^4}\int\frac{d^4l}{(2\pi)^4}\,\frac{1}{(l+q)^2-m_\pi^2+i\epsilon}\,\frac{1}{l^2-m_\pi^2+i\epsilon}(\delta_{jm}+i\epsilon^{jmn}\sigma_2^n)(l^j)(l^m+q^m) \tag{B.8}$$

$$V_{\rm b} = -i\boldsymbol{\tau}_1\cdot\boldsymbol{\tau}_2\frac{g_A^2}{4f_\pi^4}\int\frac{d^4l}{(2\pi)^4}\,\frac{1}{(l+q)^2-m_\pi^2+i\epsilon}\frac{1}{l^2-m_\pi^2+i\epsilon}(\delta_{jm}+i\epsilon^{jmn}\sigma_1^n)(l^j+q^j)(l^m) \tag{B.9}$$

where we used $q^0=0$.

Alternatively, one can derive the NLO triangle diagram contributions by using the HB formalism from the outset. Using the Feynman rules for the HB Lagrangians and propagators yields

$$\begin{aligned}V_{\rm a}^{\rm HB} &= i\frac{g_A^2}{16f_\pi^4}\int\frac{d^4l}{(2\pi)^4}\,(2l^0)\epsilon^{abc}\tau_1^c\frac{i}{(l+q)^2-m_\pi^2+i\epsilon}\,\frac{i}{l^2-m_\pi^2+i\epsilon}\\ &\quad\times\tau_2^b(\vec{\sigma}_2\cdot\vec{l})\frac{i}{-l^0+i\epsilon}\tau_2^a(-\vec{\sigma}_2\cdot(\vec{l}+\vec{q})),\end{aligned} \tag{B.10}$$

$$\begin{aligned}V_{\rm b}^{\rm HB} &= i\frac{g_A^2}{16f_\pi^4}\int\frac{d^4l}{(2\pi)^4}\,(2l^0)\epsilon^{abc}\tau_2^c\frac{i}{(l+q)^2-m_\pi^2+i\epsilon}\,\frac{i}{l^2-m_\pi^2+i\epsilon}\\ &\quad\times\tau_1^b(\vec{\sigma}_1\cdot(\vec{l}+\vec{q}))\frac{i}{-l^0+i\epsilon}\tau_1^a(-\vec{\sigma}_1\cdot\vec{l}).\end{aligned} \tag{B.11}$$

Performing the isospin sums and using the identity $(\vec{\sigma}\cdot\vec{a})(\vec{\sigma}\cdot\vec{b})=\vec{a}\cdot\vec{b}+i\vec{\sigma}\cdot(\vec{a}\times\vec{b})$, we obtain

$$V_{\rm a}^{\rm HB} = -i\,\boldsymbol{\tau}_1\cdot\boldsymbol{\tau}_2\frac{g_A^2}{4f_\pi^4}\int\frac{d^4l}{(2\pi)^4}\,\frac{1}{(l+q)^2-m_\pi^2+i\epsilon}\,\frac{1}{l^2-m_\pi^2+i\epsilon}\left[\vec{l}\cdot(\vec{l}+\vec{q})+i\vec{\sigma}_2\cdot(\vec{l}\times(\vec{l}+\vec{q}))\right], \tag{B.12}$$

$$V_{\rm b}^{\rm HB} = -i\,\boldsymbol{\tau}_1\cdot\boldsymbol{\tau}_2\frac{g_A^2}{4f_\pi^4}\int\frac{d^4l}{(2\pi)^4}\,\frac{1}{(l+q)^2-m_\pi^2+i\epsilon}\,\frac{1}{l^2-m_\pi^2+i\epsilon}\left[(\vec{l}+\vec{q})\cdot\vec{l}+i\vec{\sigma}_1\cdot((\vec{l}+\vec{q})\times\vec{l})\right]. \tag{B.13}$$

The two sets of Eqs. (B.8), (B.9) and (B.12), (B.13) obviously agree—as they should.

Since $(\vec{l}+\vec{q})\times\vec{l}=\vec{q}\times\vec{l}$ and since the integral over a term proportional to $\vec{l}$ will yield a result $\propto\vec{q}$, the spin-dependent terms vanish and the sum of both triangles is given by

$$V = V_{\rm a}+V_{\rm b} = -i\,\boldsymbol{\tau}_1\cdot\boldsymbol{\tau}_2\frac{g_A^2}{2f_\pi^4}\int\frac{d^4l}{(2\pi)^4}\,\frac{1}{(l+q)^2-m_\pi^2+i\epsilon}\,\frac{\vec{l}^{\,2}+\vec{l}\cdot\vec{q}}{l^2-m_\pi^2+i\epsilon}. \tag{B.14}$$

At this point, it might be of interest to compare with what other authors obtain for the NLO triangle diagrams. In the work of Ref. [54], time-ordered perturbation theory (TOPT) (also known as old-fashioned PT) is used in which loop integrals extend only over the three space dimensions.

Thus, we will perform the integration over the time component in Eq. (B.14) to make a comparison with TOPT possible. For convenience, we first apply the transformation $l=\frac{1}{2}(l'-q)$, which yields

$$V = -i\,\boldsymbol{\tau}_1\cdot\boldsymbol{\tau}_2\frac{g_A^2}{8f_\pi^4}\int\frac{d^4l'}{(2\pi)^4}\,\frac{1}{(l'+q)^2-4m_\pi^2+i\epsilon}\,\frac{\vec{l}^{\,\prime 2}-\vec{q}^{\,2}}{(l'-q)^2-4m_\pi^2+i\epsilon}. \tag{B.15}$$

The poles in the lower half-plane are at $l'^0 = \omega_\pm - i\epsilon$ with

$$\omega_\pm = \sqrt{(\vec{l}' \pm \vec{q})^2 + 4m_\pi^2} \tag{B.16}$$

and, so, we can write the amplitude as

$$V = -i\,\boldsymbol{\tau}_1 \cdot \boldsymbol{\tau}_2 \frac{g_A^2}{8f_\pi^4} \int \frac{d^4l'}{(2\pi)^4} \frac{1}{(l'^0)^2 - \omega_+^2 + i\epsilon} \frac{\vec{l}'^{\,2} - \vec{q}^{\,2}}{(l'^0)^2 - \omega_-^2 + i\epsilon}. \tag{B.17}$$

Now we perform the integration over l'^0 using the residue theorem

$$\begin{aligned} V &= -\boldsymbol{\tau}_1 \cdot \boldsymbol{\tau}_2 \frac{g_A^2}{8f_\pi^4} \int \frac{d^3l'}{(2\pi)^3} (\vec{l}'^{\,2} - \vec{q}^{\,2}) \left\{ \frac{1}{2\omega_+} \frac{1}{\omega_+^2 - \omega_-^2} + \frac{1}{\omega_-^2 - \omega_+^2} \frac{1}{2\omega_-} \right\} \\ &= -\boldsymbol{\tau}_1 \cdot \boldsymbol{\tau}_2 \frac{g_A^2}{8f_\pi^4} \int \frac{d^3l'}{(2\pi)^3} (\vec{l}'^{\,2} - \vec{q}^{\,2}) \left\{ \frac{1}{\omega_+^2 - \omega_-^2} \frac{\omega_- - \omega_+}{2\omega_+\omega_-} \right\} \\ &= \boldsymbol{\tau}_1 \cdot \boldsymbol{\tau}_2 \frac{g_A^2}{16f_\pi^4} \int \frac{d^3l'}{(2\pi)^3} \frac{\vec{l}'^{\,2} - \vec{q}^{\,2}}{\omega_+\omega_-(\omega_+ + \omega_-)}. \end{aligned} \tag{B.18}$$

Except for a typo in Ref. [54] and differences in notation, this agrees with the second term of Eq. (20) of Ref. [54] as well as the first term of Eq. (4.30) of Ref. [64], which both represent the triangle diagrams.

B.1.2. Dimensional regularization of the triangles

The integral is divergent and, therefore, requires regularization. In Ref. [54], this is done by introducing a Gaussian cutoff function $\exp(-\vec{l}^2/\Lambda^2)$ which, however, makes the results dependent on the cutoff parameter Λ. To avoid such cutoff dependence, we will use dimensional regularization which was first introduced by 't Hooft and Veltman in 1972 [227].[6]

For this it is convenient to go back to Eq. (B.14) and apply a trick discovered by Feynman [230],

$$\frac{1}{ab} = \int_0^1 \frac{dx}{[b + (a-b)x]^2}, \tag{B.19}$$

which allows to write the product of propagators in terms of a linear combination. Applying Feynman's trick in Eq. (B.14) yields

$$V = \boldsymbol{\tau}_1 \cdot \boldsymbol{\tau}_2 \frac{g_A^2}{2f_\pi^4} \int_0^1 dx \int \frac{d^4l}{i(2\pi)^4} \frac{\vec{l}^2 + \vec{l}\cdot\vec{q}}{[l^2 + (2lq + q^2)x - m_\pi^2 + i\epsilon]^2}. \tag{B.20}$$

The momentum integral is not yet quite ready for dimensional regularization because the integrand mixes three- and four-dimensional versions of the loop momentum l. The dimension of the integration variable l must be consistent throughout the integrand.

Formal (four-dimensional) covariance can be recovered by re-introducing the four-vector $v_\mu = (1, 0, 0, 0)$ and rewriting the numerator as $\vec{l}^2 + \vec{l}\cdot\vec{q} = (l\cdot v)^2 - l^2 - l\cdot q$. After a shift of the integration variable $l \to l + xq$, well-known formulas for the dimensional regularization of covariant integrals can be applied [see, e.g., Eqs. (10.23) and (10.32)–(10.34) of Ref. [229]].

Alternatively, one may go for consistency in three dimensions and reduce the momentum integral of Eq. (B.20) to the three space dimensions, which is what we will do here. This has the advantage that the integration variable observes an Euclidean metric from the outset (and there is no need for a Wick rotation). Moreover, the planar box diagram (see below) requires treatment in three dimensions.

The integrand of Eq. (B.20) has two poles as evidenced through

$$l^2 + (2lq + q^2)x - m_\pi^2 + i\epsilon = \left[l^0 + \sqrt{\vec{l}^2 + m_\pi^2 + (2\vec{l}\cdot\vec{q} + \vec{q}^2)x} - i\epsilon \right] \left[l^0 - \sqrt{\vec{l}^2 + m_\pi^2 + (2\vec{l}\cdot\vec{q} + \vec{q}^2)x} + i\epsilon \right] \tag{B.21}$$

where we used $q^0 = 0$. The pole in the lower half-plane is

$$l_1^0 = \sqrt{\vec{l}^2 + m_\pi^2 + (2\vec{l}\cdot\vec{q} + \vec{q}^2)x} - i\epsilon, \tag{B.22}$$

[6] Accessible introductions into dimensional regularization can be found in Refs. [228,229] and a very pedagogical presentation is provided in Appendix A.2 of the Scherer review [113].

and, using the residue theorem, one obtains

$$V = \boldsymbol{\tau}_1 \cdot \boldsymbol{\tau}_2 \frac{g_A^2}{2f_\pi^4} \int_0^1 dx \int \frac{dl^0\, d^3l}{i(2\pi)^4} \frac{\vec{l}^2 + \vec{l}\cdot\vec{q}}{(l^0 - l_1^0)^2 (l^0 + l_1^0)^2}$$
$$= \boldsymbol{\tau}_1 \cdot \boldsymbol{\tau}_2 \frac{g_A^2}{2f_\pi^4} \int_0^1 dx \int \frac{d^3l}{(2\pi)^3} \frac{1}{4} \frac{\vec{l}^2 + \vec{l}\cdot\vec{q}}{(l_1^0)^3}. \tag{B.23}$$

To proceed towards dimensional regularization, we now generalize the three-dimensional integral to $(D-1)$ dimensions. Moreover, we introduce the renormalization scale λ and multiply the integral by λ^{4-D} such that the dimension of the amplitude stays the same for any D [228,231],

$$V = \boldsymbol{\tau}_1 \cdot \boldsymbol{\tau}_2 \frac{g_A^2}{8f_\pi^4} \lambda^{4-D} \int_0^1 dx \int \frac{d^{D-1}l}{(2\pi)^{D-1}} \frac{\vec{l}^2 + \vec{l}\cdot\vec{q}}{(l_1^0)^3}. \tag{B.24}$$

For convenience, we now divide all dimension-full quantities involved in the integral by λ and denote all dimensionless quantities (except for the dimensionless momentum $\vec{k}$) by a tilde; for example, $\tilde{q} = \vec{q}/\lambda$. Furthermore, we shift the integration variable by introducing the new variable $\vec{k}$ with $\lambda\vec{k} = \vec{l} + x\vec{q}$, so that there are no terms linear in the integration variable in the denominator. Thus, we have now

$$l_1^0 = \lambda\sqrt{\vec{k}^2 + \tilde{m}_\pi^2 + \tilde{q}^2 x(1-x)} - i\epsilon, \tag{B.25}$$

and our integral reads

$$V = \boldsymbol{\tau}_1 \cdot \boldsymbol{\tau}_2 \frac{g_A^2}{8f_\pi^4} \lambda^2 \int_0^1 dx \int \frac{d^{D-1}k}{(2\pi)^{D-1}} \frac{(k - x\tilde{q})^2 + (k - x\tilde{q})\cdot\tilde{q}}{[k^2 + \tilde{m}_\pi^2 + \tilde{q}^2 x(1-x)]^{3/2}}. \tag{B.26}$$

Terms with odd powers of k vanish,

$$V = \boldsymbol{\tau}_1 \cdot \boldsymbol{\tau}_2 \frac{g_A^2}{8f_\pi^4} \lambda^2 \int_0^1 dx \int \frac{d^{D-1}k}{(2\pi)^{D-1}} \frac{k^2 - x(1-x)\tilde{q}^2}{[k^2 + \tilde{m}_\pi^2 + \tilde{q}^2 x(1-x)]^{3/2}}. \tag{B.27}$$

The volume element in $(D-1)$ dimensions is

$$d^{D-1}k = k^{D-2}\, dk\, d\Omega_{D-1} \tag{B.28}$$

with

$$\int d\Omega_{D-1} = \frac{2\pi^{(D-1)/2}}{\Gamma(\frac{D-1}{2})}. \tag{B.29}$$

Thus,

$$V = \boldsymbol{\tau}_1 \cdot \boldsymbol{\tau}_2 \frac{g_A^2}{8f_\pi^4} \frac{2\lambda^2}{\Gamma(\frac{D-1}{2})(4\pi)^{(D-1)/2}} \int_0^1 dx \int_0^\infty dk \frac{k^D - x(1-x)\tilde{q}^2 k^{D-2}}{[k^2 + \tilde{m}_\pi^2 + \tilde{q}^2 x(1-x)]^{3/2}}. \tag{B.30}$$

Using [cf. for example, Eq. (A.35) of Ref. [113]]

$$\int_0^\infty \frac{k^{D-2+n_1}}{(k^2+s)^{n/2}}\, dk = \frac{\Gamma(\frac{D+n_1-1}{2})\Gamma(\frac{n+1-D-n_1}{2})}{2\Gamma(\frac{n}{2})} \frac{1}{s^{\frac{n+1-D-n_1}{2}}}, \tag{B.31}$$

we obtain

$$V = \boldsymbol{\tau}_1 \cdot \boldsymbol{\tau}_2 \frac{g_A^2}{8f_\pi^4} \frac{\lambda^2}{\Gamma(\frac{3}{2})\Gamma(\frac{D-1}{2})(4\pi)^{(D-1)/2}} \int_0^1 dx \left\{ \frac{\Gamma(\frac{D+1}{2})\Gamma(\frac{2-D}{2})}{[\tilde{m}_\pi^2 + \tilde{q}^2 x(1-x)]^{(2-D)/2}} \right.$$
$$\left. - x(1-x)\tilde{q}^2 \frac{\Gamma(\frac{D-1}{2})\Gamma(\frac{4-D}{2})}{[\tilde{m}_\pi^2 + \tilde{q}^2 x(1-x)]^{(4-D)/2}} \right\}. \tag{B.32}$$

We choose $D = 4 - \eta$ and then take the limit $\eta \to 0$. To prepare for the latter, we expand the various expressions involved up to first order in η:

$$\frac{\Gamma(\frac{D+1}{2})}{\Gamma(\frac{D-1}{2})} = \frac{D-1}{2} = \frac{3-\eta}{2}$$

$$\Gamma\left(\frac{4-D}{2}\right)=\Gamma\left(\frac{\eta}{2}\right)=\frac{2}{\eta}-\gamma+\mathcal{O}(\eta)$$
$$\Gamma\left(\frac{2-D}{2}\right)=\frac{\Gamma(\frac{\eta}{2})}{\frac{\eta}{2}-1}=-\frac{2}{\eta}+\gamma-1+\mathcal{O}(\eta)$$
$$\frac{1}{(4\pi)^{\frac{D-1}{2}}}=\frac{1}{(4\pi)^{\frac{3}{2}}}(4\pi)^{\frac{\eta}{2}}\approx\frac{1}{(4\pi)^{\frac{3}{2}}}\left(1+\frac{\eta}{2}\ln(4\pi)\right)$$
$$\frac{1}{(\tilde{m}_\pi^2+\tilde{q}^2x(1-x))^{\frac{4-D}{2}}}\approx 1-\frac{\eta}{2}\ln(\tilde{m}_\pi^2+\tilde{q}^2x(1-x))$$
$$\frac{1}{(\tilde{m}_\pi^2+\tilde{q}^2x(1-x))^{\frac{2-D}{2}}}\approx\left[1-\frac{\eta}{2}\ln(\tilde{m}_\pi^2+\tilde{q}^2x(1-x))\right](\tilde{m}_\pi^2+\tilde{q}^2x(1-x)). \tag{B.33}$$

Concerning the properties of the Γ-function, see, e.g., Ref. [232]; $\gamma = 0.5772\ldots$ is Euler's constant; and we used $a^\epsilon=\exp(\epsilon\ln a)\approx 1+\epsilon\ln a+\cdots$.

Hence

$$V=\boldsymbol{\tau}_1\cdot\boldsymbol{\tau}_2\frac{g_A^2}{8f_\pi^4}\frac{\lambda^2}{\Gamma(\frac{3}{2})}\frac{1}{(4\pi)^{\frac{3}{2}}}\left(1+\frac{\eta}{2}\ln(4\pi)\right)\int_0^1 dx$$
$$\times\left\{\frac{3-\eta}{2}\left(-\frac{2}{\eta}+\gamma-1+\mathcal{O}(\eta)\right)\left[1-\frac{\eta}{2}\ln(\tilde{m}_\pi^2+\tilde{q}^2x(1-x))\right](\tilde{m}_\pi^2+\tilde{q}^2x(1-x))\right.$$
$$\left.-x(1-x)\tilde{q}^2\left(\frac{2}{\eta}-\gamma+\mathcal{O}(\eta)\right)\left[1-\frac{\eta}{2}\ln(\tilde{m}_\pi^2+\tilde{q}^2x(1-x))\right]\right\} \tag{B.34}$$

and neglecting terms of order η

$$V=\boldsymbol{\tau}_1\cdot\boldsymbol{\tau}_2\frac{g_A^2}{8f_\pi^4}\frac{\lambda^2}{\Gamma(\frac{3}{2})}\frac{1}{(4\pi)^{\frac{3}{2}}}\left[\left(-\frac{2}{\eta}+\gamma-1-\ln(4\pi)\right)\left(\frac{3}{2}\tilde{m}_\pi^2+\frac{5}{12}\tilde{q}^2\right)\right.$$
$$\left.+\tilde{m}_\pi^2+\frac{1}{3}\tilde{q}^2+\int_0^1 dx\left(\frac{3}{2}\tilde{m}_\pi^2+\frac{5}{2}\tilde{q}^2x(1-x)\right)\ln(\tilde{m}_\pi^2+\tilde{q}^2x(1-x))\right]. \tag{B.35}$$

The integral over the logarithmic term is

$$\int_0^1 dx\left(\frac{3}{2}\tilde{m}_\pi^2+\frac{5}{2}\tilde{q}^2x(1-x)\right)\ln(\tilde{m}_\pi^2+\tilde{q}^2x(1-x))=-\frac{4}{3}\tilde{m}_\pi^2-\frac{25}{36}\tilde{q}^2+\left(3\tilde{m}_\pi^2+\frac{5}{6}\tilde{q}^2\right)\ln(\tilde{m}_\pi)$$
$$+\frac{1}{6}(8\tilde{m}_\pi^2+5\tilde{q}^2)L(q), \tag{B.36}$$

where

$$L(q)\equiv\frac{w}{q}\ln\frac{w+q}{2m_\pi},\quad w\equiv\sqrt{4m_\pi^2+q^2},\ \text{and}\ q=|\vec{q}|. \tag{B.37}$$

Introducing the abbreviation

$$R\equiv-\frac{2}{\eta}+\gamma-1-\ln(4\pi), \tag{B.38}$$

the final result for the *triangle diagrams at NLO* in dimensional regularization reads

$$V=\boldsymbol{\tau}_1\cdot\boldsymbol{\tau}_2\frac{g_A^2}{384\pi^2f_\pi^4}\left[(18m_\pi^2+5q^2)R-4m_\pi^2-\frac{13}{3}q^2+2(18m_\pi^2+5q^2)\ln\left(\frac{m_\pi}{\lambda}\right)+(16m_\pi^2+10q^2)L(q)\right]. \tag{B.39}$$

Renormalization in a Modified Minimal Subtraction scheme ($\overline{MS}$-scheme) [228] amounts to omitting the R-term.

B.2. Football diagram

B.2.1. The football in covariant perturbation theory

The football diagram is shown in Fig. B.2. In the HB formalism, one obtains

$$V=i\frac{1}{2}\frac{1}{16f_\pi^4}\int\frac{d^4l}{(2\pi)^4}(2l^0+q^0)\epsilon^{abc}\tau_1^c\frac{i}{(l+q)^2-m_\pi^2+i\epsilon}\frac{i}{l^2-m_\pi^2+i\epsilon}(2l^0+q^0)\epsilon^{bad}\tau_2^d, \tag{B.40}$$

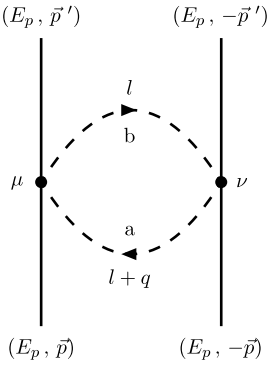

Fig. B.2. Two-pion-exchange football diagram at NLO.

where the factor $\frac{1}{2}$ is a combinatoric factor and $q = (0, \vec{p}\,' - \vec{p})$. Using $\epsilon^{abc}\tau_1^c\epsilon^{bad}\tau_2^d = -2\boldsymbol{\tau}_1\cdot\boldsymbol{\tau}_2$ and $q^0 = 0$,

$$V = i\boldsymbol{\tau}_1\cdot\boldsymbol{\tau}_2\frac{1}{4f_\pi^4}\int\frac{d^4l}{(2\pi)^4}\,\frac{1}{(l+q)^2-m_\pi^2+i\epsilon}\,\frac{(l^0)^2}{l^2-m_\pi^2+i\epsilon}. \tag{B.41}$$

It is again of interest to compare with what other authors obtain for the diagram under consideration. As discussed in conjunction with the triangle diagrams, in the work of Ref. [54], time-ordered perturbation theory (TOPT) (also known as old-fashioned PT) is used in which loop integrals extend only over the three space dimensions. Therefore, we will perform the integration over the time component in Eq. (B.41) to make a comparison with TOPT possible. Substituting $l = \frac{1}{2}(l' - q)$,

$$\begin{aligned} V &= i\boldsymbol{\tau}_1\cdot\boldsymbol{\tau}_2\frac{1}{16f_\pi^4}\int\frac{d^4l'}{(2\pi)^4}\,\frac{1}{(l'+q)^2-4m_\pi^2+i\epsilon}\,\frac{(l'^0)^2}{(l'-q)^2-4m_\pi^2+i\epsilon} \\ &= i\boldsymbol{\tau}_1\cdot\boldsymbol{\tau}_2\frac{1}{16f_\pi^4}\int\frac{d^4l'}{(2\pi)^4}\,\frac{1}{(l'^0)^2-\omega_+^2+i\epsilon}\,\frac{(l'^0)^2}{(l'^0)^2-\omega_-^2+i\epsilon} \end{aligned} \tag{B.42}$$

with

$$\omega_\pm = \sqrt{(\vec{l}\,'\pm\vec{q})^2+4m_\pi^2}, \tag{B.43}$$

and applying the residue theorem yields

$$\begin{aligned} V &= \boldsymbol{\tau}_1\cdot\boldsymbol{\tau}_2\frac{1}{16f_\pi^4}\int\frac{d^3l'}{(2\pi)^3}\,\left\{\frac{1}{2\omega_+}\,\frac{\omega_+^2}{\omega_+^2-\omega_-^2}+\frac{\omega_-^2}{\omega_-^2-\omega_+^2}\,\frac{1}{2\omega_-}\right\} \\ &= \boldsymbol{\tau}_1\cdot\boldsymbol{\tau}_2\frac{1}{32f_\pi^4}\int\frac{d^3l'}{(2\pi)^3}\,\frac{\omega_+-\omega_-}{\omega_+^2-\omega_-^2} \\ &= \boldsymbol{\tau}_1\cdot\boldsymbol{\tau}_2\frac{1}{32f_\pi^4}\int\frac{d^3l'}{(2\pi)^3}\,\frac{1}{\omega_++\omega_-}. \end{aligned} \tag{B.44}$$

This amplitude for the football diagram does not agree with Ref. [54], where the result for the football is given by the first term in Eq. (20). In our notation, the result of Ref. [54] and also of Ref. [64] [cf. Eq. (4.30) therein] is

$$V_{\rm ORK} = -\boldsymbol{\tau}_1\cdot\boldsymbol{\tau}_2\frac{1}{128f_\pi^4}\int\frac{d^3l'}{(2\pi)^3}\,\frac{1}{\omega_+\omega_-}\,\frac{(\omega_+-\omega_-)^2}{\omega_++\omega_-}. \tag{B.45}$$

B.2.2. The proper calculation of the football in time-ordered perturbation theory

We will explain now the reason for the discrepancy between Eqs. (B.44) and (B.45). In covariant PT theory one assumes for the interaction Hamiltonian density $\mathcal{H}_I = -\mathcal{L}_I$. This is strictly speaking not correct for derivative coupling, because in that case one has $\mathcal{H}_I = -\mathcal{L}_I +$ *additional noncovariant terms*. For relatively simple cases of derivative coupling, the additional terms are of the contact type. Now, in covariant PT, there are also noncovariant contributions to the propagator, and it has been shown that for certain interactions with derivative coupling these two groups of additional terms cancel. So, as a procedural matter, in covariant PT, one can use $\mathcal{H}_I = -\mathcal{L}_I$ and the usual covariant Feynman propagators, and everything comes out right (cf. e.g., Ref. [225], pp. 318–323 therein).

In TOPT the story is different. Propagators are just noncovariant energy denominators, which cancel nothing. Therefore, the full interaction Hamiltonian including all additional terms has to be use to obtain the same result as in covariant PT.

However, in Ref. [54] $\mathcal{H}_I = -\mathcal{L}_I$ is assumed in conjunction with TOPT. Thus, the contributions from the additional contact terms in the Hamiltonian are missing in the calculation of Ref. [54] and that is the reason for the discrepancy with the covariant calculation, as we will show now.

Using the notation of Ref. [225], the time component of the current associated with the Lagrangian density Eq. (A.43) reads

$$J_b^0 = \frac{1}{4f_\pi^2}\bar{N}\tau^c N\epsilon^{abc}\pi_a \tag{B.46}$$

and the additional term in the interaction Hamiltonian is [cf. Eq. (12) of Ref. [51]]

$$H_I^{\rm add}(t) = \int d^3x\,\frac{1}{2}\,(J_b^0)(J_b^0) = \int d^3x\,\frac{1}{2}\,\frac{1}{16f_\pi^4}\,\bar{N}\tau^c N\epsilon^{abc}\pi_a\bar{N}\tau^{c'}N\epsilon^{a'bc'}\pi_{a'}. \tag{B.47}$$

This generates the following leading contribution to the S-matrix

$$\begin{aligned}\langle p_1' p_2'|S|p_1 p_2\rangle &= (-i)\int dt\, H_I^{\rm add}(t) = -i\int d^4x\,\frac{1}{16f_\pi^4}\frac{1}{2}\epsilon^{abc}\epsilon^{a'bc'}\langle p_1' p_2'|\bar{N}\tau^c N\pi_a\bar{N}\tau^{c'}N\pi_{a'}|p_1 p_2\rangle \\ &= \frac{-i}{(2\pi)^6}\int d^4x\,2\frac{1}{16f_\pi^4}\frac{1}{2}\epsilon^{abc}\epsilon^{a'bc'}\tau_1^c\tau_2^{c'}e^{i(p_1'+p_2'-p_1-p_2)x}\langle 0|\pi_a\pi_{a'}|0\rangle,\end{aligned} \tag{B.48}$$

where the factor of 2 comes from the permutation of the nucleon fields and the exchange term is left out. For the pion fields, we obtain

$$\begin{aligned}\langle 0|\pi_a\pi_{a'}|0\rangle &= \frac{1}{(2\pi)^3}\int d^3k d^3k'\,\frac{1}{\sqrt{4\omega_k\omega_{k'}}}\,\langle 0|\left(a_a(\vec{k})e^{-ikx}+a_a^\dagger(\vec{k})e^{ikx}\right)\left(a_{a'}(\vec{k}')e^{-ik'x}+a_{a'}^\dagger(\vec{k}')e^{ik'x}\right)|0\rangle \\ &= \frac{1}{(2\pi)^3}\int d^3k d^3k'\,\frac{1}{\sqrt{4\omega_k\omega_{k'}}}\delta^3(\vec{k}-\vec{k}')\delta_{aa'} = \int\frac{d^3k}{(2\pi)^3}\,\frac{1}{2\omega_k}\delta_{aa'}.\end{aligned} \tag{B.49}$$

Hence,

$$\begin{aligned}\langle p_1' p_2'|S|p_1 p_2\rangle &= \frac{-i}{(2\pi)^6}\int d^4x\,\frac{1}{16f_\pi^4}\,\epsilon^{abc}\epsilon^{a'bc'}\tau_1^c\tau_2^{c'}e^{i(p_1'+p_2'-p_1-p_2)x}\int\frac{d^3k}{(2\pi)^3}\,\frac{1}{2\omega_k}\delta_{aa'} \\ &= -i(2\pi)^4\delta^4(p_1'+p_2'-p_1-p_2)\frac{1}{(2\pi)^6}\,\frac{1}{16f_\pi^4}\,\epsilon^{abc}\epsilon^{a'bc'}\tau_1^c\tau_2^{c'}\int\frac{d^3k}{(2\pi)^3}\,\frac{1}{2\omega_k}\delta_{aa'} \\ &= -i(2\pi)^4\delta^4(p_1'+p_2'-p_1-p_2)\,\frac{1}{(2\pi)^6}\,\frac{1}{8f_\pi^4}\boldsymbol{\tau}_1\cdot\boldsymbol{\tau}_2\int\frac{d^3k}{(2\pi)^3}\,\frac{1}{2\sqrt{\vec{k}^2+m_\pi^2}} \\ &= -i(2\pi)^4\delta^4(p_1'+p_2'-p_1-p_2)\frac{1}{(2\pi)^6}\,\frac{1}{32f_\pi^4}\boldsymbol{\tau}_1\cdot\boldsymbol{\tau}_2\int\frac{d^3l}{(2\pi)^3}\,\frac{1}{2\sqrt{\vec{l}^2+4m_\pi^2}},\end{aligned} \tag{B.50}$$

where $\vec{k} = \vec{l}/2$ and $\epsilon^{abc}\epsilon^{abc'}\tau_1^c\tau_2^{c'} = 2\boldsymbol{\tau}_1\cdot\boldsymbol{\tau}_2$. From the last equation, one can read off the contribution to the T-matrix [cf. Eqs. (A.35) and (A.36)], which is

$$V^{\rm add} = \boldsymbol{\tau}_1\cdot\boldsymbol{\tau}_2\frac{1}{32f_\pi^4}\int\frac{d^3l}{(2\pi)^3}\,\frac{1}{2\sqrt{\vec{l}^2+4m_\pi^2}}. \tag{B.51}$$

Obviously, this additional term does not depend on external momenta, only on m_π.

For the amplitude, calculated in TOPT and including all terms, we now get

$$V = V_{\rm ORK} + V^{\rm add} \tag{B.52}$$

$$= V_{\rm ORK} + \boldsymbol{\tau}_1\cdot\boldsymbol{\tau}_2\frac{1}{32f_\pi^4}\int\frac{d^3l}{(2\pi)^3}\,\frac{1}{2\sqrt{\vec{l}^2+4m_\pi^2}} \tag{B.53}$$

$$= V_{\rm ORK} + \boldsymbol{\tau}_1\cdot\boldsymbol{\tau}_2\frac{1}{32f_\pi^4}\int\frac{d^3l'}{(2\pi)^3}\,\frac{1}{2\omega_+} \tag{B.54}$$

$$= V_{\rm ORK} + \boldsymbol{\tau}_1\cdot\boldsymbol{\tau}_2\frac{1}{32f_\pi^4}\int\frac{d^3l'}{(2\pi)^3}\left\{\frac{1}{4\omega_+}+\frac{1}{4\omega_-}\right\} \tag{B.55}$$

$$= V_{\rm ORK} + \boldsymbol{\tau}_1 \cdot \boldsymbol{\tau}_2 \frac{1}{32 f_\pi^4} \int \frac{d^3 l'}{(2\pi)^3} \frac{(\omega_+ + \omega_-)^2}{\omega_+ + \omega_-} \frac{1}{4\omega_+ \omega_-} \tag{B.56}$$

$$= \boldsymbol{\tau}_1 \cdot \boldsymbol{\tau}_2 \frac{1}{32 f_\pi^4} \int \frac{d^3 l'}{(2\pi)^3} \frac{1}{\omega_+ + \omega_-} \tag{B.57}$$

where we used the transformations $\vec{l} = \vec{l}' + \vec{q}$ and $\vec{l}' \mapsto -\vec{l}'$. This result is now identical to the one obtained using covariant PT, Eq. (B.44), as it should. We note that the term, Eq. (B.51), left out in the calculation of Ref. [54], is a contact term $\propto m_\pi^2$, which affects the m_π dependence of the 2PE potential. Such terms are relevant for the charge dependence of the nuclear force [188] and for considerations of the chiral limit [129]. If these more subtle aspects are not of interest, then omitting the contact equation (B.51) is acceptable, since contact terms with adjustable parameters are added to the theory anyhow (cf. Section 2.3).

B.2.3. Dimensional regularization of the football

We start from Eq. (B.41),

$$V = i\boldsymbol{\tau}_1 \cdot \boldsymbol{\tau}_2 \frac{1}{4 f_\pi^4} \int \frac{d^4 l}{(2\pi)^4} \frac{1}{(l+q)^2 - m_\pi^2 + i\epsilon} \frac{(l^0)^2}{l^2 - m_\pi^2 + i\epsilon}, \tag{B.58}$$

and apply the Feynman trick equation (B.19),

$$V = -\boldsymbol{\tau}_1 \cdot \boldsymbol{\tau}_2 \frac{1}{4 f_\pi^4} \int_0^1 dx \int \frac{d^4 l}{i(2\pi)^4} \frac{(l^0)^2}{[l^2 + (2lq + q^2)x - m_\pi^2 + i\epsilon]^2}. \tag{B.59}$$

Using the residue theorem for the l^0 integration, we obtain

$$V = -\boldsymbol{\tau}_1 \cdot \boldsymbol{\tau}_2 \frac{1}{4 f_\pi^4} \int_0^1 dx \int \frac{dl^0\, d^3 l}{i(2\pi)^4} \frac{(l^0)^2}{(l^0 - l_1^0)^2 (l^0 + l_1^0)^2}$$

$$= \boldsymbol{\tau}_1 \cdot \boldsymbol{\tau}_2 \frac{1}{4 f_\pi^4} \int_0^1 dx \int \frac{d^3 l}{(2\pi)^3} \frac{1}{4} \frac{1}{l_1^0} \tag{B.60}$$

with $l_1^0 = \sqrt{\vec{l}^2 + m_\pi^2 + (2\vec{l} \cdot \vec{q} + \vec{q}^2)x} - i\epsilon$.

We treat this divergent integral by dimensional regularization (cf. Appendix B.1.2). For that purpose, we extend the integral to $(D-1)$ dimensions and shift the integration variable to $\lambda \vec{k} = \vec{l} + x\vec{q}$ with λ the renormalization scale:

$$V = \boldsymbol{\tau}_1 \cdot \boldsymbol{\tau}_2 \frac{1}{16 f_\pi^4} \lambda^2 \int_0^1 dx \int \frac{d^{D-1} k}{(2\pi)^{D-1}} \frac{1}{[\vec{k}^2 + \tilde{m}_\pi^2 + \tilde{q}^2 x(1-x)]^{1/2}}, \tag{B.61}$$

where quantities with a tilde are divided by λ and, thus, dimensionless; and $\vec{k}$ is dimensionless by definition. The angular integration yields [cf. Eqs. (B.28) and (B.29)]

$$V = \boldsymbol{\tau}_1 \cdot \boldsymbol{\tau}_2 \frac{1}{16 f_\pi^4} \frac{2\lambda^2}{\Gamma(\frac{D-1}{2})(4\pi)^{(D-1)/2}} \int_0^1 dx \int_0^\infty dk \frac{k^{D-2}}{[\vec{k}^2 + \tilde{m}_\pi^2 + \tilde{q}^2 x(1-x)]^{1/2}} \tag{B.62}$$

and applying Eq. (B.31) we obtain

$$V = \boldsymbol{\tau}_1 \cdot \boldsymbol{\tau}_2 \frac{1}{16 f_\pi^4} \frac{\lambda^2 \Gamma(\frac{2-D}{2})}{\Gamma(\frac{1}{2})(4\pi)^{(D-1)/2}} \int_0^1 dx \frac{1}{[\tilde{m}_\pi^2 + \tilde{q}^2 x(1-x)]^{(2-D)/2}}. \tag{B.63}$$

Choosing $D = 4 - \eta$ and using relations displayed in Eq. (B.33) results in

$$V = \boldsymbol{\tau}_1 \cdot \boldsymbol{\tau}_2 \frac{1}{16 f_\pi^4} \frac{\lambda^2}{\Gamma(\frac{1}{2})\,(4\pi)^{\frac{3}{2}}} \left(1 + \frac{\eta}{2} \ln(4\pi)\right) \left(-\frac{2}{\eta} + \gamma - 1\right)$$

$$\times \int_0^1 dx \left[1 - \frac{\eta}{2} \ln(\tilde{m}_\pi^2 + \tilde{q}^2 x(1-x))\right] \left(\tilde{m}_\pi^2 + \tilde{q}^2 x(1-x)\right), \tag{B.64}$$

and, neglecting terms of order η, leads to

$$V = \boldsymbol{\tau}_1 \cdot \boldsymbol{\tau}_2 \frac{1}{16 f_\pi^4} \frac{\lambda^2}{\Gamma(\frac{1}{2})\,(4\pi)^{\frac{3}{2}}} \left[\left(-\frac{2}{\eta} + \gamma - 1 - \ln(4\pi)\right) \left(\tilde{m}_\pi^2 + \frac{1}{6}\tilde{q}^2\right)\right.$$

$$\left. + \int_0^1 dx \left(\tilde{m}_\pi^2 + \tilde{q}^2 x(1-x)\right) \ln(\tilde{m}_\pi^2 + \tilde{q}^2 x(1-x))\right]. \tag{B.65}$$

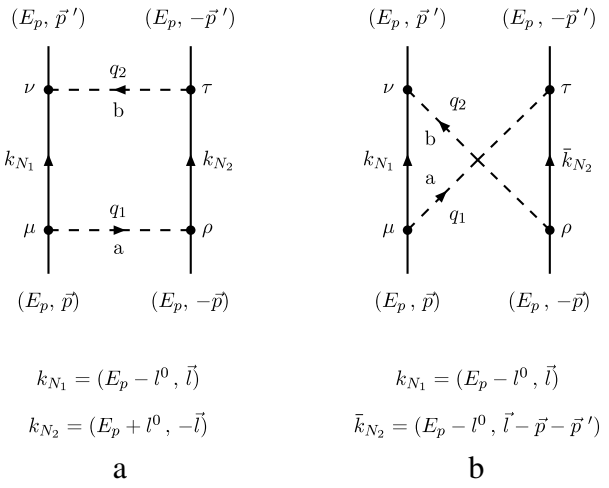

Fig. B.3. Two-pion-exchange planar box (a) and crossed box (b) diagrams at NLO.

The integral over the logarithmic term is

$$\int_0^1 dx \left(\tilde{m}_\pi^2 + \tilde{q}^2 x(1-x)\right) \ln(\tilde{m}_\pi^2 + \tilde{q}^2 x(1-x)) = -\frac{4}{3}\tilde{m}_\pi^2 - \frac{5}{18}\tilde{q}^2 + \left(2\tilde{m}_\pi^2 + \frac{1}{3}\tilde{q}^2\right)\ln(\tilde{m}_\pi) + \frac{\tilde{q}^2 + 4\tilde{m}_\pi^2}{3} L(q) \quad \text{(B.66)}$$

with $L(q)$ given in Eq. (B.37).

Thus, for the *football at NLO*, we finally get

$$V = \boldsymbol{\tau}_1 \cdot \boldsymbol{\tau}_2 \frac{1}{384\pi^2 f_\pi^4} \left[\frac{1}{2} R\,(6m_\pi^2 + q^2) - 4m_\pi^2 - \frac{5}{6}q^2 + (6m_\pi^2 + q^2)\ln\left(\frac{m_\pi}{\lambda}\right) + w^2 L(q)\right] \quad \text{(B.67)}$$

with R as defined in Eq. (B.38) and w given in Eq. (B.37).

B.3. Box and crossed box diagrams

The planar box (pb) and crossed box (cb) diagrams together with our notation are shown in Fig. B.3 and the corresponding amplitudes are given by

$$\begin{aligned} V^{\rm pb} &= i\frac{g_A^4}{16 f_\pi^4} \int \frac{d^4 l}{(2\pi)^4} \frac{i}{q_1^2 - m_\pi^2 + i\epsilon} \frac{i}{q_2^2 - m_\pi^2 + i\epsilon} \bar{u}_1(\vec{p}\,')(-q_2^\nu)\tau_1^b \gamma_\nu \gamma_5 \frac{i(\not{k}_{N_1} + M_N)}{k_{N_1}^2 - M_N^2 + i\epsilon} q_1^\mu \tau_1^a \gamma_\mu \gamma_5 u_1(\vec{p}) \\ &\quad \times \bar{u}_2(-\vec{p}\,') q_2^\tau \tau_2^b \gamma_\tau \gamma_5 \frac{i(\not{k}_{N_2} + M_N)}{k_{N_2}^2 - M_N^2 + i\epsilon} (-q_1^\rho)\tau_2^a \gamma_\rho \gamma_5 u_2(-\vec{p}), \end{aligned} \quad \text{(B.68)}$$

$$\begin{aligned} V^{\rm cb} &= i\frac{g_A^4}{16 f_\pi^4} \int \frac{d^4 l}{(2\pi)^4} \frac{i}{q_1^2 - m_\pi^2 + i\epsilon} \frac{i}{q_2^2 - m_\pi^2 + i\epsilon} \bar{u}_1(\vec{p}\,')(-q_2^\nu)\tau_1^b \gamma_\nu \gamma_5 \frac{i(\not{k}_{N_1} + M_N)}{k_{N_1}^2 - M_N^2 + i\epsilon} q_1^\mu \tau_1^a \gamma_\mu \gamma_5 u_1(\vec{p}) \\ &\quad \times \bar{u}_2(-\vec{p}\,')(-q_1^\tau)\tau_2^a \gamma_\tau \gamma_5 \frac{i(\not{\bar{k}}_{N_2} + M_N)}{\bar{k}_{N_2}^2 - M_N^2 + i\epsilon} q_2^\rho \tau_2^b \gamma_\rho \gamma_5 u_2(-\vec{p}), \end{aligned} \quad \text{(B.69)}$$

where we chose the loop momentum such that its time component is the energy transferred by the pions and its space components are the ones of an intermediate nucleon; $k_{N_1} = (E_p - l^0, \vec{l})$, $k_{N_2} = (E_p + l^0, -\vec{l})$, $q_1 = (l^0, \vec{p} - \vec{l})$, and $q_2 = (l^0, \vec{p}\,' - \vec{l})$, with $E_p = \sqrt{\vec{p}^{\,2} + M_N^2}$, for the planar box diagram. For the crossed box, only the momentum of nucleon 2 is different, $\bar{k}_{N_2} = (E_p - l^0, \vec{l} - \vec{p} - \vec{p}\,')$. The poles are located at

$$\begin{aligned} l_1^0 &= E_p \mp E_l \pm i\epsilon \\ l_2^0 &= -E_p \mp E_l \pm i\epsilon \\ \bar{l}_2^0 &= E_p \mp E_{\bar{l}} \pm i\epsilon \\ l_3^0 &= \mp\omega_1 \pm i\epsilon \\ l_4^0 &= \mp\omega_2 \pm i\epsilon \end{aligned} \quad \text{(B.70)}$$

with $\omega_1 = \sqrt{(\vec{p}-\vec{l})^2+m_\pi^2}$, $\omega_2 = \sqrt{(\vec{p}\,'-\vec{l})^2+m_\pi^2}$, $E_l = \sqrt{\vec{l}^{\,2}+M_N^2}$, and $E_{\bar{l}} = \sqrt{(\vec{l}-\vec{p}-\vec{p}')^2+M_N^2}$. The first three lines state the nucleon poles and the last two lines describe the pion poles. l_2^0 and $\bar{l}_2^0$ are the poles for nucleon 2 in the box and crossed box diagrams, respectively. We apply the Feynman trick equation (B.19) to the pion propagators and obtain

$$\begin{aligned} V^{\rm pb} &= i\frac{g_A^4}{16f_\pi^4}(3-2\boldsymbol{\tau}_1\cdot\boldsymbol{\tau}_2)\int_0^1 dx\int\frac{d^4l}{(2\pi)^4}\,\frac{1}{[l^{0\,2}-\omega_1^2+(\omega_1^2-\omega_2^2)x+i\epsilon]^2}\\ &\quad\times\bar{u}_1(\vec{p}\,')q_2^\nu\gamma_\nu\frac{\not{k}_{N_1}-M_N}{(l^0-E_p)^2-(l_1^0-E_p)^2}q_1^\mu\gamma_\mu u_1(\vec{p})\\ &\quad\times\bar{u}_2(-\vec{p}\,')q_2^\tau\gamma_\tau\frac{\not{k}_{N_2}-M_N}{(l^0+E_p)^2-(l_2^0+E_p)^2}q_1^\rho\gamma_\rho u_2(-\vec{p}), \end{aligned} \tag{B.71}$$

$$\begin{aligned} V^{\rm cb} &= i\frac{g_A^4}{16f_\pi^4}(3+2\boldsymbol{\tau}_1\cdot\boldsymbol{\tau}_2)\int_0^1 dx\int\frac{d^4l}{(2\pi)^4}\,\frac{1}{[l^{0\,2}-\omega_1^2+(\omega_1^2-\omega_2^2)x+i\epsilon]^2}\\ &\quad\times\bar{u}_1(\vec{p}\,')q_2^\nu\gamma_\nu\frac{\not{k}_{N_1}-M_N}{(l^0-E_p)^2-(l_1^0-E_p)^2}q_1^\mu\gamma_\mu u_1(\vec{p})\bar{u}_2(-\vec{p}\,')q_1^\tau\gamma_\tau\frac{\bar{\not{k}}_{N_2}-M_N}{(l^0-E_p)^2-(\bar{l}_2^0-E_p)^2}q_2^\rho\gamma_\rho u_2(-\vec{p}), \end{aligned} \tag{B.72}$$

where we used $\tau_1^b\tau_1^a\tau_2^b\tau_2^a = 3-2\boldsymbol{\tau}_1\cdot\boldsymbol{\tau}_2$ and $\tau_1^b\tau_1^a\tau_2^a\tau_2^b = 3+2\boldsymbol{\tau}_1\cdot\boldsymbol{\tau}_2$. The pion poles are now given by

$$l_{34}^0 = \mp\sqrt{(1-x)\omega_1^2+x\omega_2^2}\pm i\epsilon. \tag{B.73}$$

Performing the $1/M_N$ expansion yields

$$\bar{u}_1\gamma_\nu(\not{k}_{N_1}-M_N)\gamma_\mu u_1 \approx \delta_{\nu i}\delta_{\mu j}2M_N(\delta_{ij}+i\epsilon^{ijr}\sigma_1^r), \tag{B.74}$$

$$\bar{u}_2\gamma_\tau(\not{k}_{N_2}-M_N)\gamma_\rho u_2 \approx \delta_{\tau m}\delta_{\rho n}2M_N(\delta_{mn}+i\epsilon^{mns}\sigma_2^s), \tag{B.75}$$

$$\frac{1}{(l^0-E_p)^2-(l_1^0-E_p)^2}\times\frac{1}{(l^0+E_p)^2-(l_2^0+E_p)^2}\approx\frac{1}{4M_N^2}\frac{1}{(-l^0+i\zeta)(l^0+i\zeta)}, \tag{B.76}$$

$$\frac{1}{(l^0-E_p)^2-(l_1^0-E_p)^2}\times\frac{1}{(l^0-E_p)^2-(\bar{l}_2^0-E_p)^2}\approx\frac{1}{4M_N^2}\frac{1}{(l^0-i\epsilon)^2}, \tag{B.77}$$

where $i\zeta = \frac{\vec{p}^2-\vec{l}^2}{2M_N}+i\epsilon$, which avoids the pinch singularity (cf. discussion on p. 7 of Ref. [51]). Hence,

$$V^{\rm pb} = i\frac{g_A^4}{16f_\pi^4}(3-2\boldsymbol{\tau}_1\cdot\boldsymbol{\tau}_2)\int_0^1 dx\int\frac{d^4l}{(2\pi)^4}\,\frac{q_2^iq_1^j(\delta_{ij}+i\epsilon^{ijr}\sigma_1^r)q_2^mq_1^n(\delta_{mn}+i\epsilon^{mns}\sigma_2^s)}{(l^0-l_{34}^0)^2(l^0+l_{34}^0)^2(l^0+i\zeta)(-l^0+i\zeta)}, \tag{B.78}$$

$$V^{\rm cb} = i\frac{g_A^4}{16f_\pi^4}(3+2\boldsymbol{\tau}_1\cdot\boldsymbol{\tau}_2)\int_0^1 dx\int\frac{d^4l}{(2\pi)^4}\,\frac{q_2^iq_1^j(\delta_{ij}+i\epsilon^{ijr}\sigma_1^r)q_1^mq_2^n(\delta_{mn}+i\epsilon^{mns}\sigma_2^s)}{(l^0-l_{34}^0)^2(l^0+l_{34}^0)^2(l^0-i\epsilon)^2}. \tag{B.79}$$

In both diagrams we have a contribution from the pion poles, but in the box diagram there is also a contribution from the nucleon poles which is enhanced in the $1/M_N$ expansion and gives the iterated 1PE. We work this out by closing the l^0 contour integral in the lower half-plane and, collecting the contribution from the pole at $l^0 = -i\zeta$, results in

$$V_{\rm it}^{\rm pb} = \frac{g_A^4}{16f_\pi^4}(3-2\boldsymbol{\tau}_1\cdot\boldsymbol{\tau}_2)\int_0^1 dx\int\frac{d^3l}{(2\pi)^3}\,\frac{q_2^iq_1^j(\delta_{ij}+i\epsilon^{ijr}\sigma_1^r)q_2^mq_1^n(\delta_{mn}+i\epsilon^{mns}\sigma_2^s)}{(l_{34}^0)^4(2i\zeta)}. \tag{B.80}$$

Using

$$\int_0^1 dx\frac{1}{(l_{34}^0)^4} = \int_0^1 dx\frac{1}{[\omega_1^2-(\omega_1^2-\omega_2^2)x]^2} = \frac{1}{\omega_1^2\omega_2^2}, \tag{B.81}$$

$$q_2^iq_1^j(\delta_{ij}+i\epsilon^{ijr}\sigma_1^r)q_2^mq_1^n(\delta_{mn}+i\epsilon^{mns}\sigma_2^s) = \vec{\sigma}_1\cdot(\vec{p}\,'-\vec{l})\vec{\sigma}_1\cdot(\vec{p}-\vec{l})\vec{\sigma}_2\cdot(\vec{p}\,'-\vec{l})\vec{\sigma}_2\cdot(\vec{p}-\vec{l}), \tag{B.82}$$

$$\frac{1}{2i\zeta} = \frac{M_N}{\vec{p}^2-\vec{l}^2+i\epsilon}, \tag{B.83}$$

and changing $\vec{l}\to-\vec{l}$, we obtain

$$V_{\rm it}^{\rm pb} = \frac{g_A^4M_N}{16f_\pi^4}(3-2\boldsymbol{\tau}_1\cdot\boldsymbol{\tau}_2)\int\frac{d^3l}{(2\pi)^3}\,\frac{\vec{\sigma}_1\cdot(\vec{l}+\vec{p}\,')\vec{\sigma}_2\cdot(\vec{l}+\vec{p}\,')\vec{\sigma}_1\cdot(\vec{l}+\vec{p})\,\vec{\sigma}_2\cdot(\vec{l}+\vec{p})}{(\vec{p}^2-\vec{l}^2+i\epsilon)((\vec{l}+\vec{p})^2+m_\pi^2)((\vec{l}+\vec{p}\,')^2+m_\pi^2)} \tag{B.84}$$

which is the LO iterated 1PE.

Notice that the contribution from the nucleon pole in the crossed box diagram is zero.

Next, we calculate the contribution from the pion poles closing the l^0 contour integral in the lower half-plane with the pole of interest located at $l^0 = l^0_{34} = \sqrt{(1-x)\omega_1^2 + x\omega_2^2} - i\epsilon$:

$$V^{\rm pb} = \frac{3g_A^4}{64f_\pi^4}(3 - 2\boldsymbol{\tau}_1\cdot\boldsymbol{\tau}_2)\int_0^1 dx \int \frac{d^3l}{(2\pi)^3}\frac{(\vec{q}_1\cdot\vec{q}_2 + i\vec{\sigma}_1\cdot(\vec{q}_2\times\vec{q}_1))(\vec{q}_1\cdot\vec{q}_2 + i\vec{\sigma}_2\cdot(\vec{q}_2\times\vec{q}_1))}{(l^0_{34})^5}, \tag{B.85}$$

$$V^{\rm cb} = -\frac{3g_A^4}{64f_\pi^4}(3 + 2\boldsymbol{\tau}_1\cdot\boldsymbol{\tau}_2)\int_0^1 dx \int \frac{d^3l}{(2\pi)^3}\frac{(\vec{q}_1\cdot\vec{q}_2 + i\vec{\sigma}_1\cdot(\vec{q}_2\times\vec{q}_1))(\vec{q}_1\cdot\vec{q}_2 - i\vec{\sigma}_2\cdot(\vec{q}_2\times\vec{q}_1))}{(l^0_{34})^5}. \tag{B.86}$$

We treat the divergent integrals by dimensional regularization (cf. Appendix B.1.2). For that purpose, we extend the integrals to $(D-1)$ dimensions and shift the integration variable to $\lambda\vec{k} = \vec{p} - \vec{l} + x\vec{q}$ with λ the renormalization scale and $\vec{q} = \vec{p}\,' - \vec{p}$:

$$V^{\rm pb} = \frac{3g_A^4}{64f_\pi^4}(3 - 2\boldsymbol{\tau}_1\cdot\boldsymbol{\tau}_2)\lambda^2\int_0^1 dx \int \frac{d^{D-1}k}{(2\pi)^{D-1}}\frac{(\tilde{q}_1\cdot\tilde{q}_2 + i\vec{\sigma}_1\cdot(\tilde{q}_2\times\tilde{q}_1))(\tilde{q}_1\cdot\tilde{q}_2 + i\vec{\sigma}_2\cdot(\tilde{q}_2\times\tilde{q}_1))}{[k^2 + \tilde{m}_\pi^2 + \tilde{q}^2x(1-x)]^{5/2}}, \tag{B.87}$$

$$V^{\rm cb} = -\frac{3g_A^4}{64f_\pi^4}(3 + 2\boldsymbol{\tau}_1\cdot\boldsymbol{\tau}_2)\lambda^2\int_0^1 dx \int \frac{d^{D-1}k}{(2\pi)^{D-1}}\frac{(\tilde{q}_1\cdot\tilde{q}_2 + i\vec{\sigma}_1\cdot(\tilde{q}_2\times\tilde{q}_1))(\tilde{q}_1\cdot\tilde{q}_2 - i\vec{\sigma}_2\cdot(\tilde{q}_2\times\tilde{q}_1))}{[k^2 + \tilde{m}_\pi^2 + \tilde{q}^2x(1-x)]^{5/2}}, \tag{B.88}$$

where quantities with a tilde are divided by λ and, thus, dimensionless; and $\vec{k}$ is dimensionless by definition. Since

$$\tilde{q}_1 = \vec{k} - x\tilde{q}, \tag{B.89}$$

$$\tilde{q}_2 = \vec{k} - (x-1)\tilde{q}, \tag{B.90}$$

hence

$$\tilde{q}_1\cdot\tilde{q}_2 = k^2 + \tilde{q}^2x(x-1) - (2x-1)\vec{k}\cdot\tilde{q}, \tag{B.91}$$

$$\tilde{q}_2\times\tilde{q}_1 = \tilde{q}\times\vec{k}. \tag{B.92}$$

Terms in odd powers of $\vec{k}$ vanish. Furthermore, because of

$$\int \frac{d^{D-1}k}{(2\pi)^{D-1}}\frac{k_ik_j}{[k^2 + \tilde{m}_\pi^2 + \tilde{q}^2x(1-x)]^{5/2}} = \frac{\delta_{ij}}{D-1}\int \frac{d^{D-1}k}{(2\pi)^{D-1}}\frac{k^2}{[k^2 + \tilde{m}_\pi^2 + \tilde{q}^2x(1-x)]^{5/2}}, \tag{B.93}$$

we have

$$\begin{aligned}
&\int \frac{d^{D-1}k}{(2\pi)^{D-1}}\frac{(\vec{k}\cdot\tilde{q})^2}{[k^2 + \tilde{m}_\pi^2 + \tilde{q}^2x(1-x)]^{5/2}} = \frac{1}{D-1}\int \frac{d^{D-1}k}{(2\pi)^{D-1}}\frac{\tilde{q}^2k^2}{[k^2 + \tilde{m}_\pi^2 + \tilde{q}^2x(1-x)]^{5/2}},\\
&\int \frac{d^{D-1}k}{(2\pi)^{D-1}}\frac{(\vec{k}\cdot\tilde{q})i\vec{\sigma}_i\cdot(\tilde{q}\times\vec{k})}{[k^2 + \tilde{m}_\pi^2 + \tilde{q}^2x(1-x)]^{5/2}} = 0,\\
&\int \frac{d^{D-1}k}{(2\pi)^{D-1}}\frac{i\vec{\sigma}_1\cdot(\tilde{q}\times\vec{k})i\vec{\sigma}_2\cdot(\tilde{q}\times\vec{k})}{[k^2 + \tilde{m}_\pi^2 + \tilde{q}^2x(1-x)]^{5/2}} = \frac{1}{D-1}\int \frac{d^{D-1}k}{(2\pi)^{D-1}}\frac{i^2(\vec{\sigma}_1\times\tilde{q})\cdot(\vec{\sigma}_2\times\tilde{q})k^2}{[k^2 + \tilde{m}_\pi^2 + \tilde{q}^2x(1-x)]^{5/2}}.
\end{aligned} \tag{B.94}$$

Whence

$$\begin{aligned}
V^{\rm pb} &= \frac{3g_A^4}{64f_\pi^4}(3 - 2\boldsymbol{\tau}_1\cdot\boldsymbol{\tau}_2)\lambda^2\int_0^1 dx \int \frac{d^{D-1}k}{(2\pi)^{D-1}}\\
&\quad\times\frac{[k^2 + \tilde{q}^2x(x-1)]^2 + \frac{k^2}{D-1}\left[(2x-1)^2\tilde{q}^2 - (\vec{\sigma}_1\times\tilde{q})\cdot(\vec{\sigma}_2\times\tilde{q})\right]}{[k^2 + \tilde{m}_\pi^2 + \tilde{q}^2x(1-x)]^{5/2}},
\end{aligned} \tag{B.95}$$

$$\begin{aligned}
V^{\rm cb} &= -\frac{3g_A^4}{64f_\pi^4}(3 + 2\boldsymbol{\tau}_1\cdot\boldsymbol{\tau}_2)\lambda^2\int_0^1 dx \int \frac{d^{D-1}k}{(2\pi)^{D-1}}\\
&\quad\times\frac{[k^2 + \tilde{q}^2x(x-1)]^2 + \frac{k^2}{D-1}\left[(2x-1)^2\tilde{q}^2 + (\vec{\sigma}_1\times\tilde{q})\cdot(\vec{\sigma}_2\times\tilde{q})\right]}{[k^2 + \tilde{m}_\pi^2 + \tilde{q}^2x(1-x)]^{5/2}}.
\end{aligned} \tag{B.96}$$

Using $(\vec{\sigma}_1\times\tilde{q})\cdot(\vec{\sigma}_2\times\tilde{q}) = \lambda^{-2}[\vec{q}^{\,2}\vec{\sigma}_1\cdot\vec{\sigma}_2 - (\vec{\sigma}_1\cdot\vec{q})(\vec{\sigma}_2\cdot\vec{q})]$, the sum of the two diagrams is given by

$$V^{\rm pb} + V^{\rm cb} = W_C(\boldsymbol{\tau}_1\cdot\boldsymbol{\tau}_2) + V_S(\vec{\sigma}_1\cdot\vec{\sigma}_2) + V_T(\vec{\sigma}_1\cdot\vec{q})(\vec{\sigma}_2\cdot\vec{q}) \tag{B.97}$$

with

$$W_C = -\frac{3g_A^4}{16f_\pi^4}\,\lambda^2 \int_0^1 dx \int \frac{d^{D-1}k}{(2\pi)^{D-1}} \frac{[k^2+\tilde{q}^2x(x-1)]^2 + \frac{k^2}{D-1}(2x-1)^2\tilde{q}^2}{[k^2+\tilde{m}_\pi^2+\tilde{q}^2x(1-x)]^{5/2}}, \tag{B.98}$$

$$V_T = \frac{9g_A^4}{32f_\pi^4} \int_0^1 dx \int \frac{d^{D-1}k}{(2\pi)^{D-1}} \frac{\frac{k^2}{D-1}}{[k^2+\tilde{m}_\pi^2+\tilde{q}^2x(1-x)]^{5/2}}, \tag{B.99}$$

$$V_S = -q^2 V_T. \tag{B.100}$$

Applying the volume element in $(D-1)$ dimensions, Eqs. (B.28) and (B.29), we find

$$W_C = -\frac{3g_A^4}{16f_\pi^4} \frac{2\lambda^2}{\Gamma(\frac{D-1}{2})(4\pi)^{(D-1)/2}} \int_0^1 dx \int_0^\infty dk \frac{k^{D+2} + k^D\tilde{q}^2\left[2x(x-1)+\frac{(2x-1)^2}{D-1}\right] + k^{D-2}\tilde{q}^4x^2(x-1)^2}{[k^2+\tilde{m}_\pi^2+\tilde{q}^2x(1-x)]^{5/2}}, \tag{B.101}$$

$$V_T = \frac{9g_A^4}{32f_\pi^4} \frac{2}{\Gamma(\frac{D-1}{2})(4\pi)^{(D-1)/2}} \frac{1}{D-1} \int_0^1 dx \int_0^\infty dk \frac{k^D}{[k^2+\tilde{m}_\pi^2+\tilde{q}^2x(1-x)]^{5/2}}, \tag{B.102}$$

and performing the k-integration with the help of Eq. (B.31), we obtain

$$\begin{aligned} W_C \;=\; & -\frac{3g_A^4}{16f_\pi^4} \frac{\lambda^2}{\Gamma(\frac{5}{2})\Gamma(\frac{D-1}{2})(4\pi)^{(D-1)/2}} \int_0^1 dx \left\{ \frac{\Gamma(\frac{D+3}{2})\Gamma(\frac{2-D}{2})}{[\tilde{m}_\pi^2+\tilde{q}^2x(1-x)]^{(2-D)/2}} \right. \\ & \left. + \frac{\Gamma(\frac{D+1}{2})\Gamma(\frac{4-D}{2})\tilde{q}^2\left[2x(x-1)+\frac{(2x-1)^2}{D-1}\right]}{[\tilde{m}_\pi^2+\tilde{q}^2x(1-x)]^{(4-D)/2}} + \frac{\Gamma(\frac{D-1}{2})\Gamma(\frac{6-D}{2})\tilde{q}^4x^2(x-1)^2}{[\tilde{m}_\pi^2+\tilde{q}^2x(1-x)]^{(6-D)/2}} \right\}, \end{aligned} \tag{B.103}$$

$$V_T = \frac{9g_A^4}{32f_\pi^4} \frac{1}{\Gamma(\frac{5}{2})\Gamma(\frac{D-1}{2})(4\pi)^{(D-1)/2}} \frac{1}{D-1} \int_0^1 dx \frac{\Gamma(\frac{D+1}{2})\Gamma(\frac{4-D}{2})}{[\tilde{m}_\pi^2+\tilde{q}^2x(1-x)]^{(4-D)/2}}. \tag{B.104}$$

We choose $D = 4-\eta$ and take the limit $\eta \to 0$ [cf. Eq. (B.33)],

$$\begin{aligned} W_C \;=\; & -\frac{g_A^4}{384\pi^2 f_\pi^4}\lambda^2 \int_0^1 dx \left\{ R\left[45\tilde{m}_\pi^2 + \tilde{q}^2(-6+105x-105x^2)\right] \right. \\ & + 48\tilde{m}_\pi^2 + 6\tilde{q}^2(-1+22x-22x^2) + \frac{12\tilde{q}^4x^2(x-1)^2}{\tilde{m}_\pi^2+\tilde{q}^2x(1-x)} \\ & \left. + \left[45\tilde{m}_\pi^2 + \tilde{q}^2(-6+105x-105x^2)\right]\ln(\tilde{m}_\pi^2+\tilde{q}^2x(1-x)) \right\}, \end{aligned} \tag{B.105}$$

$$V_T = -\frac{3g_A^4}{128\pi^2 f_\pi^4} \int_0^1 dx \left\{ R + 1 + \ln(\tilde{m}_\pi^2+\tilde{q}^2x(1-x)) \right\} \tag{B.106}$$

with R as defined in Eq. (B.38). And performing the x-integration, we finally get for the *planar box plus crossed box diagrams at NLO*

$$\begin{aligned} W_C \;=\; & -\frac{g_A^4}{384\pi^2 f_\pi^4} \left\{ \left[\frac{1}{2}R + \ln\left(\frac{m_\pi}{\lambda}\right)\right](90m_\pi^2+23q^2) + 16m_\pi^2 + \frac{5}{6}q^2 \right. \\ & \left. + \left(20m_\pi^2 + 23q^2 + \frac{48m_\pi^4}{w^2}\right)L(q) \right\}, \end{aligned} \tag{B.107}$$

$$V_T = -\frac{1}{q^2}V_S = -\frac{3g_A^4}{64\pi^2 f_\pi^4}\left[\frac{1}{2}R + \ln\left(\frac{m_\pi}{\lambda}\right) - \frac{1}{2} + L(q)\right] \tag{B.108}$$

with w and $L(q)$ given in Eq. (B.37).

B.4. Summary of 2PE contributions at NLO

Adding up all 2PE contributions at NLO, namely, the box and crossed boxes, Eqs. (B.107) and (B.108), the triangles, Eq. (B.39), and the football, Eq. (B.67), we obtain

$$\begin{aligned} W_C \;=\; & -\frac{1}{384\pi^2 f_\pi^4} \left\{ \left[4m_\pi^2(5g_A^4 - 4g_A^2 - 1) + q^2(23g_A^4 - 10g_A^2 - 1) + \frac{48g_A^4m_\pi^4}{w^2}\right]L(q) \right. \\ & + \left[6m_\pi^2(15g_A^4 - 6g_A^2 - 1) + q^2(23g_A^4 - 10g_A^2 - 1)\right]\ln\left(\frac{m_\pi}{\lambda}\right) \\ & \left. + 4m_\pi^2(4g_A^4 + g_A^2 + 1) + \frac{q^2}{6}(5g_A^4 + 26g_A^2 + 5) \right\} \end{aligned} \tag{B.109}$$

$$V_T = -\frac{1}{q^2}V_S = -\frac{3g_A^4}{64\pi^2 f_\pi^4}\left[L(q) + \ln\left(\frac{m_\pi}{\lambda}\right) - \frac{1}{2}\right] \tag{B.110}$$

with w and $L(q)$ given in Eq. (B.37), and where we applied renormalization in a Modified Minimal Subtraction scheme ($\overline{MS}$-scheme) [228], i. e., the (infinite) R-terms are subtracted. The results fully agree with Ref. [55]. If one is not interested in subtle aspects, like charge dependence [188] or the chiral limit ($m_\pi \to 0$) [129], one may omit the polynomial terms in the above expressions [cf. Eqs. (4.9) and (4.10)], since contact terms are added anyhow (cf. Section 4.3) which have the same mathematical structure and, therefore, can absorb the polynomial terms. Thus, the contacts are getting renormalized by the polynomials that result from dimensional regularization.

Appendix C. Two-pion-exchange contributions to the 2NF at NNLO

Two-pion-exchange diagrams that contribute at NNLO were shown in Fig. 4. These diagrams differ from the NLO diagrams, Fig. 3, by one insertion from the dimension-two Lagrangian, the vertices of which are given in Appendix A.2.2. There are two kinds of second order vertices: The relativistic corrections of the leading order Lagrangian, which are proportional to $1/M_N$, Eqs. (A.48)–(A.50), and new contact interactions proportional to the LECs c_i, Eqs. (A.51) and (A.52). Since the shapes of the NNLO diagrams are the same as in the NLO case, the evaluation is very similar to what we presented in detail in Appendix B for the NLO diagrams. The results for the irreducible 2PE at third order (NNLO) as derived by the Munich group [55] were given in Section 4.1.2, Eqs. (4.13)–(4.18). Note that the irreducible 2PE depends on what is chosen for the (reducible) iterated 1PE. For this, the Munich group applies the expression Eq. (4.25). Alternatively, one may also use the form Eq. (4.26) implied by the BbS scheme [133], which differs in third and higher orders from the Munich expression. Therefore, when the BbS formalism is used, a (irreducible) correction term has to be added to the Munich irreducible 2PE in higher orders. In terms of the notation introduced in Eqs. (4.25) and (4.26), this correction term is given by:

$$V_{2\pi,\mathrm{it}}^{(\mathrm{KBW})} - V_{2\pi,\mathrm{it}}^{(\mathrm{EM})} = \int \frac{d^3p''}{(2\pi)^3}\left(\frac{1}{E_p} - \frac{1}{E_{p''}}\right)\frac{M_N^2}{p^2 - p''^2 + i\epsilon} V_{1\pi}(\vec{p}\,', \vec{p}\,'')\, V_{1\pi}(\vec{p}\,'', \vec{p}) \tag{C.1}$$

$$= -\int \frac{d^3p''}{(2\pi)^3}\frac{M_N^2}{E_{p''}E_p(E_{p''} + E_p)} V_{1\pi}(\vec{p}\,', \vec{p}\,'')\, V_{1\pi}(\vec{p}\,'', \vec{p}) \tag{C.2}$$

$$\approx -\int \frac{d^3p''}{(2\pi)^3}\frac{1}{2M_N} V_{1\pi}(\vec{p}\,', \vec{p}\,'')\, V_{1\pi}(\vec{p}\,'', \vec{p}), \tag{C.3}$$

with the last line showing the correction in third order or NNLO, which is what we want to calculate here. Using Eq. (4.5) and the relation $\boldsymbol{\tau}_1 \cdot \boldsymbol{\tau}_2 \boldsymbol{\tau}_1 \cdot \boldsymbol{\tau}_2 = 3 - 2\boldsymbol{\tau}_1 \cdot \boldsymbol{\tau}_2$, and defining $\vec{l} = \vec{p} - \vec{p}\,''$, yields

$$V_{2\pi,\mathrm{it}}^{(\mathrm{KBW})} - V_{2\pi,\mathrm{it}}^{(\mathrm{EM})} = -\frac{g_A^4}{32 f_\pi^4 M_N}(3 - 2\boldsymbol{\tau}_1 \cdot \boldsymbol{\tau}_2)\int \frac{d^3l}{(2\pi)^3}\frac{\vec{\sigma}_1 \cdot (\vec{l} + \vec{q})\vec{\sigma}_2 \cdot (\vec{l} + \vec{q})}{(\vec{l} + \vec{q})^2 + m_\pi^2}\frac{\vec{\sigma}_1 \cdot \vec{l}\vec{\sigma}_2 \cdot \vec{l}}{l^2 + m_\pi^2} \tag{C.4}$$

$$= -\frac{g_A^4}{32 f_\pi^4 M_N}(3 - 2\boldsymbol{\tau}_1 \cdot \boldsymbol{\tau}_2)\int_0^1 dx \int \frac{d^3l}{(2\pi)^3}\frac{\vec{\sigma}_1 \cdot (\vec{l} + \vec{q})\vec{\sigma}_2 \cdot (\vec{l} + \vec{q})\vec{\sigma}_1 \cdot \vec{l}\vec{\sigma}_2 \cdot \vec{l}}{[\vec{l}^2 + (2\vec{l} \cdot \vec{q} + \vec{q}^2)x + m_\pi^2]^2}, \tag{C.5}$$

where, in the last line, we introduced the Feynman trick. We now extend the integral to $(D-1)$ dimensions and make the change of variables $\lambda\vec{k} = \vec{l} + x\vec{q}$ (cf. Appendix B.1.2),

$$V_{2\pi,\mathrm{it}}^{(\mathrm{KBW})} - V_{2\pi,\mathrm{it}}^{(\mathrm{EM})} = -\frac{g_A^4}{32 f_\pi^4 M_N}(3 - 2\boldsymbol{\tau}_1 \cdot \boldsymbol{\tau}_2)\lambda^3 \int_0^1 dx \int \frac{d^{D-1}k}{(2\pi)^{D-1}}$$
$$\times \frac{\vec{\sigma}_1 \cdot [\vec{k} + (1-x)\tilde{q}]\vec{\sigma}_2 \cdot [\vec{k} + (1-x)\tilde{q}]\vec{\sigma}_1 \cdot (\vec{k} - x\tilde{q})\vec{\sigma}_2 \cdot (\vec{k} - x\tilde{q})}{[k^2 + \tilde{m}_\pi^2 + \tilde{q}^2 x(1-x)]^2}. \tag{C.6}$$

Since

$$\vec{\sigma}_i \cdot [\vec{k} + (1-x)\tilde{q}]\vec{\sigma}_i \cdot (\vec{k} - x\tilde{q}) = k^2 + \tilde{q}^2 x(x-1) - (2x-1)\vec{k} \cdot \tilde{q} + i\vec{\sigma}_i \cdot (\tilde{q} \times \vec{k}), \tag{C.7}$$

we obtain, making use of Eq. (B.94),

$$V_{2\pi,\mathrm{it}}^{(\mathrm{KBW})} - V_{2\pi,\mathrm{it}}^{(\mathrm{EM})} = -\frac{g_A^4}{32 f_\pi^4 M_N}(3 - 2\boldsymbol{\tau}_1 \cdot \boldsymbol{\tau}_2)\lambda^3 \int_0^1 dx \int \frac{d^{D-1}k}{(2\pi)^{D-1}}$$
$$\times \frac{[k^2 + \tilde{q}^2 x(x-1)]^2 + \frac{k^2}{D-1}[(2x-1)^2\tilde{q}^2 - (\vec{\sigma}_1 \times \tilde{q})(\vec{\sigma}_2 \times \tilde{q})]}{[k^2 + \tilde{m}_\pi^2 + \tilde{q}^2 x(1-x)]^2}. \tag{C.8}$$

Applying $(\vec\sigma_1\times\tilde q)(\vec\sigma_2\times\tilde q)=\lambda^{-2}[q^2\vec\sigma_1\cdot\vec\sigma_2-(\vec\sigma_1\cdot\vec q)(\vec\sigma_2\cdot\vec q)]$, leads to

$$V_C=-\frac{3g_A^4}{32f_\pi^4M_N}\lambda^3\int_0^1dx\int\frac{d^{D-1}k}{(2\pi)^{D-1}}\frac{[k^2+\tilde q^2x(x-1)]^2+\frac{k^2}{D-1}(2x-1)^2\tilde q^2}{[k^2+\tilde m_\pi^2+\tilde q^2x(1-x)]^2} \tag{C.9}$$

$$W_C=-\frac{2}{3}V_C \tag{C.10}$$

$$V_T=-\frac{3g_A^4}{32f_\pi^4M_N}\lambda\int_0^1dx\int\frac{d^{D-1}k}{(2\pi)^{D-1}}\frac{\frac{k^2}{D-1}}{[k^2+\tilde m_\pi^2+\tilde q^2x(1-x)]^2} \tag{C.11}$$

$$V_S=-q^2V_T \tag{C.12}$$

$$W_T=-\frac{2}{3}V_T \tag{C.13}$$

$$W_S=-q^2W_T. \tag{C.14}$$

Using the volume element in $(D-1)$ dimensions, Eqs. (B.28) and (B.29), we find

$$V_C=-\frac{3g_A^4}{32f_\pi^4M_N}\frac{2\lambda^3}{\Gamma(\frac{D-1}{2})(4\pi)^{(D-1)/2}}\int_0^1dx\int_0^\infty dk\frac{k^{D+2}+k^D\tilde q^2\left[2x(x-1)+\frac{(2x-1)^2}{D-1}\right]+k^{D-2}\tilde q^4x^2(x-1)^2}{[k^2+\tilde m_\pi^2+\tilde q^2x(1-x)]^2}, \tag{C.15}$$

$$V_T=-\frac{3g_A^4}{32f_\pi^4M_N}\frac{2\lambda}{\Gamma(\frac{D-1}{2})(4\pi)^{(D-1)/2}}\frac{1}{D-1}\int_0^1dx\int_0^\infty dk\frac{k^D}{[k^2+\tilde m_\pi^2+\tilde q^2x(1-x)]^2}. \tag{C.16}$$

Performing the k-integration yields

$$\begin{aligned}V_C\;=\;&-\frac{3g_A^4}{32f_\pi^4M_N}\frac{\lambda^3}{\Gamma(2)\Gamma(\frac{D-1}{2})(4\pi)^{(D-1)/2}}\int_0^1dx\left\{\frac{\Gamma(\frac{D+3}{2})\Gamma(\frac{1-D}{2})}{[\tilde m_\pi^2+\tilde q^2x(1-x)]^{(1-D)/2}}\right.\\&\left.+\frac{\Gamma(\frac{D+1}{2})\Gamma(\frac{3-D}{2})\tilde q^2\left[2x(x-1)+\frac{(2x-1)^2}{D-1}\right]}{(\tilde m_\pi^2+\tilde q^2x(1-x))^{(3-D)/2}}+\frac{\Gamma(\frac{D-1}{2})\Gamma(\frac{5-D}{2})\tilde q^4x^2(x-1)^2}{[\tilde m_\pi^2+\tilde q^2x(1-x)]^{(5-D)/2}}\right\},\end{aligned} \tag{C.17}$$

$$V_T=-\frac{3g_A^4}{32f_\pi^4M_N}\frac{\lambda}{\Gamma(2)\Gamma(\frac{D-1}{2})(4\pi)^{(D-1)/2}}\frac{1}{D-1}\int_0^1dx\frac{\Gamma(\frac{D+1}{2})\Gamma(\frac{3-D}{2})}{[\tilde m_\pi^2+\tilde q^2x(1-x)]^{(3-D)/2}}. \tag{C.18}$$

We choose $D=4-\eta$ and take the limit $\eta\to0$,

$$V_C=-\frac{3g_A^4}{256\pi f_\pi^4M_N}\int_0^1\frac{5m_\pi^4-m_\pi^2q^2(1-20x+20x^2)+q^4x(-1+17x-32x^2+16x^3)}{\sqrt{m_\pi^2+q^2x(1-x)}}, \tag{C.19}$$

$$V_T=\frac{3g_A^4}{256\pi f_\pi^4M_N}\int_0^1\sqrt{m_\pi^2+q^2x(1-x)}, \tag{C.20}$$

and, performing the x-integration, we finally obtain

$$V_C=-\frac{3g_A^4}{256\pi f_\pi^4M_N}(m_\pi w^2+\widetilde w^4A(q)), \tag{C.21}$$

$$V_T=\frac{3g_A^4}{512\pi f_\pi^4M_N}(m_\pi+w^2A(q)). \tag{C.22}$$

Appendix D. Two-pion-exchange contributions to the 2NF at N^{3}LO

The fourth order 2PE contributions consist of two classes: the one-loop (Fig. 5) and the two-loop diagrams (Fig. 6).

D.1. One-loop diagrams

This large pool of diagrams can be analyzed in a systematic way by introducing the following well-defined subdivisions.

D.1.1. c_i^2 contributions

The only contribution of this kind comes from the football diagram with both vertices proportional to c_i (first row of Fig. 5). One obtains [60]:

$$V_C = \frac{3L(q)}{16\pi^2 f_\pi^4}\left[\left(\frac{c_2}{6}w^2 + c_3\widetilde{w}^2 - 4c_1 m_\pi^2\right)^2 + \frac{c_2^2}{45}w^4\right], \tag{D.1}$$

$$W_T = -\frac{1}{q^2}W_S = \frac{c_4^2 w^2 L(q)}{96\pi^2 f_\pi^4}, \tag{D.2}$$

with $L(q)$ and w defined in Eq. (B.37) and

$$\widetilde{w} \equiv \sqrt{2m_\pi^2 + q^2}. \tag{D.3}$$

D.1.2. c_i/M_N contributions

This class consists of diagrams with one vertex proportional to c_i and one $1/M_N$ correction. A few graphs that are representative for this class are shown in the second row of Fig. 5. Symbols with a large solid dot and an open circle denote $1/M_N$ corrections of vertices proportional to c_i. They are part of $\widehat{\mathcal{L}}^{\Delta=2}$, Eq. (2.67). The result for this group of diagrams is [60]:

$$V_C = -\frac{g_A^2 L(q)}{32\pi^2 M_N f_\pi^4}\left[(c_2 - 6c_3)q^4 + 4(6c_1 + c_2 - 3c_3)q^2 m_\pi^2 + 6(c_2 - 2c_3)m_\pi^4 + 24(2c_1 + c_3)m_\pi^6 w^{-2}\right], \tag{D.4}$$

$$W_C = -\frac{c_4 q^2 L(q)}{192\pi^2 M_N f_\pi^4}\left[g_A^2(8m_\pi^2 + 5q^2) + w^2\right], \tag{D.5}$$

$$W_T = -\frac{1}{q^2}W_S = -\frac{c_4 L(q)}{192\pi^2 M_N f_\pi^4}\left[g_A^2(16m_\pi^2 + 7q^2) - w^2\right], \tag{D.6}$$

$$V_{LS} = \frac{c_2\, g_A^2}{8\pi^2 M_N f_\pi^4}\, w^2 L(q), \tag{D.7}$$

$$W_{LS} = -\frac{c_4 L(q)}{48\pi^2 M_N f_\pi^4}\left[g_A^2(8m_\pi^2 + 5q^2) + w^2\right]. \tag{D.8}$$

D.1.3. $1/M_N^2$ corrections

These are relativistic $1/M_N^2$ corrections of the leading order 2π exchange diagrams. Typical examples for this large class are shown in row 3–6 of Fig. 5. This time, there is no correction from the iterated 1PE, Eq. (4.25) or Eq. (4.26), since the expansion of the factor M_N^2/E_p does not create a term proportional to $1/M_N^2$. The total result for this class is [61],

$$V_C = -\frac{g_A^4}{32\pi^2 M_N^2 f_\pi^4}\left[L(q)\left(2m_\pi^8 w^{-4} + 8m_\pi^6 w^{-2} - q^4 - 2m_\pi^4\right) + \frac{m_\pi^6}{2w^2}\right], \tag{D.9}$$

$$\begin{aligned} W_C \;=\; & -\frac{1}{768\pi^2 M_N^2 f_\pi^4}\left\{L(q)\left[8g_A^2\left(\frac{3}{2}q^4 + 3m_\pi^2 q^2 + 3m_\pi^4 - 6m_\pi^6 w^{-2} - k^2(8m_\pi^2 + 5q^2)\right)\right.\right. \\ & + 4g_A^4\left(k^2\left(20m_\pi^2 + 7q^2 - 16m_\pi^4 w^{-2}\right) + 16m_\pi^8 w^{-4} + 12m_\pi^6 w^{-2} - 4m_\pi^4 q^2 w^{-2} - 5q^4 - 6m_\pi^2 q^2 - 6m_\pi^4\right) \\ & \left.\left. - 4k^2 w^2\right] + \frac{16g_A^4 m_\pi^6}{w^2}\right\}, \end{aligned} \tag{D.10}$$

$$V_T = -\frac{1}{q^2}V_S = \frac{g_A^4 L(q)}{32\pi^2 M_N^2 f_\pi^4}\left(k^2 + \frac{5}{8}q^2 + m_\pi^4 w^{-2}\right), \tag{D.11}$$

$$W_T = -\frac{1}{q^2}W_S = \frac{L(q)}{1536\pi^2 M_N^2 f_\pi^4}\left[4g_A^4\left(7m_\pi^2 + \frac{17}{4}q^2 + 4m_\pi^4 w^{-2}\right) - 32g_A^2\left(m_\pi^2 + \frac{7}{16}q^2\right) + w^2\right], \tag{D.12}$$

$$V_{LS} = \frac{g_A^4 L(q)}{4\pi^2 M_N^2 f_\pi^4}\left(\frac{11}{32}q^2 + m_\pi^4 w^{-2}\right), \tag{D.13}$$

$$W_{LS} = \frac{L(q)}{256\pi^2 M_N^2 f_\pi^4}\left[\, 16 g_A^2 \left(m_\pi^2 + \frac{3}{8}q^2\right) + \frac{4}{3} g_A^4 \left(4m_\pi^4 w^{-2} - \frac{11}{4}q^2 - 9m_\pi^2\right) - w^2 \,\right], \tag{D.14}$$

$$V_{\sigma L} = \frac{g_A^4 L(q)}{32\pi^2 M_N^2 f_\pi^4}. \tag{D.15}$$

D.2. Two-loop contributions

The two-loop contributions are quite involved. In Fig. 6, we attempt a graphical representation of this class. The gray disk stands for all one-loop πN graphs which are shown in some detail in the lower part of the figure. Not all of the numerous graphs are displayed. Some of the missing ones are obtained by permutation of the vertices along the nucleon line, others by inverting initial and final states. Vertices denoted by a small dot are from the leading order Lagrangian $\widehat{\mathcal{L}}^{\Delta=0}$, Eq. (2.65). The solid square represents vertices proportional to the LECs d_i introduced in $\mathcal{L}_{\pi N}^{(3)}$ which is part of $\widehat{\mathcal{L}}^{\Delta=2}$, Eq. (2.67). The d_i vertices occur actually in one-loop NN diagrams, but we list them among the two-loop NN contributions because they are needed to absorb divergences generated by one-loop πN graphs. Using techniques from dispersion theory, Kaiser [60] calculated the imaginary parts of the NN amplitudes, $\mathrm{Im}\, V_\alpha(i\mu)$ and $\mathrm{Im}\, W_\alpha(i\mu)$, which result from analytic continuation to time-like momentum transfer $q = i\mu - 0^+$ with $\mu \geq 2m_\pi$. From this, the momentum-space amplitudes $V_\alpha(q)$ and $W_\alpha(q)$ are obtained via the subtracted dispersion relations:

$$V_{C,S}(q) = -\frac{2q^6}{\pi}\int_{2m_\pi}^{\infty} d\mu \frac{\mathrm{Im}\, V_{C,S}(i\mu)}{\mu^5(\mu^2+q^2)}, \tag{D.16}$$

$$V_T(q) = \frac{2q^4}{\pi}\int_{2m_\pi}^{\infty} d\mu \frac{\mathrm{Im}\, V_T(i\mu)}{\mu^3(\mu^2+q^2)}, \tag{D.17}$$

and similarly for $W_{C,S,T}$.

In most cases, the dispersion integrals can be solved analytically and the following expressions are obtained [67]:

$$V_C(q) = \frac{3g_A^4 \widetilde{w}^2 A(q)}{1024\pi^2 f_\pi^6}\left[(m_\pi^2 + 2q^2)\left(2m_\pi + \widetilde{w}^2 A(q)\right) + 4g_A^2 m_\pi \widetilde{w}^2\right]; \tag{D.18}$$

$$W_C(q) = W_C^{(a)}(q) + W_C^{(b)}(q), \tag{D.19}$$

with

$$\begin{aligned} W_C^{(a)}(q) = \frac{L(q)}{18432\pi^4 f_\pi^6}\Bigg\{ & 192\pi^2 f_\pi^2 w^2 \bar{d}_3 \left[2g_A^2\widetilde{w}^2 - \frac{3}{5}(g_A^2-1)w^2\right] \\ & + \left[6g_A^2\widetilde{w}^2 - (g_A^2-1)w^2\right]\Bigg[384\pi^2 f_\pi^2\left(\widetilde{w}^2(\bar{d}_1+\bar{d}_2) + 4m_\pi^2\bar{d}_5\right) \\ & + L(q)\left(4m_\pi^2(1+2g_A^2) + q^2(1+5g_A^2)\right) - \left(\frac{q^2}{3}(5+13g_A^2) + 8m_\pi^2(1+2g_A^2)\right)\Bigg]\Bigg\} \end{aligned} \tag{D.20}$$

and

$$W_C^{(b)}(q) = -\frac{2q^6}{\pi}\int_{2m_\pi}^{\infty} d\mu \frac{\mathrm{Im}\, W_C^{(b)}(i\mu)}{\mu^5(\mu^2+q^2)}, \tag{D.21}$$

where

$$\begin{aligned} \mathrm{Im}\, W_C^{(b)}(i\mu) = & -\frac{2\kappa}{3\mu(8\pi f_\pi^2)^3}\int_0^1 dx \left[g_A^2(2m_\pi^2-\mu^2) + 2(g_A^2-1)\kappa^2x^2\right] \\ & \times \Bigg\{-3\kappa^2x^2 + 6\kappa x\sqrt{m_\pi^2+\kappa^2x^2}\ \ln\frac{\kappa x + \sqrt{m_\pi^2+\kappa^2x^2}}{m_\pi} \\ & + g_A^4\left(\mu^2 - 2\kappa^2x^2 - 2m_\pi^2\right)\left[\frac{5}{6} + \frac{m_\pi^2}{\kappa^2x^2} - \left(1+\frac{m_\pi^2}{\kappa^2x^2}\right)^{3/2}\ln\frac{\kappa x + \sqrt{m_\pi^2+\kappa^2x^2}}{m_\pi}\right]\Bigg\}; \end{aligned} \tag{D.22}$$

$$\begin{aligned} V_T(q) &= V_T^{(a)}(q) + V_T^{(b)}(q) \\ &= -\frac{1}{q^2}V_S(q) = -\frac{1}{q^2}\left(V_S^{(a)}(q) + V_S^{(b)}(q)\right), \end{aligned} \tag{D.23}$$

with

$$V_T^{(a)}(q) = -\frac{1}{q^2}V_S^{(a)}(q) = -\frac{g_A^2 w^2 L(q)}{32\pi^2 f_\pi^4}(\bar{d}_{14} - \bar{d}_{15}) \tag{D.24}$$

and

$$V_T^{(b)}(q) = -\frac{1}{q^2}V_S^{(b)}(q) = \frac{2q^4}{\pi}\int_{2m_\pi}^{\infty} d\mu\, \frac{\mathrm{Im}\, V_T^{(b)}(i\mu)}{\mu^3(\mu^2+q^2)}, \tag{D.25}$$

where

$$\mathrm{Im}\, V_T^{(b)}(i\mu) = -\frac{2g_A^6\kappa^3}{\mu(8\pi f_\pi^2)^3}\int_0^1 dx(1-x^2)\left[-\frac{1}{6} + \frac{m_\pi^2}{\kappa^2 x^2} - \left(1+\frac{m_\pi^2}{\kappa^2 x^2}\right)^{3/2}\ln\frac{\kappa x + \sqrt{m_\pi^2+\kappa^2 x^2}}{m_\pi}\right]; \tag{D.26}$$

$$W_T(q) = -\frac{1}{q^2}W_S(q) = \frac{g_A^4 w^2 A(q)}{2048\pi^2 f_\pi^6}\left[w^2 A(q) + 2m_\pi(1+2g_A^2)\right]; \tag{D.27}$$

where

$$A(q) \equiv \frac{1}{2q}\arctan\frac{q}{2m_\pi} \quad \text{and} \quad \kappa \equiv \sqrt{\mu^2/4 - m_\pi^2}. \tag{D.28}$$

Note that the analytic solutions hold modulo polynomials. We have checked the importance of those contributions where we could not find an analytic solution and where, therefore, the integrations have to be performed numerically. It turns out that the combined effect on *NN* phase shifts from $W_C^{(b)}$, $V_T^{(b)}$, and $V_S^{(b)}$ is smaller than 0.1 deg in *F* and *G* waves and smaller than 0.01 deg in *H* waves, at $T_{\rm lab} = 300$ MeV (and less at lower energies). This renders these contributions negligible. Therefore, we omit $W_C^{(b)}$, $V_T^{(b)}$, and $V_S^{(b)}$ in the construction of chiral *NN* potentials at order N^{3}LO (Section 4.6.3).

In Eqs. (D.20) and (D.24), we use the scale-independent LECs, $\bar{d}_i$, which are obtained by combining the scale-dependent ones, $d_i^r(\lambda)$, with the chiral logarithm, $\ln(m_\pi/\lambda)$, or equivalently $\bar{d}_i = d_i^r(m_\pi)$. For more details about this issue, see Ref. [123].

D.3. Impact of individual N^{3}LO *contributions on peripheral phase shifts*

The fourth order is obviously very diverse. Here, we will show how the individual fourth order contributions impact *NN* phase shifts in peripheral partial waves. For this purpose, we display in Fig. D.1 phase shifts for four important peripheral partial waves, namely, $^1F_3$, $^3F_3$, $^3F_4$, and $^3G_5$. In each frame, the following curves are shown:

(1) NNLO ("N2LO").
(2) The previous curve plus the c_i^2 graph, first row of Fig. 5, Eqs. (D.1) and (D.2), denoted by 'c2' in the figure.
(3) The previous curve plus the c_i/M_N contributions (denoted by 'c/M'), second row of Fig. 5, Eqs. (D.4)–(D.8).
(4) The previous curve plus the $1/M_N^2$ corrections ('1/M2'), row three to six of Fig. 5, Eqs. (D.9)–(D.15).
(5) The previous curve plus the two-loop contributions without the terms proportional to $\bar{d}_i$ ('2-L'); i.e. Fig. 6, but without the solid square; Eqs. (D.18)–(D.27), but with all $\bar{d}_i \equiv 0$.
(6) The previous curve plus the terms proportional to $\bar{d}_i$ (denoted by 'd' in the figure) with the parameters given in Table 2, column 'Peripheral perturbative *NN*'.

In summary, the various curves add up successively the individual N^{3}LO contributions in the order indicated in the curve label. The last curve in this series, curve (6), is the full N^{3}LO result.

The c_i^2 graph generates large attraction in all partial waves [cf. differences between curves (1) and (2) in Fig. D.1]. This attraction is compensated by repulsion from the c_i/M_N diagrams, in most partial waves; the exception is $^1F_3$ where c_i/M_N adds more attraction [curve (3)]. The $1/M_N^2$ corrections [difference between curves (3) and (4)] are typically small. Finally, the two-loop contributions create substantial repulsion in $^1F_3$ and $^3G_5$ which brings $^1F_3$ into good agreement with the data while causing a discrepancy for $^3G_5$. In $^3F_3$ and $^3F_4$, there are large cancelations between the 'pure' two-loop graphs and the $\bar{d}_i$ terms, making the net two-loop contribution rather small.

A pivotal role in the above game is played by W_S, Eq. (D.6), from the c_i/M_N group. This attractive term receives a factor of 9 in $^1F_3$, a factor (-3) in $^3G_5$, and a factor of 1 in $^3F_3$ and $^3F_4$. Thus, this contribution is very attractive in $^1F_3$ and repulsive in $^3G_5$. The latter is the reason for the overcompensation of the c_i^2 graph by the c_i/M_N contribution in $^3G_5$ which is why the final N^{3}LO result in this partial wave comes out too repulsive. One can expect that $1/M_N$ corrections that occur at order five or six will resolve this problem.

Before finishing this appendix, we like to point out that the problem with the $^3G_5$ is not as dramatic as it may appear from the phase shift plots—for two reasons. First, the $^3G_5$ phase shifts are about one order of magnitude smaller than the *F* and most of the other *G* phases. Thus, in absolute terms, the discrepancies seen in $^3G_5$ are small. In a certain sense, we are looking at 'higher order noise' under a magnifying glass. Second, the $^3G_5$ partial wave contributes 0.06 MeV to the energy per nucleon in nuclear matter, the total of which is -16 MeV. Consequently, small discrepancies in the reproduction of $^3G_5$ by a *NN* potential will have negligible influence on the microscopic nuclear structure predictions obtained with that potential.

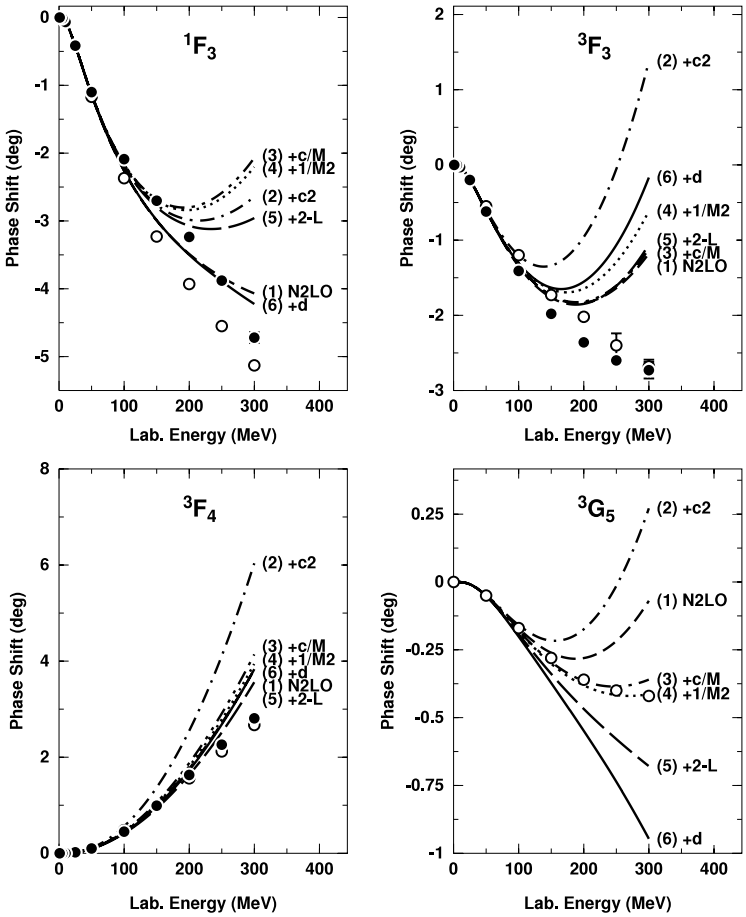

Fig. D.1. The effect of individual fourth order contributions on the neutron–proton phase shifts in some selected peripheral partial waves. The individual contributions are added up successively in the order given in parentheses next to each curve. Curve (1) is NNLO ("N2LO") and curve (6) completes N^{3}LO. For further explanations, see Appendix D.3. Empirical phase shifts (solid dots and open circles) as in Fig. 8.

Appendix E. Fourth order *NN* contact potential: partial-wave decomposition

The contact potential of order four, Eq. (4.43), decomposes into partial waves as follows

$$V_{\rm ct}^{(4)}(^1S_0) = \widehat{D}_{^1S_0}(p'^4 + p^4) + D_{^1S_0}p'^2p^2$$
$$V_{\rm ct}^{(4)}(^3P_0) = D_{^3P_0}(p'^3p + p'p^3)$$
$$V_{\rm ct}^{(4)}(^1P_1) = D_{^1P_1}(p'^3p + p'p^3)$$
$$V_{\rm ct}^{(4)}(^3P_1) = D_{^3P_1}(p'^3p + p'p^3)$$
$$V_{\rm ct}^{(4)}(^3S_1) = \widehat{D}_{^3S_1}(p'^4 + p^4) + D_{^3S_1}p'^2p^2$$
$$V_{\rm ct}^{(4)}(^3D_1) = D_{^3D_1}p'^2p^2$$
$$V_{\rm ct}^{(4)}(^3S_1 - {}^3D_1) = \widehat{D}_{^3S_1-{}^3D_1}p^4 + D_{^3S_1-{}^3D_1}p'^2p^2$$
$$V_{\rm ct}^{(4)}(^3D_1 - {}^3S_1) = \widehat{D}_{^3S_1-{}^3D_1}p'^4 + D_{^3S_1-{}^3D_1}p'^2p^2$$
$$V_{\rm ct}^{(4)}(^1D_2) = D_{^1D_2}p'^2p^2$$
$$V_{\rm ct}^{(4)}(^3D_2) = D_{^3D_2}p'^2p^2$$
$$V_{\rm ct}^{(4)}(^3P_2) = D_{^3P_2}(p'^3p + p'p^3)$$
$$V_{\rm ct}^{(4)}(^3P_2 - {}^3F_2) = D_{^3P_2-{}^3F_2}p'p^3$$
$$V_{\rm ct}^{(4)}(^3F_2 - {}^3P_2) = D_{^3P_2-{}^3F_2}p'^3p$$

$$V_{\rm ct}^{(4)}({}^3D_3) = D_{{}^3D_3} p'^2 p^2 \tag{E.1}$$

with the coefficients given by

$$\begin{aligned}
\widehat{D}_{{}^1S_0} &= 4\pi\left(D_1+\frac{1}{16}D_2+\frac{1}{4}D_3-3D_5-\frac{3}{16}D_6-\frac{3}{4}D_7-D_{11}-\frac{1}{4}D_{12}-\frac{1}{4}D_{13}-\frac{1}{16}D_{14}\right)\\
D_{{}^1S_0} &= 4\pi\left(\frac{10}{3}D_1+\frac{5}{24}D_2+\frac{1}{6}D_3+\frac{2}{3}D_4-10D_5-\frac{5}{8}D_6-\frac{1}{2}D_7-2D_8-\frac{10}{3}D_{11}\right.\\
&\quad\left.-\frac{1}{6}D_{12}-\frac{1}{6}D_{13}-\frac{5}{24}D_{14}-\frac{2}{3}D_{15}\right)\\
D_{{}^3P_0} &= 4\pi\left(-\frac{4}{3}D_1+\frac{1}{12}D_2-\frac{4}{3}D_5+\frac{1}{12}D_6-\frac{2}{3}D_9-\frac{1}{6}D_{10}+\frac{8}{3}D_{11}+\frac{1}{3}D_{12}-\frac{1}{3}D_{13}-\frac{1}{6}D_{14}\right)\\
D_{{}^1P_1} &= 4\pi\left(-\frac{4}{3}D_1+\frac{1}{12}D_2+4D_5-\frac{1}{4}D_6+\frac{4}{3}D_{11}-\frac{1}{12}D_{14}\right)\\
D_{{}^3P_1} &= 4\pi\left(-\frac{4}{3}D_1+\frac{1}{12}D_2-\frac{4}{3}D_5+\frac{1}{12}D_6-\frac{1}{3}D_9-\frac{1}{12}D_{10}-2D_{11}-\frac{1}{6}D_{12}+\frac{1}{6}D_{13}+\frac{1}{8}D_{14}\right)\\
\widehat{D}_{{}^3S_1} &= 4\pi\left(D_1+\frac{1}{16}D_2+\frac{1}{4}D_3+D_5+\frac{1}{16}D_6+\frac{1}{4}D_7+\frac{1}{3}D_{11}+\frac{1}{12}D_{12}+\frac{1}{12}D_{13}+\frac{1}{48}D_{14}\right)\\
D_{{}^3S_1} &= 4\pi\left(\frac{10}{3}D_1+\frac{5}{24}D_2+\frac{1}{6}D_3+\frac{2}{3}D_4+\frac{10}{3}D_5+\frac{5}{24}D_6+\frac{1}{6}D_7+\frac{2}{3}D_8+\frac{10}{9}D_{11}\right.\\
&\quad\left.+\frac{1}{18}D_{12}+\frac{1}{18}D_{13}+\frac{5}{72}D_{14}+\frac{2}{9}D_{15}\right)\\
D_{{}^3D_1} &= 4\pi\left(\frac{8}{15}D_1+\frac{1}{30}D_2-\frac{2}{15}D_3-\frac{2}{15}D_4+\frac{8}{15}D_5+\frac{1}{30}D_6-\frac{2}{15}D_7-\frac{2}{15}D_8\right.\\
&\quad\left.+\frac{2}{5}D_9-\frac{1}{10}D_{10}-\frac{4}{9}D_{11}+\frac{1}{9}D_{12}+\frac{1}{9}D_{13}-\frac{1}{36}D_{14}-\frac{16}{45}D_{15}\right)\\
\widehat{D}_{{}^3S_1-{}^3D_1} &= 4\pi\left(-\frac{2\sqrt{2}}{3}D_{11}-\frac{\sqrt{2}}{6}D_{12}-\frac{\sqrt{2}}{6}D_{13}-\frac{\sqrt{2}}{24}D_{14}\right)\\
D_{{}^3S_1-{}^3D_1} &= 4\pi\left(-\frac{14\sqrt{2}}{9}D_{11}+\frac{\sqrt{2}}{18}D_{12}+\frac{\sqrt{2}}{18}D_{13}-\frac{7\sqrt{2}}{72}D_{14}+\frac{2\sqrt{2}}{9}D_{15}\right)\\
D_{{}^1D_2} &= 4\pi\left(\frac{8}{15}D_1+\frac{1}{30}D_2-\frac{2}{15}D_3-\frac{2}{15}D_4-\frac{8}{5}D_5-\frac{1}{10}D_6+\frac{2}{5}D_7+\frac{2}{5}D_8-\frac{8}{15}D_{11}\right.\\
&\quad\left.+\frac{2}{15}D_{12}+\frac{2}{15}D_{13}-\frac{1}{30}D_{14}+\frac{2}{15}D_{15}\right)\\
D_{{}^3D_2} &= 4\pi\left(\frac{8}{15}D_1+\frac{1}{30}D_2-\frac{2}{15}D_3-\frac{2}{15}D_4+\frac{8}{15}D_5+\frac{1}{30}D_6-\frac{2}{15}D_7-\frac{2}{15}D_8+\frac{2}{15}D_9-\frac{1}{30}D_{10}\right.\\
&\quad\left.+\frac{4}{5}D_{11}-\frac{1}{5}D_{12}-\frac{1}{5}D_{13}+\frac{1}{20}D_{14}+\frac{4}{15}D_{15}\right)\\
D_{{}^3P_2} &= 4\pi\left(-\frac{4}{3}D_1+\frac{1}{12}D_2-\frac{4}{3}D_5+\frac{1}{12}D_6+\frac{1}{3}D_9+\frac{1}{12}D_{10}-\frac{2}{15}D_{11}+\frac{1}{30}D_{12}-\frac{1}{30}D_{13}+\frac{1}{120}D_{14}\right)\\
D_{{}^3P_2-{}^3F_2} &= 4\pi\left(\frac{4\sqrt{6}}{15}D_{11}-\frac{\sqrt{6}}{15}D_{12}+\frac{\sqrt{6}}{15}D_{13}-\frac{\sqrt{6}}{60}D_{14}\right)\\
D_{{}^3D_3} &= 4\pi\left(\frac{8}{15}D_1+\frac{1}{30}D_2-\frac{2}{15}D_3-\frac{2}{15}D_4+\frac{8}{15}D_5+\frac{1}{30}D_6-\frac{2}{15}D_7-\frac{2}{15}D_8-\frac{4}{15}D_9+\frac{1}{15}D_{10}-\frac{2}{15}D_{15}\right).
\end{aligned} \tag{E.2}$$

Appendix F. Parameters of N^{3}LO *NN* potentials

This appendix provides detailed information on parameters involved in the Idaho N^{3}LO *NN* potentials [68]. The πN LECs were shown already in Table 2 (column '*NN* potential'). In Table F.1, the LECs are listed, which are associated with the contact

Table F.1
LECs for two N^{3}LO fits by the Idaho group [68] using $\Lambda = 500$ and 600 MeV in the regulator function $f(p', p)$, Eq. (4.63). The C_S and C_T of the zero order counterterms given in Eq. (4.38) are in units of 10^4 GeV^{-2}; the C_i, Eq. (4.40), in 10^4 GeV^{-4}; and the D_i, Eq. (4.43), in 10^4 GeV^{-6}.

LEC	$\Lambda = 500$ MeV	$\Lambda = 600$ MeV
C_S^{pp}	−0.009991	−0.009943
C_S^{nn}	−0.010011	−0.009949
C_S^{np}	−0.010028	−0.009955
C_T^{pp}	0.000523	0.000695
C_T^{nn}	0.000543	0.000701
C_T^{np}	0.000561	0.000707
C_1	0.051949	0.046433
C_2	0.163034	0.174354
C_3	0.003249	0.006562
C_4	−0.048954	−0.050066
C_5	−0.075081	−0.086978
C_6	−0.013343	−0.013639
C_7	−0.225500	−0.214188
D_1	−0.016674	−0.004441
D_2	2.480231	2.751960
D_3	0.915240	0.086650
D_4	−0.811591	−0.061000
D_5	0.138064	0.126881
D_6	1.249801	1.266717
D_7	0.148074	0.268796
D_8	−0.153405	−0.239967
D_9	−0.516607	−0.538043
D_{10}	2.379565	2.429102
D_{11}	−0.125289	−0.132228
D_{12}	0.081807	−0.053835
D_{13}	0.008037	−0.081804
D_{14}	−1.393312	−1.204164
D_{15}	0.164684	−0.005571

terms, Eqs. (4.38), (4.40) and (4.43), and, in Table F.2, the contact LECs are given in terms of partial-wave parameters. Notice that through Eqs. (4.39), (4.42) and (E.2) there is a one-to-one correspondence between these two representations of the contact LECs. The partial-wave parameters appear one order of magnitude larger, because they are multiplied by (4π) in the partial-wave decomposition. The partial-wave contact parameters of the Jülich N^{3}LO potentials can be found in Ref. [171]. There are similarities between the parameter sets.

At this point, one may raise the question of the *naturalness* of the LECs. LECs may be perceived as *natural* if they are roughly of the following sizes:

$$C_{S,T} \sim \frac{1}{f_\pi^2} \approx 0.01 \, \frac{10^4}{\text{GeV}^2}, \tag{F.1}$$

$$C_i \sim \frac{1}{f_\pi^2 \, \Lambda^2} \approx 0.05 \frac{10^4}{\text{GeV}^4}, \tag{F.2}$$

$$D_i \sim \frac{1}{f_\pi^2 \, \Lambda^4} \approx 0.2 \frac{10^4}{\text{GeV}^6}, \tag{F.3}$$

where we used $\Lambda = 0.5$ GeV for the numerical estimates. Comparison with Table F.1 reveals that the values of the contact LECs that result from a fit to the *NN* data are in general natural, indeed. Exceptions are D_2 and D_{10} which are an order of magnitude too large.

The charge-dependent LO contact parameters $\widetilde{C}_{^1S_0}^{pp}$, $\widetilde{C}_{^1S_0}^{nn}$, and $\widetilde{C}_{^1S_0}^{np}$ of Table F.2 can be analyzed as follows. Based upon the isospin-symmetric Lagrangian equation (2.61) and the isospin violating ones, Eqs. (4.80) and (4.81), the charge-dependent non-derivative contact parameters in the $^1S_0$ state are given by

$$\widetilde{C}_{pp} = \widetilde{C}_{\text{sym}} + \widetilde{C}_{\text{CIB}} + \widetilde{C}_{\text{CSB}}, \tag{F.4}$$

$$\widetilde{C}_{nn} = \widetilde{C}_{\text{sym}} + \widetilde{C}_{\text{CIB}} - \widetilde{C}_{\text{CSB}}, \tag{F.5}$$

$$\widetilde{C}_{np} = \widetilde{C}_{\text{sym}} - \widetilde{C}_{\text{CIB}}, \tag{F.6}$$

where $\widetilde{C}_{\text{sym}}$ is the same as $\widetilde{C}_{^1S_0}$ of Eq. (4.39). The charge-symmetric and the CSB and CIB contributions can then be obtained from

$$\widetilde{C}_{\text{sym}} = \frac{1}{2}\left[\frac{1}{2}\left(\widetilde{C}_{pp} + \widetilde{C}_{nn}\right) + \widetilde{C}_{np}\right], \tag{F.7}$$

Table F.2
Partial-wave LECs for two N^{3}LO fits by the Idaho group [68] using $\Lambda = 500$ and 600 MeV in the regulator function $f(p', p)$, Eq. (4.63). The $\widetilde{C}_i$ of the zero order partial-wave counterterms given in Eq. (4.39) are in units of 10^4 GeV^{-2}; the C_i, Eq. (4.41), in 10^4 GeV^{-4}; and the D_i, $\widehat{D}_i$, Eq. (E.1), in 10^4 GeV^{-6}. The last column lists the exponent n of the regulator function, which is applied to the corresponding partial-wave counterterm.

Partial-wave LEC	$\Lambda = 500$ MeV	$\Lambda = 600$ MeV	n
$\widetilde{C}^{pp}_{^1S_0}$	−0.145286	−0.151165	3
$\widetilde{C}^{nn}_{^1S_0}$	−0.146285	−0.151467	3
$\widetilde{C}^{np}_{^1S_0}$	−0.147167	−0.151745	3
$C_{^1S_0}$	2.380	2.200	2
$\widehat{D}_{^1S_0}$	−2.545	−4.890	2
$D_{^1S_0}$	−16.00	−5.84	2
$C_{^3P_0}$	1.487	1.548	2
$D_{^3P_0}$	0.245	−0.215	3
$C_{^1P_1}$	0.656	0.790	2
$D_{^1P_1}$	5.25	4.40	2
$C_{^3P_1}$	−0.630	−0.488	2
$D_{^3P_1}$	2.35	3.24	4
$\widetilde{C}_{^3S_1}$	−0.118972496	−0.116210	3
$C_{^3S_1}$	0.760	0.775	2
$\widehat{D}_{^3S_1}$	7.00	4.8004	2
$D_{^3S_1}$	6.55	10.8654	2
$D_{^3D_1}$	−2.80	−2.35	2
$C_{^3S_1-^3D_1}$	0.826	0.796	2
$\widehat{D}_{^3S_1-^3D_1}$	2.25	2.86	2
$D_{^3S_1-^3D_1}$	6.61	5.58	2
$D_{^1D_2}$	−1.770	−1.764	4
$D_{^3D_2}$	−1.46	−1.27	2
$C_{^3P_2}$	−0.538	−0.548	2
$D_{^3P_2}$	2.295	2.554	2
$D_{^3P_2-^3F_2}$	−0.465	−0.525	4
$D_{^3D_3}$	5.66	6.26	2, 3[a]

[a] $f(p', p) = 0.5\{\exp[-(p'/\Lambda)^4 - (p/\Lambda)^4] + \exp[-(p'/\Lambda)^6 - (p/\Lambda)^6]\}$ is applied.

$$\widetilde{C}_{\rm CSB} = \frac{1}{2}\left(\widetilde{C}_{pp} - \widetilde{C}_{nn}\right), \tag{F.8}$$

$$\widetilde{C}_{\rm CIB} = \frac{1}{2}\left[\frac{1}{2}\left(\widetilde{C}_{pp} + \widetilde{C}_{nn}\right) - \widetilde{C}_{np}\right]. \tag{F.9}$$

Using the numbers from the $\Lambda = 500$ MeV fit listed in Table F.2, the following values are produced:

$$\widetilde{C}_{\rm sym} = -0.1465\ \frac{10^4}{\rm GeV^2}, \tag{F.10}$$

$$\widetilde{C}_{\rm CSB} = 0.0005\ \frac{10^4}{\rm GeV^2}, \tag{F.11}$$

$$\widetilde{C}_{\rm CIB} = 0.0007\ \frac{10^4}{\rm GeV^2}. \tag{F.12}$$

Note that these are partial-wave parameters, which carry a factor of (4π) as compared to the parameters of, e.g., Eq. (F.1). As discussed in Section 4.6.2, the Idaho N^{3}LO potential [68] does not include explicitly the CIB effect from the pion-mass splitting in the NLO 2PE. Thus, the above value for $\widetilde{C}_{\rm CIB}$ is not the pure contact contribution since it includes a simulation of this omitted (small) effect (causing $\Delta a_{CIB} \approx -0.5$ fm). Moreover, also the CSB effect from nucleon-mass difference in the NLO 2PE is not calculated explicitly and, thus, effectively contained in $\widetilde{C}_{\rm CSB}$. The exact size of this effect when evaluated in ChPT at NLO is not known, but could be a large fraction of the total CSB [179].

The regulator function $f(p', p)$, Eq. (4.63), has two parameters, namely, the 'cutoff' Λ and the power parameter n. Fits were made for $\Lambda = 500$ and 600 MeV [denoted by N^{3}LO(500) and N^{3}LO(600)]. The parameter n has to be chosen such that the higher powers generated by the multiplication with the regulator [cf. Eq. (4.64)] are beyond the order at which we are working, which is $\nu = 4$. In short, the requirement is

$$2n + \nu_i > 4, \tag{F.13}$$

where ν_i denotes the order of a specific contribution to the potential. Thus, $n \geq 3$ for LO contributions, $n \geq 2$ for NLO contributions, etc. In the case of the Idaho N^{3}LO potentials, $n = 4$ is used for the 1PE and $n = 2$ for all 2PE contributions (which are NLO or higher). For the contact contributions, n is chosen in a partial-wave-dependent way and in accordance with Eq. (F.13), see Table F.2.

Table F.3
pp phase shifts (in degrees) by the Idaho N^{3}LO(500) potential [68].

T_{lab} (MeV)	$^1S_0$	$^3P_0$	$^3P_1$	$^1D_2$	$^3P_2$	$^3F_2$	ϵ_2	$^3F_3$	$^1G_4$	$^3F_4$
1	32.76	0.13	−0.08	0.00	0.01	0.00	0.00	0.00	0.00	0.00
5	54.71	1.58	−0.90	0.04	0.21	0.00	−0.05	0.00	0.00	0.00
10	55.01	3.73	−2.05	0.17	0.64	0.01	−0.20	−0.03	0.00	0.00
25	48.37	8.57	−4.91	0.70	2.47	0.10	−0.80	−0.23	0.04	0.02
50	38.75	11.47	−8.31	1.70	5.87	0.33	−1.65	−0.69	0.15	0.10
100	25.74	9.30	−13.39	3.68	11.11	0.80	−2.54	−1.48	0.41	0.42
150	16.66	4.34	−17.63	5.28	14.01	1.22	−2.83	−1.96	0.66	0.87
200	8.73	−0.87	−21.48	6.59	15.67	1.56	−2.76	−2.16	0.88	1.37
250	0.51	−5.78	−25.43	7.95	16.85	1.81	−2.35	−2.11	1.05	1.83
300	−8.53	−10.43	−29.54	9.16	17.73	1.94	−1.67	−1.83	1.14	2.17

Table F.4
nn phase shifts (in degrees) by the Idaho N^{3}LO(500) potential [68].

T_{lab} (MeV)	$^1S_0$	$^3P_0$	$^3P_1$	$^1D_2$	$^3P_2$	$^3F_2$	ϵ_2	$^3F_3$	$^1G_4$	$^3F_4$
01	57.51	0.21	−0.12	0.00	0.02	0.00	0.00	0.00	0.00	0.00
05	60.86	1.85	−1.04	0.05	0.26	0.00	−0.06	−0.01	0.00	0.00
10	57.62	4.10	−2.25	0.18	0.73	0.01	−0.22	−0.04	0.00	0.00
25	48.89	8.92	−5.15	0.73	2.66	0.11	−0.82	−0.24	0.04	0.02
50	38.67	11.60	−8.57	1.76	6.16	0.34	−1.68	−0.71	0.16	0.11
100	25.48	9.16	−13.66	3.75	11.42	0.81	−2.55	−1.50	0.42	0.43
150	16.34	4.08	−17.89	5.33	14.31	1.23	−2.82	−1.98	0.67	0.88
200	8.31	−1.18	−21.69	6.63	15.99	1.58	−2.74	−2.17	0.89	1.39
250	−0.06	−6.11	−25.56	7.97	17.19	1.83	−2.31	−2.11	1.06	1.86
300	−9.24	−10.79	−29.44	9.13	18.07	1.95	−1.63	−1.82	1.15	2.19

Table F.5
$I = 1$ *np* phase shifts (in degrees) by the Idaho N^{3}LO(500) potential [68].

T_{lab} (MeV)	$^1S_0$	$^3P_0$	$^3P_1$	$^1D_2$	$^3P_2$	$^3F_2$	ϵ_2	$^3F_3$	$^1G_4$	$^3F_4$
1	61.95	0.18	−0.11	0.00	0.02	0.00	0.00	0.00	0.00	0.00
5	63.34	1.63	−0.94	0.04	0.25	0.00	−0.05	0.00	0.00	0.00
10	59.55	3.66	−2.06	0.16	0.70	0.01	−0.18	−0.03	0.00	0.00
25	50.28	8.16	−4.86	0.68	2.56	0.09	−0.74	−0.20	0.03	0.02
50	39.82	10.75	−8.25	1.71	5.98	0.30	−1.57	−0.62	0.14	0.09
100	26.51	8.37	−13.35	3.75	11.17	0.75	−2.46	−1.38	0.39	0.39
150	17.35	3.36	−17.58	5.37	14.05	1.15	−2.76	−1.84	0.64	0.84
200	9.29	−1.86	−21.39	6.68	15.72	1.49	−2.70	−2.03	0.87	1.33
250	0.89	−6.76	−25.26	8.04	16.92	1.74	−2.29	−1.98	1.04	1.80
300	−8.31	−11.40	−29.17	9.19	17.81	1.87	−1.63	−1.70	1.14	2.13

Table F.6
$I = 0$ *np* phase shifts (in degrees) by the Idaho N^{3}LO(500) potential [68].

T_{lab} (MeV)	$^1P_1$	$^3S_1$	$^3D_1$	ϵ_1	$^3D_2$	$^1F_3$	$^3D_3$	$^3G_3$	ϵ_3	$^3G_4$
1	−0.19	147.76	−0.01	0.11	0.01	0.00	0.00	0.00	0.00	0.00
5	−1.55	118.18	−0.19	0.67	0.22	−0.01	0.00	0.00	0.01	0.00
10	−3.19	102.58	−0.68	1.15	0.85	−0.07	0.00	0.00	0.08	0.01
25	−6.67	80.45	−2.81	1.76	3.72	−0.43	−0.03	−0.05	0.55	0.17
50	−10.03	62.28	−6.41	2.05	8.99	−1.16	0.05	−0.26	1.61	0.72
100	−14.05	42.31	−11.94	2.32	17.56	−2.35	0.89	−0.95	3.50	2.14
150	−17.49	29.79	−15.83	2.67	22.68	−3.22	2.32	−1.77	4.83	3.51
200	−21.43	20.63	−19.01	3.16	24.71	−3.86	3.66	−2.56	5.66	4.62
250	−26.08	13.33	−21.94	3.72	24.29	−4.27	4.51	−3.19	6.02	5.35
300	−31.28	7.24	−24.48	4.02	22.00	−4.41	5.35	−3.53	5.91	5.57

Phase shifts of *NN* scattering as produced by the Idaho N^{3}LO(500) potential [68] are shown in Tables F.3–F.6 up to laboratory energies of 300 MeV.

References

[1] H. Yukawa, Proc. Phys. Math. Soc. Japan 17 (1935) 48.
[2] Prog. Theor. Phys. (Kyoto) 3 (1956) (supplement).
[3] M. Taketani, S. Machida, S. Onuma, Prog. Theor. Phys. (Kyoto) 7 (1952) 45.
[4] K.A. Brueckner, K.M. Watson, Phys. Rev. 90 (1953) 699; 92 (1953) 1023.

[5] A.R. Erwin, et al., Phys. Rev. Lett. 6 (1961) 628;
B.C. Maglić, et al., Phys. Rev. Lett. 7 (1961) 178.
[6] Prog. Theor. Phys. (Kyoto) 39 (1967) (supplement).
[7] R.A. Bryan, B.L. Scott, Phys. Rev. 135 (1964) B434; 177 (1969) 1435.
[8] K. Erkelenz, Phys. Rep. 13C (1974) 191.
[9] K. Holinde, R. Machleidt, Nuclear Phys. A247 (1975) 495; A256 (1976) 479, 497.
[10] M.M. Nagels, T.A. Rijken, J.J. de Swart, Phys. Rev. D 17 (1978) 768.
[11] R. Machleidt, Adv. Nuclear Phys. 19 (1989) 189.
[12] V.G.J. Stoks, R.A.M. Klomp, C.P.F. Terheggen, J.J. de Swart, Phys. Rev. C 49 (1994) 2950.
[13] R. Machleidt, Phys. Rev. C 63 (2001) 024001.
[14] F. Gross, A. Stadler, Phys. Rev. C 78 (2008) 014005.
[15] A.D. Jackson, D.O. Riska, B. Verwest, Nuclear Phys. A249 (1975) 397.
[16] G.E. Brown, A.D. Jackson, The Nucleon-Nucleon Interaction, North-Holland, Amsterdam, 1976.
[17] R. Vinh mau, in: M. Rho, D.H. Wilkinson (Eds.), Mesons in Nuclei, vol. I, North-Holland, Amsterdam, 1979, p. 151.
[18] M. Lacombe, B. Loiseau, J.M. Richard, R. Vinh mau, J. Côté, P. Pires, R. de Tourreil, Phys. Rev. C 21 (1980) 861.
[19] M.H. Partovi, E.L. Lomon, Phys. Rev. D 2 (1970) 1999; 5 (1972) 1192.
[20] R. Machleidt, K. Holinde, Ch. Elster, Phys. Rep. 149 (1987) 1.
[21] C.E. de Tar, Nuclear Phys. A335 (1980) 203.
[22] M. Harvey, Nuclear Phys. A352 (1981) 301–326.
[23] M. Oka, K. Yazaki, Prog. Theor. Phys. 66 (1981) 551–577.
[24] A. Faessler, F. Fernandez, G. Luebeck, K. Shimizu, Nuclear Phys. A402 (1983) 555.
[25] A.W. Thomas, Adv. Nuclear Phys. 13 (1983) 1.
[26] F. Myhrer, J. Wroldsen, Rev. Modern Phys. 60 (1988) 629.
[27] S. Takeuchi, K. Shimizu, K. Yazaki, Nuclear Phys. A504 (1989) 777.
[28] T. Barnes, S. Capstick, M.D. Kovarik, E.S. Swanson, Phys. Rev. C 48 (1993) 539.
[29] D.R. Entem, F. Fernandez, A. Valcarce, Phys. Rev. C 62 (2000) 034002.
[30] G.H. Wu, J.L. Ping, L.J. Teng, F. Wang, T. Goldman, Nuclear Phys. A673 (2000) 279.
[31] C. Downum, J. Stone, T. Barnes, E. Swanson, I. Vidana, Nucleon–nucleon interactions from the quark model, arXiv:1001.3320 [nucl-th].
[32] S. Weinberg, Physica 96A (1979) 327.
[33] J. Schwinger, Ann. Phys. (N.Y.) 2 (1957) 407.
[34] M. Gell-Mann, M. Levy, Nuovo Cimento 16 (1960) 705.
[35] T. Ericson, W. Weise, Pions and Nuclei, Clarendon Press, Oxford, 1988.
[36] S. Weinberg, Phys. Rev. Lett. 18 (1967) 188.
[37] S. Weinberg, Phys. Rev. Lett. 17 (1966) 616.
[38] Y. Tomozawa, Nuovo Cimento A 46 (1966) 707.
[39] S. Weinberg, Phys. Rev. 166 (1968) 1568.
[40] S. Coleman, J. Wess, B. Zumino, Phys. Rev. 177 (1969) 2239;
C.G. Callan, S. Coleman, J. Wess, B. Zumino, Phys. Rev. 177 (1969) 2247.
[41] G.E. Brown, A.M. Green, W.J. Gerace, Nuclear Phys. A115 (1968) 435.
[42] G.E. Brown, Comments Nuclear Part. Phys. 4 (1970) 140.
[43] G.E. Brown, in: M. Rho, D.H. Wilkinson (Eds.), Mesons in Nuclei, vol. I, North-Holland, Amsterdam, 1979, p. 330.
[44] J. Fleischer, J.A. Tjon, Phys. Rev. D 21 (1980) 87.
[45] R. Brockmann, R. Machleidt, Phys. Lett. 149B (1984) 283;
Phys. Rev. C 42 (1990) 1965.
[46] F. Gross, J.W. van Orden, K. Holinde, Phys. Rev. C 45 (1992) 2094.
[47] S. Weinberg, Effective Field Theory Past and Future, arXiv:0908:1964 [hep-th].
[48] J. Gasser, H. Leutwyler, Ann. Phys. 158 (1984) 142; Nuclear Phys. B250 (1985) 465.
[49] J. Gasser, M.E. Sainio, A. Švarc, Nuclear Phys. B307 (1986) 779.
[50] S. Weinberg, Phys. Lett. B 251 (1990) 288.
[51] S. Weinberg, Nuclear Phys. B363 (1991) 3.
[52] S. Weinberg, Phys. Lett. B 295 (1992) 114.
[53] C. Ordóñez, L. Ray, U. van Kolck, Phys. Rev. Lett. 72 (1994) 1982.
[54] C. Ordóñez, L. Ray, U. van Kolck, Phys. Rev. C 53 (1996) 2086.
[55] N. Kaiser, R. Brockmann, W. Weise, Nuclear Phys. A625 (1997) 758.
[56] N. Kaiser, S. Gerstendörfer, W. Weise, Nuclear Phys. A637 (1998) 395.
[57] N. Kaiser, Phys. Rev. C 61 (2000) 014003.
[58] N. Kaiser, Phys. Rev. C 62 (2000) 024001.
[59] N. Kaiser, Phys. Rev. C 63 (2001) 044010.
[60] N. Kaiser, Phys. Rev. C 64 (2001) 057001.
[61] N. Kaiser, Phys. Rev. C 65 (2002) 017001.
[62] C.A. da Rocha, M.R. Robilotta, Phys. Rev. C 49 (1994) 1818; 52 (1995) 531;
M.R. Robilotta, Nuclear Phys. A595 (1995) 171;
M.R. Robilotta, C.A. da Rocha, Nuclear Phys. A615 (1997) 391;
J.-L. Ballot, C.A. da Rocha, M.R. Robilotta, Phys. Rev. C 57 (1998) 1574.
[63] R. Higa, M.R. Robilotta, Phys. Rev. C 68 (2003) 024004.
[64] E. Epelbaum, W. Glöckle, U.-G. Meißner, Nuclear Phys. A637 (1998) 107.
[65] E. Epelbaum, W. Glöckle, U.-G. Meißner, Nuclear Phys. A671 (2000) 295.
[66] D.R. Entem, R. Machleidt, Phys. Lett. B 524 (2002) 93.
[67] D.R. Entem, R. Machleidt, Phys. Rev. C 66 (2002) 014002.
[68] D.R. Entem, R. Machleidt, Phys. Rev. C 68 (2003) 041001.
[69] R. Machleidt, D.R. Entem, J. Phys. G: Nuclear Phys. 31 (2005) S1235..
[70] U. van Kolck, Phys. Rev. C 49 (1994) 2932.
[71] E. Epelbaum, A. Nogga, W. Glöckle, H. Kamada, U.-G. Meißner, H. Witala, Phys. Rev. C 66 (2002) 064001.
[72] S. Ishikawa, M.R. Robilotta, Phys. Rev. C 76 (2007) 014006.
[73] V. Bernard, E. Epelbaum, H. Krebs, U.-G. Meißner, Phys. Rev. C 77 (2008) 064004.
[74] A. Deltuva, A.C. Fonseca, Phys. Rev. Lett. 98 (2007) 162502; Phys. Rev. C 76 (2007) 021001. arXiv:1005.1308 [nucl-th].
[75] L. Coraggio, A. Covello, A. Gargano, N. Itaco, T.T.S. Kuo, D.R. Entem, R. Machleidt, Phys. Rev. C 66 (2002) 021303.
[76] L. Coraggio, A. Covello, A. Gargano, N. Itaco, T.T.S. Kuo, R. Machleidt, Phys. Rev. C 71 (2005) 014307.
[77] L. Coraggio, A. Covello, A. Gargano, N. Itaco, Phys. Rev. C 81 (2010) 064303.
[78] P. Navrátil, E. Caurier, Phys. Rev. C 69 (2004) 014311.
[79] C. Forssen, P. Navratil, W.E. Ormand, E. Caurier, Phys. Rev. C 71 (2005) 044312.

[80] K. Kowalski, D.J. Dean, M. Hjorth-Jensen, T. Papenbrock, P. Piecuch, Phys. Rev. Lett. 92 (2004) 132501.
[81] D.J. Dean, M. Hjorth-Jensen, Phys. Rev. C 69 (2004) 054320.
[82] M. Wloch, D.J. Dean, J.R. Gour, M. Hjorth-Jensen, K. Kowalski, T. Papenbrock, P. Piecuch, Phys. Rev. Lett. 94 (2005) 21250.
[83] D.J. Dean, J.R. Gour, G. Hagen, M. Hjorth-Jensen, K. Kowalski, T. Papenbrock, P. Piecuch, M. Wloch, Nuclear Phys. 752 (2005) 299.
[84] J.R. Gour, P. Piecuch, M. Hjorth-Jensen, M. Wloch, D.J. Dean, Phys. Rev. C 74 (2006) 024310.
[85] G. Hagen, T. Papenbrock, D.J. Dean, M. Hjorth-Jensen, Phys. Rev. Lett. 101 (2008) 092502.
[86] G. Hagen, T. Papenbrock, D.J. Dean, M. Hjorth-Jensen, Phys. Rev. C 82 (2010) 034330.
[87] S. Fujii, R. Okamoto, K. Suzuki, Phys. Rev. C 69 (2004) 034328.
[88] S. Fujii, R. Okamoto, K. Suzuki, Phys. Rev. Lett. 103 (2009) 182501.
[89] K. Ermisch, et al., Phys. Rev. C 71 (2005) 064004.
[90] S. Kistryn, et al., Phys. Rev. C 72 (2005) 044006.
[91] H. Witala, J. Golak, R. Skibinski, W. Glöckle, A. Nogga, E. Epelbaum, H. Kamada, A. Kievsky, M. Viviani, Phys. Rev. C 73 (2006) 044004.
[92] J. Ley, et al., Phys. Rev. C 73 (2006) 064001.
[93] E. Stephan, et al., Phys. Rev. C 76 (2007) 057001.
[94] N. Kalantar-Nayestanaki, E. Epelbaum, The three-nucleon system as a laboratory for nuclear physics: the need for 3N forces, Nuclear Phys. News 17 (2007) 22. arXiv:nucl-th/0703089, and references therein.
[95] L.C. Marcucci, A. Kievsky, L. Girlanda, S. Rosati, M. Viviani, Phys. Rev. C 80 (2009) 034003.
[96] A. Kievsky, M. Viviani, L. Girlanda, L.E. Marcucci, Phys. Rev. C 81 (2010) 044003.
[97] M. Viviani, L. Giarlanda, A. Kievsky, L.E. Marcucci, S. Rosati, arXiv:1004.1306 [nucl-th].
[98] A. Nogga, P. Navratil, B.R. Barrett, J.P. Vary, Phys. Rev. C 73 (2006) 064002.
[99] P. Navratil, V.G. Gueorguiev, J.P. Vary, W.E. Ormand, A. Nogga, Phys. Rev. Lett. 99 (2007) 042501.
[100] G. Hagen, T. Papenbrock, D.J. Dean, A. Schwenk, A. Nogga, M. Wloch, P. Piecuch, Phys. Rev. C 76 (2007) 034302.
[101] T. Otsuka, T. Susuki, J.D. Holt, A. Schwenk, Y. Akaishi, Phys. Rev. Lett. 105 (2010) 032501.
[102] S.K. Bogner, A. Schwenk, R.J. Furnstahl, A. Nogga, Nuclear Phys. A763 (2005) 59;
S.K. Bogner, R.J. Furnstahl, A. Nogga, A. Schwenk, Nuclear matter from chiral low-momentum interactions, arXiv:0903.3366 [nucl-th].
[103] K. Hebeler, A. Schwenk, Phys. Rev. C 82 (2010) 014314.
[104] R. Machleidt, I. Slaus, J. Phys. G: Nuclear Part. Phys. 27 (2001) R69.
[105] U. van Kolck, Prog. Part. Nuclear Phys. 43 (1999) 337.
[106] P.F. Bedaque, U. van Kolck, Ann. Rev. Nuclear Part. Sci. 52 (2002) 339.
[107] E. Epelbaum, Prog. Part. Nuclear Phys. 57 (2006) 654.
[108] E. Epelbaum, H.-W. Hammer, U.-G. Meißner, Rev. Modern Phys. 81 (2009) 1773.
[109] S.R. Beane, P.F. Bedaque, K. Orginos, M.J. Savage, Phys. Rev. Lett. 97 (2006) 012001.
[110] N. Ishii, S. Aoki, T. Hatsuda, Phys. Rev. Lett. 99 (2007) 022001.
[111] T. Inoue, N. Ishii, S. Aoki, T. Doi, T. Hatsuda, Y. Ikeda, K. Murano, H. Nemura, K. Sasaki, Baryon–Baryon interactions in the flavor $SU(3)$ limit from full QCD simulations on the lattice, arXiv:1007.3559 [hep-lat].
[112] A concise and pedagogical introduction into low-energy QCD is contained in: W. Weise, The QCD vacuum and its hadronic excitations, arXiv:nucl-th/0504087.
[113] S. Scherer, Adv. Nuclear Phys. 27 (2003) 277.
[114] S. Scherer, M.R. Schindler, arXiv:hep-ph/0505265.
[115] K. Nakamura, et al., (Particle Data Group), J. Phys. G: Nuclear Part. Phys. 37 (2010) 075021.
[116] J. Goldstone, Nuovo Cimento 19 (1961) 154.
[117] J. Goldstone, A. Salam, S. Weinberg, Phys. Rev. 127 (1962) 965.
[118] V. Bernard, N. Kaiser, J. Kambor, U.-G. Meißner, Nuclear Phys. B388 (1992) 315.
[119] V. Bernard, N. Kaiser, U.-G. Meißner, Internat. J. Modern Phys. E 4 (1995) 193.
[120] E. Jenkins, A.V. Manohar, Phys. Lett. B 255 (1991) 558.
[121] H. Georgi, Phys. Lett. B 240 (1990) 447.
[122] N. Fettes, U.-G. Meißner, M. Mojžiš, S. Steininger, Ann. Phys. (NY) 283 (2000) 273; 288 (2001) 249.
[123] N. Fettes, U.-G. Meißner, S. Steiniger, Nuclear Phys. A640 (1998) 199.
[124] E. Epelbaum, Ph.D. Thesis, University of Bochum, 2000 (unpublished).
[125] L. Girlanda, S. Pastore, R. Schiavilla, M. Viviani, Phys. Rev. C 81 (2010) 034005.
[126] J.L. Friar, Few-Body Syst. 22 (1997) 161.
[127] S.N. Yang, W. Glöckle, Phys. Rev. C 33 (1986) 1774.
[128] S.A. Coon, J.L. Friar, Phys. Rev. C 34 (1986) 1060.
[129] E. Epelbaum, U.-G. Meißner, W. Glöckle, Nuclear Phys. A714 (2003) 535.
[130] J. Liu, et al., Phys. Rev. Lett. 105 (2010) 181803.
[131] R.A. Arndt, R.L. Workman, M.M. Pavan, Phys. Rev. C 49 (1994) 2729.
[132] V. Stoks, R. Timmermans, J.J. de Swart, Phys. Rev. C 47 (1993) 512.
[133] R. Blankenbecler, R. Sugar, Phys. Rev. 142 (1966) 1051.
[134] K.G. Richardson, Chiral symmetry and the nucleon–nucleon interaction, Ph.D. Thesis, University of Manchester, 1999, arXiv:hep-ph/0008118.
[135] M.C. Birse, J.A. Mcgovern, Phys. Rev. C 70 (2004) 054002.
[136] R. Higa, arXiv:nucl-th/0411046.
[137] G.Q. Li, R. Machleidt, Phys. Rev. C 58 (1998) 3153.
[138] P. Büttiker, U.-G. Meißner, Nuclear Phys. A668 (2000) 97.
[139] V.G.J. Stoks, R.A.M. Klomp, M.C.M. Rentmeester, J.J. de Swart, Phys. Rev. C 48 (1993) 792.
[140] SAID, Scattering Analysis Interactive Dial-in computer facility, George Washington University (formerly Virginia Polytechnic Institute), solution SM99 (Summer 1999);
for more information see, e.g. R.A. Arndt, I.I. Strakovsky, R.L. Workman, Phys. Rev. C 50 (1994) 2731.
[141] In fact preliminary calculations which take an important class of diagrams of order five into account, indicate that the N^4LO contribution may prevailingly be repulsive (N. Kaiser, private communication).
[142] K. Erkelenz, R. Alzetta, K. Holinde, Nuclear Phys. A176 (1971) 413; note that there is an error in equation (4.22) of this paper where it should read ${}^{-}W^J_{LS} = 2qq' \frac{J-1}{2J-1}\left[A^{J-2,(0)}_{LS} - A^{J(0)}_{LS}\right]$ and ${}^{+}W^J_{LS} = 2qq' \frac{J+2}{2J+3}\left[A^{J+2,(0)}_{LS} - A^{J(0)}_{LS}\right]$.
[143] E.E. Salpeter, H.A. Bethe, Phys. Rev. 84 (1951) 1232.
[144] R. Machleidt, in: K. Langanke, J.A. Maruhn, S.E. Koonin (Eds.), Computational Nuclear Physics 2 — Nuclear Reactions, Springer, New York, 1993, p. 1.
[145] D.B. Kaplan, M.J. Savage, M.B. Wise, Nuclear Phys. B478 (1996) 629; Phys. Lett. B 424 (1998) 390; Nuclear Phys. B534 (1998) 329.
[146] S. Fleming, T. Mehen, I.W. Stewart, Nuclear Phys. A677 (2000) 313; Phys. Rev. C 61 (2000) 044005.
[147] D.R. Phillips, S.R. Beane, T.D. Cohen, Ann. Phys. (N.Y.) 263 (1998) 255.
[148] T. Frederico, V.S. Timoteo, L. Tomio, Nuclear Phys. A653 (1999) 209.
[149] M.C. Birse, Phys. Rev. C 74 (2006) 014003; Phys. Rev. C 76 (2007) 034002.
[150] S.R. Beane, P.F. Bedaque, M.J. Savage, U. van Kolck, Nuclear Phys. A700 (2002) 377.
[151] M. Pavon Valderrama, E. Ruiz Arriola, Phys. Rev. C 72 (2005) 054002.

[152] A. Nogga, R.G.E. Timmermans, U. van Kolck, Phys. Rev. C 72 (2005) 054006.
[153] M. Pavon Valderrama, E. Ruiz Arriola, Phys. Rev. C 74 (2006) 054001.
[154] M. Pavon Valderrama, E. Ruiz Arriola, Phys. Rev. C 74 (2006) 064004; Phys. Rev. C 75 (2007) 059905 (Erratum).
[155] E. Epelbaum, U.-G. Meißner, On the renormalization of the one-pion exchange potential and the consistency of Weinberg's power counting, arXiv:nucl-th/0609037.
[156] M. Pavon Valderrama, E. Ruiz Arriola, Ann. Phys. (N.Y.) 323 (2008) 1037.
[157] D.R. Entem, E. Ruiz Arriola, M. Pavón valderrama, R. Machleidt, Phys. Rev. C 77 (2008) 044006.
[158] C.-J. Yang, Ch. Elster, D.R. Phillips, Phys. Rev. C 77 (2008) 014002; 80 (2009) 034002, 044002.
[159] B. Long, U. van Kolck, Ann. Phys. (N.Y) 323 (2008) 1304.
[160] S.R. Beane, D.B. Kaplan, A. Vuorinen, Phys. Rev. C 80 (2009) 011001.
[161] M. Pavon Valderrama, A. Nogga, E. Ruiz Arriola, D.R. Phillips, Eur. Phys. J. A 36 (2008) 315.
[162] R. Machleidt, D.R. Entem, J. Phys. G: Nuclear Phys. 37 (2010) 064041.
[163] M.P. Valderrama, Phys. Rev. C 83 (2011) 024003.
[164] R. Machleidt, P. Liu, D.R. Entem, E. Ruiz Arriola, Phys. Rev. C 81 (2010) 024001.
[165] B.H. Brandow, Rev. Modern Phys. 39 (1967) 771.
[166] B.D. Day, Rev. Modern Phys. 39 (1967) 719.
[167] H.A. Bethe, Ann. Rev. Nuclear Sci. 21 (1971) 93.
[168] B.D. Day, R.B. Wiringa, Phys. Rev. C 32 (1985) 1057.
[169] E. Epelbaum, J. Gegelia, Eur. Phys. J. A41 (2009) 341.
[170] G.P. Lepage, How to renormalize the Schrödinger equation, nucl-th/9706029.
[171] E. Epelbaum, W. Glöckle, U.-G. Meißner, Nuclear Phys. A747 (2005) 362.
[172] E. Epelbaum, W. Glöckle, U.-G. Meißner, Eur. Phys. J. A19 (2004) 401.
[173] The 1999 *NN* data base is defined in Ref. [13].
[174] R.B. Wiringa, V.G.J. Stoks, R. Schiavilla, Phys. Rev. C 51 (1995) 38.
[175] R. Machleidt, F. Sammarruca, Y. Song, Phys. Rev. C 53 (1996) 1483.
[176] J.R. Bergervoet, P.C. van Campen, W.A. van der Sanden, J.J. de Swart, Phys. Rev. C 38 (1988) 15.
[177] E.M. Henley, G.A. Miller, in: M. Rho, D.H. Wilkinson (Eds.), Mesons in Nuclei, vol. I, North-Holland, Amsterdam, 1979, p. 406.
[178] G.A. Miller, M.K. Nefkens, I. Slaus, Phys. Rep. 194 (1990) 1.
[179] G.Q. Li, R. Machleidt, Phys. Rev. C 58 (1998) 1393.
[180] A. Gardestig, J. Phys. G: Nuclear Part. Phys. 36 (2009) 053001.
[181] D.E. González Trotter, et al., Phys. Rev. C 73 (2006) 034001.
[182] Q. Chen, et al., Phys. Rev. C 77 (2008) 054002.
[183] U.L. van Kolck, Soft physics: applications of effective chiral Lagrangians to nuclear physics and quark models, Ph.D. Thesis, University of Texas, Austin, USA, 1993.
[184] U. van Kolck, Few-Body Syst. Suppl. 9 (1995) 444.
[185] U. van Kolck, J.L. Friar, T. Goldman, Phys. Lett. B 371 (1996) 169.
[186] E. Epelbaum, U.-G. Meißner, Phys. Rev. C 72 (2005) 044001.
[187] J. Friar, U. van Kolck, Phys. Rev. C 60 (1999) 034006.
[188] M. Walzl, U.-G. Meißner, E. Epelbaum, Nuclear Phys. A693 (2001) 663.
[189] J.L. Friar, U. van Kolck, G.L. Payne, S.A. Coon, Phys. Rev. C 68 (2003) 024003 and references to earlier work therein.
[190] J.L. Friar, U. van Kolck, M.C.M. Rentmeester, R.G.E. Timmermans, Phys. Rev. C 70 (2004) 044001.
[191] U. van Kolck, M.C.M. Rentmeester, J.L. Friar, T. Goldman, J.J. de Swart, Phys. Rev. Lett. 80 (1998) 4386.
[192] N. Kaiser, Phys. Rev. C 73 (2006) 044001.
[193] N. Kaiser, Phys. Rev. C 73 (2006) 064003.
[194] N. Kaiser, Phys. Rev. C 74 (2006) 067001.
[195] G.J.M. Austin, J.J. de Swart, Phys. Rev. Lett. 50 (1983) 2039.
[196] W.A. van der Sanden, A.H. Emmen, J.J. de Swart, Report No. THEF-NYM-83.11, Nijmegen, 1983 (unpublished); quoted in Ref. [176].
[197] A. Huber, Th. Udem, B. Gross, J. Reichert, M. Kourogi, K. Pachucki, M. Weitz, T.W. Hansch, Phys. Rev. Lett. 80 (1998) 468.
[198] W. Glöckle, H. Witala, D. Hüber, H. Kamada, J. Golak, Phys. Rep. 274 (1996) 107.
[199] D.R. Entem, R. Machleidt, H. Witala, Phys. Rev. C 65 (2002) 064005 and references to earlier work therein.
[200] E. Caurier, P. Navratil, W.E. Ormand, J.P. Vary, Phys. Rev. C 66 (2002) 024314.
[201] E. Epelbaum, U.-G. Meißner, J.E. Palomar, Phys. Rev. C 71 (2005) 024001.
[202] J.-I. Fujita, H. Miyazawa, Prog. Theor. Phys. 17 (1957) 360.
[203] S.A. Coon, M.D. Scadron, P.C. Mcnamee, B.R. Barrett, D.W.E. Blatt, B.H.J. Mckeller, Nuclear Phys. A317 (1979) 242.
[204] H.T. Coelho, T.K. Das, M.R. Robilotta, Phys. Rev. C 28 (1983) 1812;
M.R. Robilotta, H.T. Coelho, Nuclear Phys. A460 (1986) 645.
[205] J.L. Friar, D. Hüber, U. van Kolck, Phys. Rev. C 59 (1999) 53.
[206] S.A. Coon, H.K. Han, Few-Body Syst. 30 (2001) 131.
[207] A. Gårdestig, D.R. Philips, Phys. Rev. Lett. 96 (2006) 232301.
[208] C. Hanhart, U. van Kolck, G.A. Miller, Phys. Rev. C 85 (2000) 2905.
[209] D. Gazit, S. Quaglioni, P. Navrátil, Phys. Rev. Lett. 103 (2009) 102502.
[210] S.X. Nakamura, Phys. Rev. C 77 (2008) 054001.
[211] B.M. Fisher, C.R. Brune, H.J. Karwowski, D.S. Leonard, E.J. Ludwig, T.C. Black, M. Viviani, A. Kievsky, S. Rosati, Phys. Rev. C 74 (2006) 034001.
[212] M.R. Robilotta, Phys. Rev. C 74 (2006) 044002.
[213] N. Fettes, U.-G. Meißner, Nuclear Phys. A676 (2000) 311.
[214] E. Epelbaum, Eur. Phys. J. A34 (2007) 197.
[215] E. Epelbaum, Phys. Lett. B 639 (2006) 456.
[216] D. Rozpedzik, J. Golak, R. Skibinski, H. Witala, W. Glöckle, E. Epelbaum, A. Nogga, H. Kamada, Acta Phys. Polon. B37 (2006) 2889, arXiv:nucl-th/0606017.
[217] K. Holinde, R. Machleidt, Nuclear Phys. A280 (1977) 429.
[218] T.R. Hemmert, B.R. Holstein, J. Kambor, J. Phys. G 24 (1998) 1831.
[219] V. Bernard, N. Kaiser, U.-G. Meißner, Nuclear Phys. A615 (1997) 483.
[220] C. Ordóñez, U. van Kolck, Phys. Lett. B 291 (1992) 459.
[221] H. Krebs, E. Epelbaum, U.-G. Meißner, Eur. Phys. J. A32 (2007) 127.
[222] E. Epelbaum, H. Krebs, U.-G. Meißner, Nuclear Phys. A806 (2008) 65.
[223] N. Fettes, U.-G. Meißner, Nuclear Phys. A679 (2001) 629.
[224] S.C. Pieper, V.R. Pandharipande, R.B. Wiringa, J. Carlson, Phys. Rev. C 64 (2001) 014001.
[225] S. Weinberg, The Quantum Theory of Fields, Vol. I, Cambridge University Press, Cambridge, New York, 1995.
[226] I.S. Gerstein, R. Jackiw, B.W. Lee, S. Weinberg, Phys. Rev. D 3 (1971) 2486.
[227] G.'t. Hooft, M. Veltman, Nuclear Phys. B44 (1972) 189.
[228] J.C. Collins, Renormalization, Cambridge University Press, Cambridge, 1984.
[229] F. Mandl, G. Shaw, Quantum Field Theory, revised ed., Wiley, New York, 1984.
[230] R.P. Feynman, Phys. Rev. 76 (1949) 769.
[231] G. 't Hooft, Nuclear Phys. B61 (1973) 455.
[232] M. Abramovitz, I.A. Stegun, Handbook of Mathematical Functions, Dover, New York, 1970.